Correlation of Tribological Properties with Chemical Structure of Modified DLC Films

By

SYAMALARAO POLAKI

Enrolment no: PHYS02 2010 04 018

Indira Gandhi Centre for Atomic Research,
Kalpakkam, Tamil Nadu, India, 603102

A thesis submitted to the
Board of studies in Physical Sciences

In partial fulfilment of requirements
for the degree of

DOCTOR OF PHILOSOPHY

of

HOMI BHABHA NATIONAL INSTITUTE

October, 2016

Homi Bhabha National Institute

Recommendations of the Viva Voce Board

As members of the Viva Voce Board, we certify that we have read the dissertation prepared by **Syamalarao Polaki** entitled **"Correlation of tribological properties with chemical structure of modified DLC films"** and recommend that it may be accepted as fulfilling the thesis requirement for the award of Degree of Doctor of Philosophy.

for N.V. Chandra

Chairman: Prof. Dr. Sitaram Dash (Dean) Date: 12/6/17

Guide: Prof. Dr. A .K. Tyagi Date:

12/6/2017.

Examiner: Prof. Dr. B. R. Mehta Date:

Amarendra June 12, 2017

Member: Prof. Dr. G. Amarendra Date:

12/6/17

Member: Prof. Dr. M. Kamruddin Date:

Final approval and acceptance of this dissertation is contingent upon the candidates' submission of the final copies of the dissertation to HBNI.

I hereby certify that I have read this dissertation prepared under my direction and recommend that it may be accepted as fulfilling the dissertation requirement.

Date: 12/6/17

Place: KALPAKKAM

Prof. Dr. A. K. Tyagi
(Guide)

STATEMENT OF AUTHOR

This dissertation has been submitted in the partial fulfilment of requirements for an advanced degree at Homi Bhabha National Institute (HBNI) and is deposited in the Library to be made available for borrowers under rules of the HBNI.

Brief quotations from this dissertation are allowable without special permission, provided that accurate acknowledgement of source is made. Requests for permission for extended quotation from or reproduction of this manuscript in whole or in part may be granted by the Competent Authority of HBNI when in his or her judgement the proposed use of the material is in the interests of the scholarship. In all other instances, however, permission must be obtained from the author.

SYAMALARAO POLAKI

DECLARATION

I, hereby declare that the investigation presented in the thesis has been carried out by me. The work is original and has not been submitted earlier as a whole or in part for a degree/diploma at this or any other Institution/University.

SYAMALARAO POLAKI

LIST OF PUBLICATIONS

Publications in Journals/Preprints arising from thesis

1. Tribological properties of chemically modified diamond like carbon films in hydrogen plasma, **S.R. Polaki**, N. Kumar, Nanda Gopala Krishna, T.R. Ravindran, M. Kamruddin, S. Dash, A.K. Tyagi, **Tribology International** 81(**2015**)283–290.
2. Tribological behavior of hydrogenated DLC film: Chemical and physical transformations at nano-scale, **S.R. Polaki**, N. Kumar, K. Ganesan, Kishore Madapu, Ashok Bahuguna, M. Kamruddin, S. Dash, A.K. Tyagi, **Wear** 338-339 (**2015**)105–113.
3. Interpretation of Friction and Wear in DLC Film: Role of Surface Chemistry and Test Environment, **S. R. Polaki**, N. Kumar, Kishore Madapu, K. Ganesan, Nanda Gopala Krishna, S.K. Srivastava, S. Abhaya, M. Kamruddin, S. Dash and A.K. Tyagi, **Journal of physics D: applied physics 49 (2016) 445302**
4. "The role of substrate bias and nitrogen doping on structural evolution and local indentation modulus of diamond-like carbon films", **S. R. Polaki**, K. Ganesan, Kishore Madapu, S.K. Srivastava, M. Kamruddin and A.K. Tyagi, **Journal of physics D: applied physics 50 (2017) 175601**
5. "Chemical reconstruction of diamond-like carbon film surface in microwave plasma medium", **S. R. Polaki**, N. Kumar,* N. G. Krishna, K. Madapu, M. Kamruddin, S. Dash and A. K. Tyagi, **Advanced Materials Interfaces** (**under review**)
6. Role of duty ratio and pulse frequency of substrate biasing on local indentation modulus of DLC films, **S. R. Polaki**, K. Ganesan, Kishore Madapu, S.K. Srivastava, R. Ramaseshan, M. Kamruddin and A.K. Tyagi (**to be communicated**)

Conferences

1. Friction behavior of H_2 plasma treated diamond-like carbon films, **S. R. Polaki**, N. Kumar, M. Kamruddin, A.K. Tyagi, Conference proceedings, RAINSAT 2015.
2. Acoustic force atomic microscopy investigations of nitrogen doped DLC films, **S.R.Polaki**, K. Ganesan, N. Kumar, M. Kamruddin, A.K. Tyagi, Conference proceedings, NANOS 2015.

SYAMALARAO POLAKI

Dedicated to

To My Revered Parents and loving family

ACKNOWLEDGEMENTS

From the first moment of journey towards this dissertation, time moves on her way. In this page, I want to recall all, without them this dissertation would not have been possible.

First and foremost, I sincerely thank and express my deepest gratitude to my supervisor, Dr. A. K. Tyagi, and Dr. M. Kamruddin my section Head, for their guidance, encouragement and patience support throughout the course of present dissertation.

I would like to express my gratitude to Dr. A. K. Bhaduri, Dr. S.A.V. Satya Murty, Dr. Vasudev Rao, and Dr. S. C. Chetal, present and former Directors, IGCAR for permitting me to pursue Ph. D at IGCAR. I am highly thankful to Dr. G. Amarendra, Dr. C. S. Sundar, and Dr. M. P. Janawadkar, present and former Group Directors, MSG for providing the conductive atmosphere for my smooth research.

I am also very grateful to all the professors of my doctoral committee; Dr. Sitaram Dash, Dr. G. Amarendra and Dr. Kamruddin for sharing their valuable time and for providing me with helpful feedback and evaluating my work at each stage.

I am deeply indebted to Dr. Niranjan Kumar, without him this dissertation would not have shaped up to this level. He helped me a lot in carrying out tribology studies, data analysis and communicating the manuscripts. His valuable suggestions on scientific issues helped me to excel in this area.

I would like to thank my other collaborators who helped me in analysing my samples using variety of characterization techniques. Mr. Kishore Madapu for Raman spectroscopy measurements, Mr. Nanda Gopala Krishna for XPS measurements and data analysis, Dr. K. Ganesan for topography, AFAM measurements and technical discussions, Dr. S. K. Srivastava for RBS and ERDA measurements, Mr. Ashok Bahaguna for Dektak measurements, Mr. Subrata Ghosh for contact angle measurements and Dr. Rama Seshan for nano indentation measurements, Dr. S. Abhaya for Auger spectroscopy measurements, Dr. Avinash Patsa for Raman analysis and Smt. J. Parimala for giving me DC power supply.

I am also thankful to my colleagues Dr. P. K. Aji Kumar, Mr. P.A. Manoj Kumar, Dr. G. Mangamma, Dr. R. Pandian, Dr. Tom Mathews, Dr. R. N. Viswanath, Dr. Kamala Kannan and Mr. Gopinath Sahoo who helped in learning various stages of Ph.D. career.

I would not have been able to complete my work without the support from Dept. of Atomic Energy, Govt. of India. I would like to thank Homi Bhabha National Institute for accepting this dissertation towards Ph.D. degree. I am also thankful to all reviewers and examiner for their time and careful evaluation.

I wish to extend my sincere gratitude to all my teachers, who had taught me at educational career. I am also thanks to my friends, batch mates, and all other colleagues of the centre.

I am Thankful to my friends Mr. Anji Reddy and Mr. A. Viswanath and their family whom with I have many memorable moments.

I am deeply indebted to my beloved parents, and my whole family, for their moral support over the years. They have shown me that who I am and who I'd like to become.

Last but not least, I will never have the words of appreciation for my wife, Smt.Lalitha Kumari and my little one Mr. Rutvik Polaki who made my life so beautiful.

Thank you all for your love, patience and support to make it possible.

SYAMALARAO POLAKI

Table of CONTENTS

Synopsis i

List of Figures vii

List of Tables xii

List of Abbreviation xiii

Chapter 1. Introduction

1.1 Historical over view of amorphous carbon 1

1.2 Classification of amorphous carbon family 2

1.3 Properties and applications of DLC films 3

1.4 Synthesis techniques and growth mechanism of DLC films 4

1.5 Motivation and Research objectives 14

1.6 References 16

Chapter 2. Experimental Techniques

2.1 Growth techniques

2.1.1 Substrate cleaning 21

2.1.2 Electron Cyclotron Resonance Chemical Vapour Deposition (ECR-CVD) setup 22

2.1.3 Process conditions for the film growth 24

2.2 Characterization techniques

2.2.1 Field Emission Scanning Electron Microscope (FESEM) 25

2.2.2 Scanning Probe Microscopy (SPM) 26

2.2.3 Raman spectroscopy 30

2.2.4 X-ray Photoelectron Spectroscopy (XPS) 31

2.2.5 Auger Electron Spectroscopy (AES) 33

2.2.6 Rutherford Back Scattering spectroscopy (RBS) 34

2.2.7 Elastic Recoil Detection Analysis (ERDA) 35

2.2.8 Tribometer 36

2.2.9 Surface profilometer 38

2.2.10 Contact Angle Measurements 38

2.3 References 40

Chapter 3. Effect of gas composition and pulse DC biasing on structural and mechanical properties of DLC films

3.1 Introduction 41

3.2 Experimental section

3.2.1 Film growth 42

3.2.2 Characterization 42

3.3 Results and discussion

3.3.1 Effect of gas composition 43

3.3.2 Effect of duty cycle and frequency of pulsed DC bias 47

3.3.3 Effect of substrate biasing 50

3.4 Conclusions 62

3.5 References 63

Chapter 4. Effect of sliding speed and normal load on the tribological properties of DLC films

4.1 Introduction 65

4.2 Experimental details 66

4.3 Results and discussion

4.3.1 Morphology, topography and chemical structure of DLC film 67

4.3.2 Tribology behavior of DLC films 68

4.3.3 Raman analysis of wear track 72

4.3.4 AFAM analysis of wear tracks 76

4.3.5 Friction and wear mechanism 79

4.4 Conclusions 81

4.5 References 83

Chapter 5. Mechanical and tribological properties of nitrogen doped DLC films

5.1. Introduction 85

5.2. In-situ nitrogen doping 86

5.3. Results and discussion

5.3.1 Topography and film thickness 86

5.3.2 Raman Spectroscopy studies 87

5.3.3 XPS Analysis 89

5.3.4 Film density and hydrogen content 92

5.3.5 AFAM analysis 92

5.3.6 Tribology studies 95

5.4.Conclusions 98

5.5.References 99

Chapter 6. Effect of gas medium on friction behavior of the DLC films

6.1. Introduction 101

6.2. Film preparation and measurements 102

6.3. Results and discussion

6.3.1 Morphology of wear tracks 103

6.3.2 Raman spectroscopy analysis 104

6.3.3 Tribology studies in different gas medium 105

6.4 Conclusions 111

6.5 References 112

Chapter 7. Friction and wetting characteristics of plasma treated DLC films

7.1 Introduction 114

7.2 Plasma exposure and post exposure characterization of DLC surfaces 116

7.3 Results and discussion

- 7.3.1 Topography and film thickness 116
- 7.3.2 Raman and X-ray photoelectron spectroscopy 120
- 7.3.3 Contact angle analysis 129
- 7.3.4 Tribology studies 134

7.4 Conclusions 136

7.5 References 137

Chapter 8. Conclusions and Future prospects

8.1 Conclusions 139

8.2 Future prospects 141

SYNOPSIS

Friction is the foremost barrier in energy conservation towards achieving eco friendly society. Novel materials minimizing friction and wear in the machineries to make them economical and energy efficient are always in great demand. Owing to unique properties of Diamond Like Carbon (DLC) films that include high hardness, chemical inertness, tunable band gap, ultra-low friction coefficient and extremely high wear resistance it has become an obvious choice for electronic, optical and wear protection applications in nano to micro and macro-scale. Diamond Like Carbon is an amorphous network of solid carbon with mixed bonding states (sp^2 and sp^3) often with hydrogen. DLC films have been used to meet demands of outstanding tribological properties in wide variety of operating environments. Its spectrum of applications spreads over a wide range starting from the protective coatings for miniature devices like MEMS/NEMS to the sturdy machinery tools, surface coating on engine parts, anti reflecting coatings in optics and recently extended into the field of biomedicine and bio sensors. Usage of DLC films as protective as well as antireflection coating on silicon solar cell and space solar cells helped towards increasing the efficiency. DLC films are also considered to be next generation solid lubricant material for space applications.

DLC is a generalized term and further classified based on the amount of sp^3 fraction and hydrogen content. The films with high sp^3 fraction are known as tetrahedral amorphous carbon (ta-C), one with lower sp^3 fraction known to be amorphous carbon (a-C) and their hydrogenated counter parts are ta-C:H and a-C:H. The sp^3 fraction and hydrogen content is important factor to quantify the quality of the films and its suitability for various applications. Hydrogenated and hydrogen free DLC films have contrasting tribological behavior. They possess ultra low friction coefficient in vacuum/inert and in humid air, respectively. Despite these differences, DLC films have an advantage of tunable mechanical and tribological properties over a wide range.

Various deposition techniques like magnetron sputtering (DC or RF), pulsed laser deposition, ion beam deposition, filtered cathodic arc deposition, hot filament chemical vapor deposition (CVD), microwave enhanced plasma CVD and electron cyclotron resonance plasma CVD (ECR-CVD) are employed for the synthesis of DLC thin films. Among all these methods, ECR-CVD is the most preferred technique because of its high plasma density, larger deposition area, superior electron temperatures and flexibility in operating at lower pressures. Moreover, ECR CVD doesn't contain any electrodes which enable to maintain the substrate at a desired voltage, which in turn helps to tune the ion flux density and energy independently. Recent advances in physical and chemical deposition methods allow growth of DLC film with desired sp^2/sp^3 bonding state and hydrogen concentration. There are a few experimental parameters which need to be manipulated for achieving controlled chemistry of a film. Irrespective of the kind of deposition method adopted for synthesis the ion energy and growth temperature used in the process controls the sp^2/sp^3 fraction and hydrogen content in the film. Doping of DLC film to modify its properties with various metals as well as non metals is extensively reported in recent times. Nitrogen doping is an effective way to chemically modify the DLC film. It forms localized C-N bonds and improves their mechanical properties and film-substrate adhesion. The significance of chemisorbed species like O_2, N_2 and H_2O in determining the tribological properties has also been reported. Recent studies on the surface functionalization/ passivaion of the DLC film by hydrogen and oxygen with plasma exposure further proves the influence of the surface absorbents on friction coefficient. This phenomenon has also been substantiated by numerous MD simulation studies reported recently.

The bonding, surface chemistry and test environment are the key factors in determining the friction coefficient and wear resistance. Plentiful recently published scientific reports in this area emphasizes the scope for elaborate tribological studies on DLC films with varying sp^2/sp^3 fraction, doping, surface functionalization / passivation and test environments. In this study the focus lies on studying the role of chemical bonding and surface chemistry on structural, mechanical and wetting characteristics of the DLC films. The significance of the surface chemistry and role of surface oxidation is investigated. This study extends to establish the mechanism of the tribo chemical reactions associated with different gas medium and its role in determining the friction coefficient and wear resistance.

Chapter 1: Introduction

Chapter 1 presents a brief introduction to DLC films. It covers the classification of the DLC films and their morphology, structural, tribological properties and potential applications. Detailed and upto date literature survey on synthesis methods and process parameter optimization is presented. A brief motivation and objective of the work towards modified and improved DLC films is given at the end of the chapter.

Chapter 2: Experimental details

This chapter describes in detail the experimental procedures involved in the synthesis and characterization of DLC films. The details of Electron Cyclotron Resonance Chemical Vapor Deposition (ECR-CVD) used to grow DLC films are given. The process parameters like gas composition (argon/methane ratio), substrate bias (voltage, frequency, duty cycle), used for the growth are given in detail. The parameters used for in-situ doping of the films, plasma exposure studies are discussed. The details of the analytical techniques like FESEM, AFM, RAMAN, RBS, XPS and AES etc. used to characterize the films are elaborated.

Chapter 3: Effect of gas composition and pulse DC biasing on structural and mechanical properties of DLC films

This chapter discusses the influence of gas compostion and pulsed DC parameters on the structural and tribological properties of the DLC films. In this work, high pure argon (Ar) and methane (CH_4) gases were used as dilution and process gases, respectively. It is understood that the ratio of these gases influence the properties of the DLC films to a great extent. The variation in morphology, thickness, film density and hydrogen content are elaborated. The variation in chemical bonding with the gas ratio is analyzed using Raman spectra of these films. Further the optimized gas ratio maintained constantly and films grown as a function of substrate biasing voltage, pulse frequency and duty cycle. The morphology, thickness, film density and hydrogen content of these films are also analyzed. It is observed that biasing voltage and duty cycle has a significant influence on the properties of the films. The nano indentation measurements were carried out on these set of samples to obtain hardness and elastic modulus. Relationship of biasing voltages with phase composition in DLC film and its tribological properties were investigated. Phase composition with mechanical and tribological properties was correlated. At the end this chapter presents the optimized process parameters for the improved DLC films.

Chapter 4: Effect of sliding speed and normal load on the tribological properties of DLC films

Main focus of this chapter lies on the optimization of sliding speed and normal load to obtain the tribological properties of the DLC films. It is well known that the sliding speed and normal load alter chemical bonding, structure and phase due to the applied stress and heat generated in sliding contact. It is observed that increase in sliding speed reduced the friction coefficient. Whereas increase in normal load increased the friction coefficient and the film failed at higher load. Raman and acoustic force mapping of the wear tracks are explored to find the changes in chemical bonding and elastic modulus. The wear track dimension also changes along with sliding speed and normal load. Stylus profilometer is extensively used to obtain the wear track dimensions for wear rate calculation. It is observed that the increase in normal load has severe effect than increase in sliding speed. This chapter discusses in detail about the physical and chemical changes occurred in the DLC films due to contact stress during tribology test. Optimum sliding speed and normal load suitable for effective tribological performance of these films are reported. These parameters are maintained constantly henceforth throughout the thesis work.

Chapter 5: Mechanical and tribological properties of nitrogen doped DLC films

Chapter 5 details the in-situ nitrogen doping of the DLC films by allowing high pure nitrogen gas at different flow rates into the process chamber along with methane during the growth. The variation in growth rate and morphology are studied and growth rate was found to reduce with the nitrogen doping. However, the rms roughness of the films does not change much. The films characterized using Raman spectroscopy and XPS to obtain the changes in chemical structure with the doping. It was observed that the graphitization of the films increased with the doping. XPS results confirmed the formation of the carbonitride bonds and it increased with nitrogen flow rate. Further these films characterized by Acoustic Force Atomic Microscopy (AFAM) technique to obtained the elastic properties. The modulus of the films reduced with the nitrogen doping. Friction coefficient was increased with nitrogen content but the film does not fails, implying an improved toughness. The wear rate of the films observed to be reduced with the nitrogen doping.

Chapter 6: Effect of gas medium on the friction behavior of the DLC films

This chapter deals with the tribology studies of DLC films in presence of five different mediums. It is known that friction behavior of DLC films is sensitive to test environment. Here, high pure argon, nitrogen, methane and oxygen gas medium was used for tribological studies and the results was compared with ambient atmospheric tribology test. These tests were carried out on undoped and nitrogen doped films and films were selected based on their difference in surface chemistry. Several gases such as argon, oxygen, nitrogen and methane were used to study the role of active and passive gaseous species on friction and wear. The interaction mechanism exhibited by the DLC films in each gas medium during the tribo test is elaborated in this chapter.

Chapter 7: Friction and wetting characteristics of plasma treated DLC films

Chapter 7 describes the interaction of DLC films with hydrogen, nitrogen and oxygen radicals or ions by exposing them to desired plasma. The plasma exposure studies are carried out as a function of exposure time and energy. The etching rate of the plasma is calculated by measuring the variation in films thickness after plasma exposure. Plasma exposed films were characterized by XPS to understand the change occurred in surface chemistry. The friction coefficient of these films increased with plasma exposure. Additionally a significant run in behavior is observed in friction for the film exposed to hydrogen and nitrogen plasmas. The run in behavior is seen in case of lower energy plasma exposure film only and it vanished in higher energy plasma exposure. On the other hand oxygen plasma exposure doesn’t show any run in behavior at all. The contact angle measurements showed that both the hydrogen and nitrogen plasma exposure make the films hydrophobic. Whereas, on exposed to oxygen plasma the films became hydrophilic. This chapter elaborates the change in surface chemistry with plasma exposure and correlates it with friction coefficient and wetting characteristics.

Chaper 8: Conclusion and future prospects

This chapter gives the summary of the observations and findings from the obtained results of the entire thesis work. It also briefs the future prospects or directions for this work.

List of Figures

Figure 1.1 Ternary phase diagram of bonding in C-H alloys 2

Figure 1.2 Various applications of DLC films 4

Figure 2.1 A schematic of ECR CVD system used for the growth of DLC films 24

Figure 2.2 A schematic of Field Emission Scanning Electron Microscopy (FESEM) 25

Figure 2.3 Probable emissions during electron beam interaction with material surface 26

Figure 2.4 A schematic representation of a) force displacement curve of tip and sample and b) Atomic Force Microscope (AFM) 27

Figure 2.5 Schematic view of a) excitation process and b) instrumentation setup 30

Figure 2.6 Schematic representation of XPS a) instrumental setup and b) Photo electron emission process 32

Figure 2.7 Schematic view of Auger electron emission process (KLL transition) 33

Figure 2.8 Schematic representation of the ion beam analysis setup with both RBS and ERDA detectors 34

Figure 2.9 A schemcatic representation of tribometer setup 36

Figure 2.10 (a) Schematic of contact angles (CA) formed by sessile liquid drops on smooth homogeneous solid surface, (b) table of CA with wetting property and (c) Contact angle measurement set up in our lab 39

Figure 3.1 FESEM cross section images of DLC films grown under different gas concentrations, (a-d) Ar series and (e-h) methane series 43

Figure 3.2 Raman spectra of DLC films grown under different gas concentration a) Ar and b) CH_4 series 46

Figure 3.3 Film density and hydrogen content of DLC films a) Ar and b) CH_4 series 47

Figure 3.4 Variations in film density and hydrogen content of DLC films grown as function of a) duty cycle b) pulsing frequency of pulse bias 48

Figure 3.5 Elastic modulus of DLC films grown as a function of a) duty cycle and b) frequency of pulse bias 49

Figure 3.6 Friction coefficient of DLC films grown as a function of a) duty cycle and b) frequency of pulse bias 50

Figure 3.7 AFM topography of DLC films grown at substrate bias of (a) -50, (b) -100, (c) -150 and (d) -200 V, FESEM cross sectional micrograph is given in inset 51

Figure 3.8 Raman spectra of DLC films grown as a function of substrate bias 52

Figure 3.9 Contact resonance frequency mapping of DLC films grown at different substrate biases of (a) Si (100), b) -50, (c) -100, (d) -150, and (e) -200V 56

Figure 3.10 The calculated elastic modulii of the DLC films grown at different bias 56

Figure 3.11 XPS survey spectra and deconvoluted high resolution C1s spectra of DLC films grown at different substrate bias 58

Figure 3.12 Friction coefficient of DLC films grown at different substrate bias 58

Figure 3.13 FESEM images of wear tracks on DLC films grown at different substrate bias 61

Figure 4.1 Typical (a) FESEM image of surface and cross-section (b) AFM topography and (c) nano indentation data of the film 67

Figure 4.2 (a) RBS spectra (b) Raman spectra and (c) XPS of hydrogenated DLC film 67

Figure 4.3 Friction behavior of DLC film at sliding speed of (a) 0.2 (b) 0.5 (c) 1 and (d) 3 cm/s 69

Figure 4.4 2D wear tack profiles at sliding speeds of (a) 0.2 (b) 0.5 (c) 1 and (d) 3 cm/s 70

Figure 4.5 Friction coefficient of DLC films tested under different normal loads 70

Figure 4.6 2D wear tack profiles at normal loads (a) 2 (b) 5 and (c) 8 N 71

Figure 4.7 I_D/I_G ratio mapping of wear tracks formed at sliding speeds of (a) 0.2 (b) 0.5 (c) 1 and (d) 3 cm/s at load 1 N 73

Figure 4.8 Sliding speed dependent I_D/I_G ratio in wear track of DLC film at locations (a), (b), and (c) indicated in Fig. 4.7 74

Figure 4.9 Sliding speed dependent FWHM of G band in wear track of DLC film at locations (a), (b), and (c) indicated in Fig. 4.7 74

Figure 4.10 I_D/I_G ratio and FWHM of G peak inside wear tracks obtained at different normal loads 75

Figure 4.11 First order contact resonance frequency spectra of the cantilever on pristine DLC film at different loads 76

Figure 4.12 Simultaneously measured (a) topography (b) AFAM amplitude images at two different frequencies in which one is above the contact resonance frequency (CRF) and (c) other is below the CRF 77

Figure 4.13 Line profile topography of (a) AFAM amplitude at higher to contact resonance frequency (CRF) (b) at lower CRF (c) and CRF for the wear track with sliding speed of 3 cm/s 78

Figure 4.14 Schematic representation of *sp*^{3} and *sp*^{2} phase across the wear track at (a) less and (b) high sliding speed 79

Figure 4.15 Raman spectra of ball scar showing evidence of a-C. In inset optical image of the scar is shown 81

Figure 5.1 AFM topography of undoped and nitrogen doped DLC films at various nitrogen flow rates of (a) 0, (b) 0.5, (c) 1 and (d) 2.5 sccm 87

Figure 5.2 Raman spectra of nitrogen doped DLC films at various nitrogen flow rates of (a) 0, (b) 0.5, (c) 1 and (d) 2.5 sccm 88

Figure 5.3 Raman parameter with N_2 flow rate (a) G peak position, (b) FWHM of G band, (c) I_D/I_G ratio and (d) intensity of G band 89

Figure 5.4 XPS survey spectra and C1s spectra of DLC films with different nitrogen concentrations such as 0, 0.5, 1 and 2.5 sccm, respectively 90

Figure 5.5 C/O ratio of nitrogen doped DLC films 91

Figure 5.6 a) RBS and b) ERDA spectra of nitrogen doped DLC films 92

Figure 5.7 CRF mapping of various sample surfaces a) Si (100), b) B_{2-0}, c) $B_{2-0.5}$, d) $B_{2-1.0}$ and e) $B_{2-2.5}$ 93

Figure 5.8 Calculated elastic modulus of nitrogen doped DLC films 94

Figure 5.9 Friction coefficient of nitrogen doped DLC films 95

Figure 5.10 Film thickness and failure distance *vs* nitrogen flow rate 97

Figure 6.1 FESEM images of wear tracks of DLC film tested in various gaseous medium 103

Figure 6.2 Raman spectra of wear tracks under different gas medium a) B_{2-0} b) B_{2-1} 104

Figure 6.3 I_D/I_G ratio and G position inside wear track of B_{2-0} and B_{2-1} films tested in different gas medium 105

Figure 6.4 Friction coefficient of B_{2-0} and B_{2-1} films in different gas medium 106

Figure 6.5 Wear track profiles of both B_{2-0} and B_{2-1} DLC films at different medium such as ambient (a, f), argon (b, g), nitrogen (c, h), methane (d, i) and oxygen (e, j) 107

Figure 6.6 Wear rates of DLC films B_{2-0}, B_{2-1} in different gas medium 108

Figure 6.7 Auger spectra of the as grown (B_{2-0}) and nitrogen doped (B_{2-1}) DLC films 109

Figure 6.8 Schematic representation of bonding at the surface of the films 110

Figure 7.1 Surface topography, chemical structure and wetting characteristics of untreated DLC film: (a) AFM topography, (b) Raman spectra and (c) XPS survey spectra and (d) water contact angle 117

Figure 7.2 Surface topography of plasma exposed DLC films, inset in each image showed cross section of film thickness 119

Figure 7.3 Film thickness of DLC films exposed to a) Hydrogen, b) Oxygen plasma and c) Nitrogen plasmas 120

Figure 7.4 Surface topography of bias assisted hydrogen plasma exposed DCL films a) 15 mins, b) 30 mins and c) 60 mins 120

Figure 7.5 Rama spectra of plasma treated DLC films 122

Figure 7.6 I_D/I_G ratio and G peak position of DLC films exposed to a) H_2, b) O_2 and c) N_2 plasmas 123

Figure 7.7 XPS survey spectra DLC films exposed to a) H_2, b) O_2 and c) N_2 plasmas 126

Figure 7.8 C/O ratio and roughness of DLC films exposed to (a) H_2 (b) O_2 and (c) N_2 plasmas 127

Figure 7.9 C1s spectra of bias assisted H_2 plasma exposed DLC films a) 15, b) 30 and c) 60 mins 128

Figure 7.10 Contact angle of DLC film exposed to (a) H_2 (b) O_2 and (c) N_2 plasmas 129

Figure 7.11 Schematic representation of DLC film surface exposed to (a) H_2 (b) O_2 and (c) N_2 plasmas 131

Figure 7.12 Friction plot and corresponding wear rate of plasma exposed DLC films 135

List of Tables

Table 3.1 Film thickness, density and H content of Ar and CH_4 series DLC films 44

Table 3.2 Properties of DLC films grown as a function of substrate biasing 54

Table 4.1 Physical and chemical properties of hydrogenated DLC film 68

Table 4.2 Wear rate of DLC film as a function of sliding speed and normal load 72

Table 5.1 Properties of nitrogen doped DLC films 97

Table 7.1 Roughness, sp^2/sp^3 ratio, coefficient of friction (COF) and contact angle (CA) with plasma processing time 129

List of Abbreviations

2D	Two Dimensional
µ	micron
a-C	Amorphous carbon
AES	Auger Electron Spectroscopy
AFM	Atomic Force Microscopy
AFAM	Acoustic Force Atomic Microscopy
BE	Binding Energy
CA	Contact Angle
cc	Cubic centimeter
cm	Centimeter
CRF	Contact Resonance Frequency
CVD	Chemical Vapor Deposition
DLC	Diamond Like Carbon
ECR	Electron Cyclotron Resonance
ERDA	Elastic Recoil Detection Analysis
eV	Electron volt
FESEM	Field Emission Scanning Electron Microscope
FWHM	Full Width at Half Maximum
GPa	Giga Pascal
N	Newton
nm	Nano Meter
RBS	Rutherford Back scattering Spectroscopy
rms	Root Mean Square
RH	Relative Humidity
sccm	Standard Cubic Centimeter
ta-C	Tetrahedral Amorphous Carbon
V	volt
W	Watt
XPS	X-ray Photo electron Spectroscopy

Friction is the foremost barrier in energy conservation towards achieving economical and eco friendly machineries that help in developing green industrialization. Friction and wear decides the efficiency and life time of any machinery. A significant fraction of the global GDP has been invested on reducing frictional losses in industrial and transportation machineries. A recent report by Holmberg *et al.* covers detailed frictional losses that occur in automobiles used for road transport and its contribution towards pollution and global warming.[1] Novel materials would minimize the loss of friction and wear in machineries that can improve the above mentioned aspects. For the past three decades lot of research activity revolved around developing coating materials with very low friction coefficient and high wear resistance. This research activity continues to draw the attention forever because of huge demand for wear resistant materials. Carbon is a most remarkable element with large number of allotropes pays a major role in today's science and technology. It is also used to grow variety of materials starting from nano/ultra nanocrystalline diamond, amorphous carbon, transition metal carbides and carbo-nitrides coatings. All of them attracted a lot of interest due to their superior mechanical properties, low friction coefficient and high wear resistance.[2]

1.1 Historical over view of amorphous carbon

Diamond Like Carbon (DLC) is one among the most studied carbon based coating material for the purpose of friction and wear resistance applications. Historically, the DLC films were first discovered in 1950's by Heinz Schmellenmeier.[3] However, it was brought into limelight after the work of Eisenberg and Chabot in 1970's and continued by a few other research groups.[4] Eventually DLC films gained momentum in late 90's. DLC is more popular because of its ability to mimic the diamond in terms of optical, electrical and mechanical properties.[5] Moreover, DLC has the advantage of room temperature growth in contrast to the high temperatures needed for the growth of diamond which limits the usage as substrate materials to a few.

1.2 Classification of amorphous carbon family

DLC is the solid amorphous carbon network with a mixture of sp^2 and sp^3 bonding. It represents the whole family of amorphous carbon with highly sp^2 bonding (amorphous carbon, a-C) to highly sp^3 bonding (tetrahedral amorphous carbon, ta-C) and their hydrogenated counter parts a-C:H, ta-C:H.[5-8] A ternary diagram of bonding between C-H alloys shown in Fig. **1.1** illustrates the variety of amorphous carbon forms. The hardness of the DLC film compared to diamond and other hard coatings is also showed in Fig. **1.1**

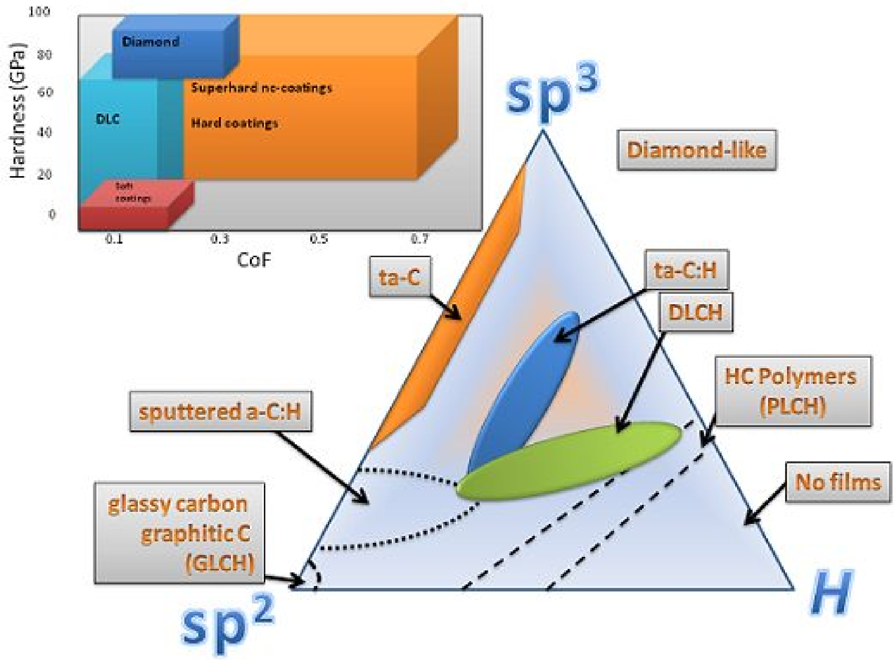

Figure 1.1 Ternary phase diagram of bonding in C-H alloys [9]

The ternary phase diagram consists of three major regions at three corners. The left corner starts with highly sp^2 a-C which is soft and generally known as glass carbon. Hydrogenated a-C:H forms at the intermediate stage while moving from left to right corner. They possess higher sp^3 bonding than a-C films but too soft. These films are generally known as polymeric DLC films. The right extreme does not form any film because the lack of carbon source gas. On the other hand the top corner shows highly sp^3 C-C bonded DLC films known as ta-C which mimic the properties of diamond. The left corner to top corner shows the transition of soft a-C to hard ta-C films. Whereas right most corner to top corner starts with no film to hydrogenated ta-C:H to finally highly hard ta-C. All the four variants differed by the amount of sp^3 bonding and hydrogen content and it is found that no two types of the DLC films have similar physical or chemical characteristics.[5-8] The bonding and hydrogen content governs the physical/mechanical properties of DLC films. DLC films exhibit wide range of bonding from highly sp^2 to highly sp^3 bonding. Hence, bonding can be easily tuned between sp^2 and sp^3 by changing the process parameter. This is one of the important factors behind promoting this material for various technological applications.[5-7] Moreover; the presence of hydrogen also plays a major role in stabilizing the sp^3/sp^2 ratio in a-C films. Hence, controlling of chemical bonding is very crucial because the performance of a-C / ta-C films extensively depends on the bonding nature.[5-7]

1.3 Properties and applications of DLC films

DLC thin films got immense scientific interest due to their exceptional properties. For instance, their high chemical inertness, superior mechanical properties, low friction coefficient, high resistance to wear, high optical transparency and tunable band gap make them potential candidate for countless applications. DLC films find wide range of applications as protective coating on magnetic storage disks, as low friction and wear resistant coating on cutting tools, automobile spares and engine parts**,** as antireflective coating for solar cell and IR windows, as heat sink material for electronic devices, protective coating for miniaturized electromechanical devices (MEMS/NEMS), electroluminescence materials, field emission devices, as gas diffusion barrier coating on PET bottles used for storage of food and beverages, biosensors and biomedical coatings.[10-13] A few exotic areas in which DLC films used are illustrated in Fig. **1.2**.

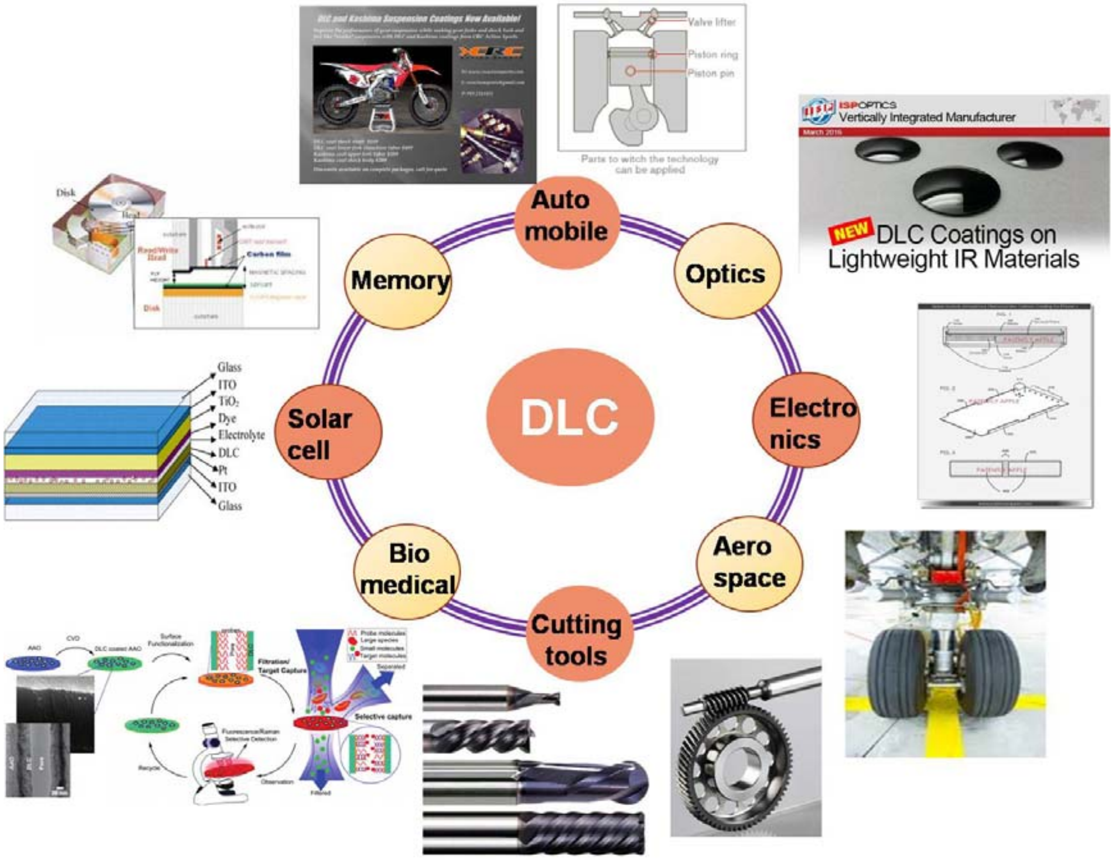

Figure 1.2 Various applications of DLC films [14-21]

1.4 Synthesis techniques and growth mechanism of DLC films

Since, from the discovery, a variety of deposition techniques of both Physical Vapor deposition (PVD) and Chemical Vapor Deposition (CVD) methods have been adopted to grow DLC films. The PVD techniques include magnetron sputtering (DC or RF), pulsed laser deposition (PLD), ion beam deposition and filtered cathodic arc deposition.[2, 5] The CVD techniques include hot filament chemical vapor deposition (HF-CVD), plasma enhanced plasma CVD (PECVD) (RF and DC) and Microwave assisted plasma CVD.[2, 5] Solid graphite is used as target material for growth of DLC through PVD methods, whereas high pure hydrocarbon gases are used in case of CVD methods. Thus the DLC films grown under PVD methods are hydrogen free. On the other hand hydrogen is an inherently inevitable component in CVD grown DLC films. However, hydrogen is an essential constituent of DLC films which helps in stabilizing the sp^3 bonding network and passivates the dangling bonds which in-turn results in lower friction coefficient and wear rates.[6] Thus CVD methods were widely employed for the growth of DLC films because of their advantages in getting ultra smooth and defect free coatings over large areas and of irregular shapes. Among all, the ECR CVD technique gives high density plasma in the range of 10^{12} per cm^3 with narrow ion energy distribution (< 5%) and maximum dissociation efficiency. Additionally, it allows controlling the ion flux and energy independently by means of substrate bias.[22]

A variety of hydrocarbon gases such as acetylene (C_2H_2), methane CH_4, benzene C_6H_6 are tried for the growth of DLC films.[5, 23, 24] Amount of hydrogen content and the growth rate of DLC films vary with the type of gaseous source used for growth. High C/H ratio results in high growth rate and less hydrogen content.[5] On the other hand lower C/H ratio reduces the growth rate and increases the hydrogen content.[5] Moreover, the presence or absence of hydrogen further influences the bonding state and in-turn the mechanical properties of DLC film. However, CH_4 was preferred over other two due to its availability and high pure state which reduces contamination, necessary for electronics applications.[5] Moreover; it also helps in stabilizing sp^3 bonding due to high fraction of hydrogen. This is required for improving mechanical properties. Few studies showed effect of gas composition i.e the amount of dilution with other gases in controlling bonding (sp^2/sp^3 ratio) as well as hydrogen content. This was further extended to find out its influences on the mechanical properties.[25-27] Additionally, it has been reported that dilution of the hydrocarbon source gas with the high pure argon (Ar) and hydrogen (H_2) is also found to influence the growth rate and hydrogen content.[25-30] Dilution with Ar found to increase the film density, sp^3 bonding and hardness due to Ar^+ ion bombardment during growth.[31, 32] This ion bombardment also helps in reducing the hydrogen content in the DLC films. On the other hand DLC films grown in highly hydrogenated plasma containing higher amounts of hydrogen helps in chemically stable films with less dangling bonds. These films possess very low friction coefficients and high resistant to wear.[26, 30]

The key parameter of DLC films is sp^3 C-C bonding which gives the maximum hardness and high film density.[5] In addition to feedstock gas composition many researchers focused on the external growth parameters like ion energy, ion density/flux to find out their role in controlling the chemical bonding of DLC films, especially grown in plasma assisted growth methods.[33-36] Similarly, theoretical modeling studies were also carried out to establish the growth mechanism of the DLC network.[37-40] These studies proposed a growth model named as “subimplantation” growth which emphasizes the role of ion energy in determining the chemical bonding and deciding the quality of the DLC films. This model is based on the physical process and describes the stabilization of sp^3 bonding due to the ion bombardment. It is proposed that the minimum incident carbon ion energy required to stabilize sp^3 bonding is Ep ~30 eV.[37-40] The sp^3 bonding fraction increases with ion energy and reaches a maximum at ~100 eV.[5] In plasma based growth methods the ion energy is tuned by varying plasma source power. In general, external substrate bias is provided to control the ion energy independently, irrespective of the plasma source power. Many studies were carried out to find out the effect of substrate bias on the properties of DLC films and reported the stabilization of sp^3 bonding with increase in substrate bias. Additionally, it is observed that the increase in sp^3 bonding helps in improving the film density. This helps to improve the mechanical and tribological properties.[5]

Two major components are required to grow dense DLC films with high sp^3 content. They are 1) ion energy and 2) gas composition. Almost all the growth methods adopted for synthesis of DLC films involves either high energy species or the ion energy increased by external means (substrate biasing).[5-7] High kinetic energies of the species during growth impose compressive stresses into DLC films.[5] These intrinsic stresses lead to catastrophic failure of these films in both cohesive and adhesive manner during their lifetime. Moreover, high residual stress limits the achievable film thickness. Above the threshold thickness, film buckles and ultimately delaminates from the substrate which further curtails its usage in various applications.[7] Role of thermal stress can be minimized by growing the DLC film at room temperature. Moreover, various approaches have been adopted to grow DLC films for reducing the residual stresses. Among which the most popular ones are thermal annealing and doping/alloying.[41-46] However, thermal annealing is proved to alter the chemical bonding as well as microstructure and thereby deteriorate the physical properties of the films.[41-44] Incorporation of metal or non metals into DLC matrix is found to be the right choice to achieve lower residual stresses and thus improving the film adhesion. Incorporation of wide range of heavy metallic elements namely, Ti, Cr, V, Nb, W, Cu, Al, Ag and Mo and lighter elements Si, S, P, F, O, N and B have been extensively studied.[45-51] Doped /alloyed DLC films exhibited improved properties like thermal stability, bio compatibility, electrical conductivity, wear resistance and ultra low friction coefficient. Among all the non-metallic dopants, nitrogen draws more attention because of its easy availability in ultra high pure gaseous state. Nitrogen doping is an effective way to chemically modify the DLC film due to its electronic structure. It forms C-N bonds and improves their mechanical properties, toughness and film-substrate adhesion.[45- 48] Nitrogen also found to reduce the intrinsic compressive stresses in DLC films. In addition, electrical conductivity of DLC films also improved with nitrogen incorporation.[45- 48] However, high substrate bias and nitrogen doping enhance the amount of C=C sp^2 bonding and leads to formation of graphitic clustering in the films. It can introduce structural inhomogeneity into the DLC films. Usage of DLC films in MEMS/NEMS devices demands ultra thin films with high structural integrity and elastically homogenous. Earlier reports showed that the elastic modulus and hardness have influence on friction coefficient and wear resistance. Friction coefficient is inversely proportional to elastic modulus. It is also reported that film with higher elastic modulus shows lower wear rates. Evaluating elastic properties of such an ultra thin films at nanometer-scale resolution demand specialized characterization tools due to complexity in the film-substrate elastic coupling. Novel tools like nano-indentation, Surface Brillouin light Scattering (SBS), surface wave ultrasonic techniques and Acoustic Force Atomic Microscope (AFAM) are most commonly used to obtain elastic properties of thin films.[52-54]Among all these techniques, AFAM is one of popular tools to measure the elastic modulus quantitatively.

Recent advances in physical and chemical deposition methods allow growth of DLC film with desired sp^2/sp^3 bonding state and hydrogen concentration.[5-7] Tribological properties of DLC films were extensively studied and known for their ultra low friction coefficients. In real time applications, a tribological coating operates at high temperature, high loads and higher sliding speeds. To maintain the efficiency, in the aggressive tribo conditions, the DLC films are useful due to their high thermal conductivity, high hardness, low friction and high wear resistance.[5-7] However, DLC films are known for their tribologically sensitiveness to test atmospheres, due to the presence of chemically susceptible carbon atoms which easily interact with oxygen and moisture.[55, 56] The compressive residual stress in DLC creates the repulsive force between carbon atoms which pushes the free carbon atoms at the surface or defected regions into electronegative state thus enhances the reactivity on exposure to surrounding atmospheres.[57] Depending upon the chemical nature of DLC films and test conditions, these interactions may either enhance or degrade the tribological properties. This is confirmed by the difference in tribological behavior exhibited by the hydrogenated and hydrogen free DLC films.[58] The hydrogenated DLC film possess ultra low friction coefficient and very low wear rates in vacuum and inert atmospheres.[59] Because of the passivation of free dangling bonds by the hydrogen. In oxygen rich environments, a-C:H films get oxidized due to tribo chemical interactions. This forms a covalent bonding at the sliding interface resulting in high friction coefficient and high wear rates.[60] On the other hand, hydrogen free DLC film showed low friction coefficient and wear rate in humid atmosphere.[59] This is because of the saturation of dangling bonds by oxygen and OH groups due to dissociation of water in humid environments. In vacuum or inert atmospheres, friction and wear rate increase due to interaction of dangling bonds of sliding surfaces.[56]

A few theoretical studies were carried out to find out the tribo chemical interactions in different testing environments. A charge transfer concept was used to explain the friction behavior and wear rates of DLC films. Absorbed oxygen react with C-H bonds and forms C-

O-H and COOH in humid or oxygen medium.[56] In such cases, the surface becomes more electronegative due to the charge transfer from the C and H to O atoms.[61] Hence, the increase in oxygen content decreases the electrostatic repulsive interaction between the surfaces which in turn destroy the low friction behavior. On the contrary humidity enhances adhesion due to capillary force persists between the film surface and ball, causing an increase in friction coefficient. The humidity level decreases in the inert medium which could be correlated with the extremely low friction coefficient and wear rate in hydrogenated DLC film. Apart from humidity, the wear induced electrostatic charge on both film surface and alumina ball causes strong repulsion. This repulsive force reduces the shear strength of the contact that acts to lower the friction coefficient and wear rates.[49]

However, the external parameters like sliding counter bodies, applied load and sliding speed also influence the frictional behavior of the DLC films.[62-70] The results show significance of chemical and mechanical nature of sliding interfaces which influence friction behavior of DLC films.[71] Such films for machine applications must withstand high loads and high sliding speeds where the phase stability and deformation resistance are the key issues. Interfacial shearing may cause oxidation of contact interfaces. Mainly, at high sliding speeds, the chemical stability of the film degrades due to surface oxidation and this causes deformation in sliding interfaces resulting in less wear resistance.[68] Chemical stability of a DLC film is governed by shear induced graphitization due to mechanical energy and passivation of the dangling bonds caused by hydrogen and oxygen atoms/molecules.[64, 66, 67] Most of the work describes that low friction in DLC film is contributed by graphitization.[64–67] However, this matter is largely debated and discussed whether graphitization or passivation is dominating factor to explain low friction behavior in DLC film.[67, 68] On the other hand, in view of contact mechanics, applied normal load would be a crucial parameter for tribological behavior. A few recent reports discussed the friction and wear properties in the context of deformation governed by normal load.[68, 69, 72, 73] Liu *et al*. showed the effect of various counter bodies on DLC film and found that the wear rate mainly depends on the contact stress generated by the counter body.[74] This study proved that the physical properties of the counter body are more important than the chemical reactions and testing environment. Studies on hydrogenated DLC films against Si_3N_4 and Al_2O_3 in vacuum showed that the lower friction is observed against later than the former.[75] Recent findings showed that stainless steel ball used against DLC film get oxidized in humid environment and no signature of oxidation was seen in dry air or oxygen medium.[60] This is due to the formation of electrochemical galvanic corrosion cell by the tribo chemical interactions.[60] The mass spectroscopy analysis of evolved gases during tribology studies of DLC films showed the signature of CO_2 formation in dry air and hydrocarbon or carboxyl groups while testing under humid environment.[57] These studies emphasis the significance of the understanding of the tribo chemical interactions occurred during tribo testing of DLC films.

In general DLC films are prone to oxidation on exposure to ambient or oxygen environment. However, the oxidation phenomenon of DLC is more complex. Many studies proved that the absorbed oxygen plays a crucial role in deciding the friction coefficient of DLC films.[76-80] It shows that in addition to parameters discussed above some other importance factors such as absorbed oxygen, surface chemistry and surface roughness are also proved to be strong contenders for controlling friction behavior of DLC films.[76-80] In general DLC films are known for their sensitive friction behavior. Because DLC film surface either left with free dangling bonds or saturated with the hydrogen atoms/molecules, depends on the type of

DLC films and growth process.[71, 56] Due to unique covalency of carbon atoms in *sp*^{2} and *sp*^{3} hybridized state, the DLC films with dangling bonds easily interacts with reactive gases and water vapor.[56] Tuning the surface chemistry and passivating unsaturated dangling bonds to avoid adhesive covalent interaction between mating parts and further reduce the friction and wear is of scientific importance. Recent studies on molecular level interaction of DLC films showed that surface reactivity is mostly controlling the friction behavior and hydrogen terminated DLC films possessed ultra low friction coefficient.[49, 81-84] Molecular dynamics and quantum chemical calculations carried out by Shandan Bai *et. al.* showed that fluorine terminated DLC films results in lower friction coefficient than the hydrogen terminated ones due to higher electronegativity of fluorine which alters the surface charge of DLC films.[84] However, controlled experimental studies are needed to support these theoretical models and to find out the practicality of such controlled studies. Plasma treatment of DLC films is found to be an effective method to alter the surface chemistry in a controlled manner to get terminated surface with desired surface reactivity required to tune the wettability characteristics.[85, 86] Surface wettability is one of the important factors to control the friction of DLC surface.

Till date, majority of research studies on DLC films are explored only for their mechanical properties.[2, 5, 9] Recently, the focus is shifted towards the surface modification methods for specialized applications such as self cleaning and super hydrophobic surface for anti fogging.[87-89] All these characteristics are derived from surface chemistry of the films. DLC films are ideal for bio transplants because of its biocompatibility and chemical inertness that prevent side effect in cell growth.[90] Mechanical stability, anti corrosion and anti wear in bio-aqueous medium are important properties of these films for sustainable functionality in bio environments.[91] Increasing demand for DLC films in bio-medical devices and bio-sensors have grown due to its unique tunable wetting characteristics derived by surface chemical modification.[92-94] Developing DLC/diamond films with desired wettability characteristics in the range of hydrophilic to super hydrophobic is highly demanded for wide range of applications. Wettability is an essential property of materials and is influenced by both surface chemistry as well as surface topography.[95] It in-turn alters the surface energy to achieve desirable wetting characteristics. Generally the energy of diamond surfaces is tuned by hydrogenation, oxidation and surface termination by functional groups.[91, 86] This basically works on the principle of modified reconstruction and termination of dangling bonds. However, the long term sustainability of these surfaces in fluidic media is not reliable. Surface modification through doping is the other important method to modify the surface chemistry and bonding aspects.[86,93] Doping with atomic species alters bonding configurations and it reconstructs the surface chemistry.[49, 91] On the other hand hierarchical structures created by micro or nano texturing on surface also alters the wetting characteristics of the materials.[96] Advanced lithography techniques are useful in pattering nanostructures on the surface to play with the surface energy. However, they are expensive and involve complex processing methods.[97] Plasma etching is another promising method to modify the surface both physically and chemically, which creates hierarchical rough surface of high energy that further enables functionalization of surface.[86, 96,98] Maskless pattering array of nano rods or needle like structures on diamond surfaces by plasma etching is quite a relevant technique.[86] Plasma treatment of DLC films is an useful method to modify the surface chemistry for desired wetting characteristic. Wetting characteristics of plasma exposed DLC films is decided by the type of gases, plasma energy and time of exposure.

Earlier studies showed that plasma exposed DLC films get functionalized with hydroxyl, carboxylic, carbonyl and nitrile groups which in-turn influence the wetting characteristics.[85, 98] The super hydrophobic and hydrophilic characteristic of the DLC surfaces extend its applications into textile industry to develop both highly wetting as well as highly water repellent clothes.[85] This gives potential features like ultra fast drying and self cleaning of the fabric used for medical applications. Detailed analysis of microstructure and surface chemistry is significant towards understanding the wetting characteristics of plasma exposed films.

1.5 Motivation and Research objectives

In recent times, DLC has emerged as most renowned wear resistant coating material and has become a part of several appliances. However, modernization demands multifunctional devices in miniaturized form where DLC films with versatile properties come handy. Therefore, it brings an opportunity to have a relook into this amazing material for tailoring the properties suitable for these applications. Although plentiful scientific reports on various aspects of the DLC films are readily available, certain scientific aspects are yet to be addressed. A few studies have focused on detailed analysis of the wear tracks to establish the mechanism responsible for ultra low friction coefficient. Not many studies are found in the areas of tuning surface chemistry by functionalization or passivation towards achieving superior tribological properties. Tuning surface energy of DLC films is an important concern in tribology and biomedical implants. Plasma exposure conditions need to be optimized to achieve superior properties for the above applications.

The present study is mainly focused on to the tribological properties of chemically modified DLC films. Tetrahedral sp^3 dominated ultra-smooth hydrogenated DLC films were prepared using ECRCVD technique by optimizing the feed stock gas composition and substrate bias. Laser Raman spectroscopy was extensively used to study the variation in chemical structure. Rutherford Back Scattering (RBS) and Elastic recoil Detection Analysis (ERDA) were employed to measure the elemental composition, film density and hydrogen content, respectively. Surface chemistry and absorbed oxygen content were obtained by X-ray Photo Electron Spectroscopy (XPS) and correlated with the friction behavior of these films. In situ nitrogen doping was carried out to enhance the wear resistance. Elastic modulus mapping was carryout by AFAM to find the variation in local indentation modulus due to change in chemical bonding at high substrate bias and high nitrogen concentrations. Quantitative modulus was also calculated from the contact resonance curves using established theories. The observed elastic inhomogenity induced by bias and nitrogen doping provided a microscopic evidence for the graphitic clustering discussed by the established “subimplantation” growth model of DLC films. The elastic modulus mapping across the wear track using AFAM technique was carried out to substantiate the role of graphitization phenomenon in controlling the ultra low friction coefficient of DLC films. Tribo tests were carried out under various gas mediums such as Ar, N_2, O_2, CH_4, to study the possible tribo chemical interactions. Controlled surface reconstruction of DLC films was carried out by post growth exposure of the films to variety of plasmas (H_2, N_2 and O_2) as a function of time and ion energies to tune the wetting characteristics. Influence of altered micro structure and surface chemistry on wetting characteristics of plasma exposed DLC films was studied. The variation in friction behavior and wear rates due to plasma exposure was also correlated with surface chemistry.

1.6 References

1. K. Holmberg *et al., Tribol. Int.* **2012**, 47, 221.
2. A. Erdemir and C. Donnet, *J. Phys. D: Appl. Phys.* **2006**, 39, R311.
3. H. Schmellenmeier, *Exp. Tech. Phys.* **1953**, 1, 49.
4. S. Eisenberg and R. Chabot, *J. Appl. Phys.* **1971**, 42, 2953.
5. J. Robertson, *Mat. Sci. Engg.* **2002**, R 37, 129.
6. A. Grill, *Diamond Relat. Mater.* **1999**, 8, 428.
7. Y. Lifshitz, *Diamond Relat. Mater.* **1999**, 8, 1659.
8. A. C. Ferrari and J. Robertson, *Phil. Trans. R. Soc. Lond. A* 2004, 362, 2477.
9. C. A. Charitidis, *et al., Lubricants* **2013**, 1, 22.
10. W. S. Choi, *et al., Mater. Lett.* **2008**, 62, 577.
11. N. Dwivedi, *et al., J. Appl. Phys.* **2012**, 111, 014908.
12. D. S. da Silva, *et al., J. Appl. Phys.* **2011**, 110, 043510.
13. E. Rismani, *et al., J. Appl. Phys.* **2012**, 111, 084902.
14. C. Casiraghi, *et al., Materials Today* **2007**, 10 (1–2), 44.
15. http://racetechtitanium.com/category/racetech-news/page/2/.
16. https://www.highpowermedia.com/blog/3103/dlc-for-pistons.
17. https://jm.linkedin.com/topic/dlc.
18. M. Aramesh, *et al., Nano Scale* **2015**, 7, 5998.
19. http://www.dpaonthenet.net/article/49987/New-Diamonex-diamond-like-carbon-coating-for-the-aerospace-industry.aspx
20. http://www.nissan-global.com/EN/TECHNOLOGY/OVERVIEW/dlc.html
21. Zadesky, *et al., U.S.A patent* **2013**, US 2013/0128462 A1.

22. S.I. Hosseini, *et al.*, *Thin solid Films* **2011**, 519, 3090.

23. A. Erdemir, *et al.*, *Surf. Coat. Technol*. **1999**, 120 –121, 589.

24. A. Erdemir, *et al.*, *Diamond Relat. Mater.* **2000**, 9, 632.

25. D. Caschera, *et al.*, *Thin Solid Films* **2011**, 519, 4087.

26. Y. Jeng, *et al.*, *Thin Solid Films* **2013**, 529, 301.

27. J. Libardi, *et al.*, *Thin Solid Films* **2004**, 459, 282.

28. G. Cicala, *et al.*, *Surf. Coat. Technol.* **2004**, 180 –181, 222.

29. G. Cicala, *et al.*, *Diamond Relat. Mater.* **2004**, 13, 1361.

30. A. Erdemir, *et al.*, *Surf. Coat. Technol.* **2000**, 133 –134, 448.

31. J. Zhou, *et al.*, *Plasma Sources Sci. Technol.* **2006**, 15, 714.

32. Y. H. Liu, *et al.*, *Surf. Coat. Technol.* **2006**, 200, 5819.

33. M. Moseler, *et al.*, *Science* **2005**, 309, 1545.

34. S. F. Yoon, *et al.*, *J. Appl. Phys.* **2001**, 89 (9), 4830.

35. L. Martinu, *et al.*, *J. Vac. Sci. Technol. A* **1994**, 12 (4), 1360.

36. Q. Zhang, *et al.*, *J. Appl. Phys.* **1998**, 84, 5538.

37. S. Uhlmann and T. Frauenheim, *Phys. Rev. Lett.* **1998**, **81** (3), 641.

38. K. Kohary and S. Kugler, *Phys. Rev .B* **2001**, 63, 193404.

39. M. Kaukonen and R. M. Nieminen, *Phys. Rev. B* **2000**, 61 (4), 2806.

40. H.P. Kaukonen and R. M. Nieminen, *Phys. Rev. Lett.* **1999**, 68 (5), 620.

41. H. Li, *et al.*, *Thin Solid Films.* **2006**, 515, 2153.

42. A. C. Ferrari, *et al.*, *J. Appl. Phys.* **1999**, 85(10), 7191.

43. T. A. Friedmann, *et al*., *Appl. Phys. Lett.* **1997**, 71 (26), 3820.

44. R. Kalish, *et al.*, *Appl. Phys. Lett.* **1999**, 74 (20), 2936.

45. D. Bootkul, *et al.*, *Appl. Surf. Sci.* **2014,** *310*, 284.
46. S. E. Rodil, *et al.*, *Phys. stat. sol. A* **1999**, 174, 25.
47. M. Kaukonen, *et al*., *Phys. Rev. Lett.* **1999**, 83 (25), 5346.
48. M. K. Fung, *et al.*, *Diamond Relat. Mater.* **1999**, 8, 472.
49. L. Zhang, *et al.*, *RSC Adv.* **2015**, *5*, 9635.
50. Z. Wu, *et al.*, *Appl. Surf. Sci.* **2012**, 258, 7918.
51. M. Kaukonen, *et al.*, *Appl. Phys. Lett.* **2005**, 87, 251918.
52. R. Pastorelli, *et al.*, *Diamond Relat. Mater.* **2000**, **9**, 825.
53. C.A. Charitidis, *Int. J. Refr. Met. Hard Mater.* **2010**, 28, 51.
54. M. Muraoka and S. Komatsu, *Nanoscale Res. Lett.* **2011**, **6:33**, 1.
55. J. A. Heimberg, *et al.*, *Appl. Phys. Lett.* **2001**, 78, 2449.
56. J. Andersson, *et al.*, *Wear* **2003**, 254, 1070.
57. X. Wu, *et al.*, *Tribo. Lett.* **2015**, 57 (5), 1-7.
58. H. Ronkainen and K. Holmberg, *Tribology of Diamond-Like Carbon Films. New York (USA): Springer*, **2008**, 158.
59. H. Ronkainen, *et al.*, *Wear*, **2001**, 249, 260.
60. A. Alazizi, *et al.*, *Langmuir* **2016**, 32, 1996.
61. S. Dag and S. Ciraci, *Phys. Rev. B* **2004**, 70, 241401.
62. H. Meerkamm, et al., *Int. J. Refr. Met. Hard Mater.* **1999**, 17, 201.
63. A. M. Pfupfu, *et al.*, *Diamond Relat. Mater.* **2011**, 20, 1143.
64. Y. Liu, *et al.*, *Surf. Coat. Technol.* **1996**, 86–87, 564.
65. Y. Liu, *et al.*, *Surf. Coat. Technol.* **1996**, 82, 48.
66. A.A. Voevodin, *et al.*, *Diamond Relat. Mater.* **1996**, 5, 1264.

67. C. Longchen, *et al., Carbon* **2014**, 66, 259.

68. D. W. Kim, *et al., Wear* **2013**, 297, 722.

69. M. Tian-Bao, *et al., Sci. Rep.* **2014**, 4, 3662.

70. B. Lichun, *et al., J. Appl. Phys.* **2011**, 110, 33521.

71. A. Erdemir, *Surf. Coat. Technol.* **2001**, 146 –147, 292.

72. X B Yan, *et al., J. Phys. D: Appl. Phys.* **2004**, 37, 2416.

73. S. Kaciulis, *Surf. Interface Anal.* **2012**, 44, 1155.

74. X. Liu, *et al., Wear* **2012**, 292–293, 124.

75. R. Zhang, *et al., RSC Adv.* **2015**, 5, 32690.

76. A. Erdemir, *Tribo. Int.* **2004**, 37, 1005.

77. S. J. Park, *et al., Diamond Relat. Mater.* 2003, 12, 1517.

78. C. Donnet, *et al., Surf. Coat. Technol.* **1994**, 68 – 69, 626.

79. C. Donnet and A. Grill, *Surf. Coat. Technol.* **1997**, 94 – 95, 456.

80. J. Fontaine, *et al., Surf. Coat. Technol.* **2001**, 146 – 147, 286.

81. A. R. Konicek, *et al., Phys. Rev. B* **2012**, 85, 155448.

82. M.I. D. B. Bouchet, *et al., J. Phys. Chem. C* **2012**, *116*, 6966.

83. Y. N. Chen, *et al., J. Phys. Chem. C* **2015**, 119, 16148.

84. S. Bai, *et al., J. Phys. Chem. C* **2012**, 116, 12559.

85. D. Caschera, *et al., Langmuir* **2013**, 29, 2775.

86. S. Tian, *et al., Langmuir* **2014**, 30, 12647.

87. R. Blossey, *Nature Materials* **2003**, 2(5), 301.

88. N. R. Chio, *et al., Nature Nanotechnology* **2007**, 2, 354.

89. S. Meng, *et al., Phys. Rev. Lett.* **2006**, 97, 036107.

90. R. K. Roy and K. R Lee, *J. Biomed. Mat. Res. B Appl. Biomater.* **2007**, 83(1), 72.

91. J. W. Yi, *et al.*, *Langmuir* **2010**, 26 (22), 17203.

92. M. K. Kuntumalla, *et al., J. Phys. Chem. Chem. Phys.* **2015**, 17, 21331.

93. F. Liu, *et al.*, *ACS Nano* **2010**, 4 (5), 2643.

94. H. Zhuang, *et al., J. Phys. Chem. C* **2010**, 114, 20207.

95. B. Cortese and H. Morgan, *Langmuir* **2012**, 28, 896.

96. Y. Rahmawan, *et al.*, *Langmuir* **2010**, 26 (1), 484.

97. M. Karlsson, *et al.*, *Langmuir* **2010**, 26 (2), 889.

98. S. R. Polaki, *et al.*, *Tribol. Int.* **2015**, 81, 283.

The present chapter describes the detailed experimental procedure followed in growth and characterization of the DLC films. The experimental work starts with thorough substrate cleaning and loading into the vacuum chamber of Electron Cyclotron Resonance Chemical Vapor Deposition (ECR-CVD) system in which DLC films were grown. The growth methodology started with choosing argon (Ar), methane (CH_4) gases as dilution and process gases, respectively. The compositional variation and tuning of process parameters were rigorously varied to obtain optimum growth rate. The growth process further extended to the *in-situ* nitrogen doping of these films.

A variety of characterization tools were employed for detailed analysis of physical and chemical structure of the DLC films. Field Emission Scanning Electron Microscopy (FESEM) and Atomic Force Microscopy (AFM) were employed to obtain morphology, growth rate and rms roughness of these films. Visible laser Raman spectroscopy is extensively used to analyze the variation in chemical structure as a function of process parameters. X-ray Photo electron Spectroscopy (XPS) is deployed to evaluate the elemental characterization and bonding state of the carbon (sp^2 or sp^3) in these films. The film density and hydrogen content of films were obtained using Rutherford Backscattering (RBS) and Elastic Recoil Detection Analysis (ERDA). The influence of growth parameters on the chemical bonding of film was studied. This aspect was correlated with the friction and wear properties of films. Wetting characteristics of the plasma exposed DLC films with water is also carried out.

2.1 Growth techniques

2.1.1 Substrate cleaning

DLC films were grown on single crystal Si (100) wafer. The growth process starts with the cleaning of the substrate to avoid contamination. Firstly, Si wafer into 25 × 25 mm size pieces by mechanically cleaving. The Si substrates dipped into de ionized water and sonicated for 10 mins. Then the Si wafer took out from the beaker and dried with hair drier. The dried Si wafer dipped in absolute alcohol and sonicated again for 10 mins and then dried.

2.1.2 Electron Cyclotron Resonance Chemical Vapor Deposition (ECR-CVD) setup

The DLC films for this thesis work were grown using ECR-CVD system. The ECR ion source was first proposed by R. Geller in late 1960's for the purpose of fusion plasma studies, since then it has been widely utilized in a variety of research areas ranging from atomic and nuclear physics to material sciences.[1] ECR ion sources have unique capability of producing highly charged ion beams, because of which they become increasingly popular in heavy-ion accelerators. The ECR ion sources in operation nowadays adopt a minimum-**B** (magnetic field) configuration for the confinement of ECR plasma and commonly uses single-frequency microwave with a narrow bandwidth.[2] Electron cyclotron resonance is a phenomenon observed both in plasma and condensed matter physics. ECR involves transfer of energy from microwave to electrons when the electric field of externally launched microwaves is in phase with the gyro frequency of electrons. This is widely known as resonance condition and occurs under an applied magnetic field.[1-5] An electron in a static and uniform magnetic field revolves in a circular motion due to the Lorentz force. The circular motion superimposed by a uniform axial motion and result into a helical motion. The angular frequency ($\omega = 2\pi f$) of cyclotron motion for a given magnetic field strength B is

$$\boldsymbol{\omega = eB/m} \qquad (2.1)$$

where e is the elementary charge and m is the mass of the electron.

Various deposition techniques were employed for the synthesis of DLC thin films. Among all the methods, ECR-CVD is the most preferred technique because it gives high plasma density, larger deposition area, superior electron temperatures, presence of multivalent ions, flexibility in operating at lower pressures, Moreover, ECR CVD doesn't consist of any electrodes which enable to maintain the substrate at a desired voltage, which in turn helps to tune the ion flux density and ion energy independently. [3-5]

The ECR CVD mainly consists of

- Vacuum systems
  Rotary pump: 350 lit/min (for both roughing and backing)
  Turbo molecular pump: 1100 lit/s
- Vacuum chamber
  Process chamber: 150 mm dia., 200 mm height
  Deposition chamber: 54 cm dia., 64 cm height
- Plasma source
  Microwave generator: 2.45 GHz, Max 1200 Watt
  Electro magnet: 875 gauss

The microwave generator used in the present study is a magnetron type of source. Schematic representation of the ECR CVD is illustrated in Fig. **2.1**. The microwave generated at the source reaches to the processing chamber via circulator, traverse inside rectangular wave guide and finally passes through dielectric window. The circulator is connected mainly to protect microwave source from the reflected waves. Once the microwave enters into the rectangular wave guide it converts into rectangular mode. The rectangular wave guide consists of 3 stub tuners to tune wave form of the microwave it in-turn reduces the reflecting power. A water cooled antenna located at the end of the wave guide converts the microwave into circular mode and pushes it into the process chamber through a quartz window. The process chamber is the resonance zone where the energy transfer takes place between microwave and stray electrons. A tunable electro magnet sits over the process chamber to get 875 gauss magnetic field required for creating resonance condition. The energized electrons further contribute towards the plasma generation. The plasma further extends to the deposition chamber due to the spread of divergent magnetic field and helps for the film growth.

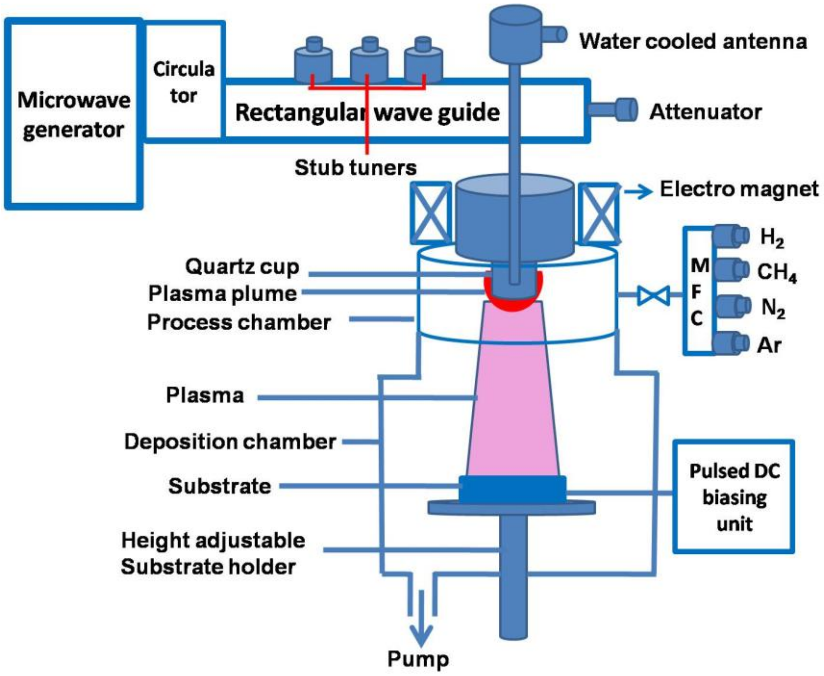

Figure 2.1 A schematic of ECR –CVD system used for growth of DLC films

2.1.3 Process conditions for the film growth

After loading the cleaned and dried Si wafer into ultra high vacuum chamber it was evacuated to rough vacuum $5x10^{-3}$ mbar pressure. Thereafter the chamber is further evacuated to high vacuum upto $2x10^{-6}$ mbar using a turbo-molecular pump backed by mechanical pump. Followed by purging the chamber with high pure Ar (99.999 %) to reduce the oxygen partial pressure and avoid contamination of the films. This process was repeated for minimum 2 times. Thereafter mixture of high pure Ar and CH_4 were leaked into the chamber and taken it to $5x10^{-3}$ mbar pressure. Plasma is strikes by switching on the microwave generator and electro magnet. Once the plasma seems stable pulse DC biasing was given to the substrate and maintained it at a desired potential for the film growth.

2.2 Characterization techniques

2.2.1 Field Emission Scanning Electron Microscopy (FESEM)

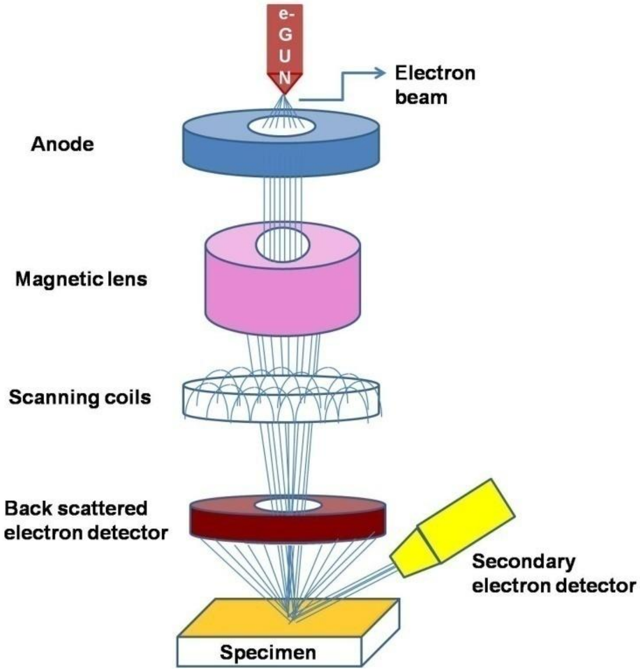

Figure 2.2 A schematic of Field Emission Scanning Electron Microscopy (FESEM)

FESEM is a powerful imaging technique idle for imaging morphology and to measure the film thickness. In principle, electrons were extracted from a sharp tip of the filament by applying very high voltages. These emitted electrons get focused by electromagnetic condenser lens to form a sharp electron beam with a narrow energy spread. A schematic representation of FESEM is illustrated in Fig. **2.2**. The focused electron beam is used to raster on the material surface to get the morphology. The possible emission characteristics upon interaction of incident electron beam with matter are shown in Fig. **2.3**. Secondary electrons (SE) and back scattered electrons (BSE) are used to analyze by corresponding detectors for obtaining morphology.[6]

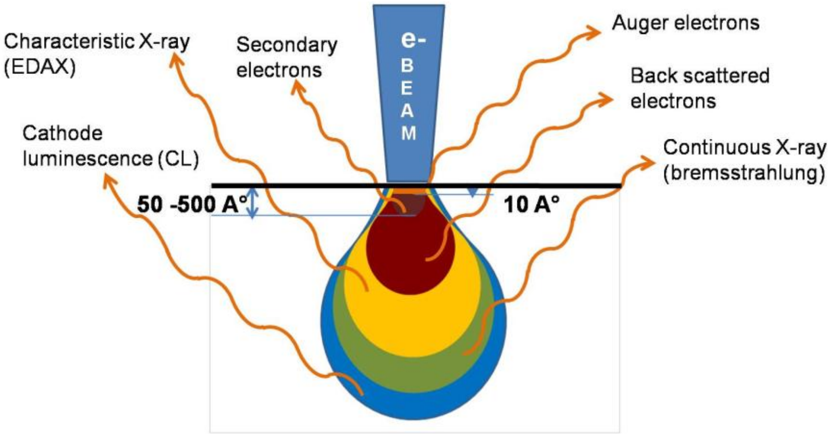

Figure 2.3 Probable emissions during electron beam interaction with material surface

In addition to morphology the back scattering electrons gives Z contrast also, which is useful for mapping of different phases. FESEM system consists of field emission gun, SE and BSE detectors. In this study we used FESEM to obtain the morphology and film thickness of the DLC films. Additionally we used FESEM for the wear track analysis after tribology tests at different conditions. Wear tracks widths were measured which is important parameter to calculate the wear rate. We have used FESEM to evaluate the post deformation analysis of the wear tracks in the DLC films. Apart from this, the film thicknesses were also measured using cross section FESEM imaging of the freshly cleaved edge of DLC/Si system.

2.2.2 Scanning Probe Microscopy (SPM)

Since its invention by Binning in 1986 the Scanning Probe Microscopy emerged as a powerful imaging tool with sub nanometric spatial resolution.[7] It works on the principle of the force distance relation between the probe and material surface. This is a versatile technique with various modes like electrical, magnetic, friction force and acoustic force.[8] Moreover, the SPM imaging is a non destructive method and it can be used to probe insulators, semiconductors and conducting materials too. Atomic force microscope probes materials surface with a sharp tip, of few micron length often 30 to 50 nm radius of curvature. The tip is attached to a free end of a hanging cantilever with few hundred microns length and fixed at the other end.

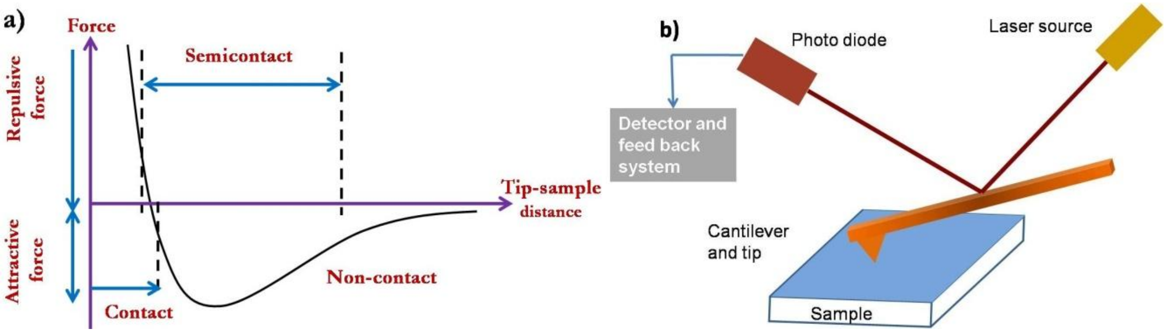

Figure 2.4 A schematic representation of a) force displacement curve of tip and sample and b) Atomic Force Microscope (AFM)

A micro fabricated cantilever with optical lever detection makes it possible to measure the applied force in terms of deflection. As the tip approaches close to the sample surface the interaction of forces between tip and sample cause deflection of the tip. The force distance curve shown in Fig. **2.4 a)** indicate range of attractive to repulsive force regime experienced by the tip while brings in contact with the sample surface with a constant load. In AFM measurements vertical/lateral elastic forces, adhesion force and friction force operates between tip and sample.[9] A photodiode detector with a focused laser beam on the back side of the cantilever measures the deflection of the tip. The schematically representation is shown in Fig. **2.4 b)**. The tip deflections are further processed to generate the topography map of sample surface. Acoustic Force mode is a used to map the variation in local elastic modulus (E) at nano scale. A multi mode scanning probe microscope (Ntegra Aura, M/s. NT-MDT, The Netherlands) was used to carry out AFAM measurements. Silicon cantilevers having force constant of 20 N/m and length of about 250 microns were used for the study. In

AFAM setup, the sample is coupled to a piezoelectric transducer which produces longitudinal mechanical waves that cause out-of-plane vibrations in the sample's surface. The sample's vibrations cause the AFM cantilever to resonate at contact resonance frequency (CRF). Under this condition, there are two different forces acting on the AFM tip viz. sample - tip interaction by van der walls forces and cantilever vibrations. While the former one is used for obtaining topography. Whereas the elastic properties of the unknown materials were meaured using the cantilever vibrations.**[10]** The CRF of the cantilever depends on the stiffness of tip-sample contact and on the contact radius. The tip-sample contact stiffness depends on the Young's modulus of the sample and the tip, the load exerted by the tip and the geometry of the surface.**[9-12]** Thus, AFAM can be used to determine the Young's modulus of materials from the contact stiffness when the cantilever properties are known.

According to Hertzian contact model for elastic deformation, contact stiffness (k*) of a hemispherical indenter with contact radius of R on a flat surface with a force F_c can be expressed as **[11, 12]**

$$k^* = \sqrt[3]{6RF_C E^{*2}} \qquad (2.2)$$

where E* is the reduced modulus, and can be expressed as

$$\frac{1}{E^*} = \frac{1-\nu_t}{E_t^*} + \frac{1-\nu_s}{E_s^*} \qquad (2.3)$$

E_t, υ_t, E_s, υ_s are modulus and Poisson ratio of tip and sample respectively. According to equation 1, the radius of curvature of the tip is an important factor in estimation of elastic modulus but it is not constant during measurements due to wearable nature of tip. In addition, it is also difficult to measure exact radius of the tip. The uncertainty in the measurement of R creates a large error in calculated elastic modulus. In order to avoid such error, it is believed that a calibration on a reference sample can substitute the characterization of cantilever parameters. Further, the AFM tips are allowed to scan several cursory measurements so that the tip loses its sharpness and does not wear further during AFAM measurements. The cantilever vibration mechanics can be solved numerically by several methods to calculate the elastic modulus of unknown materials. According to a simplified point mass model, in which elastic clamp is fixed at one end and the other end is with a point mass. Then, the contact stiffness of the coupled system can be written as [11]

$$f_s = \sqrt{k_s^* + k/m} \qquad (2.4)$$

Where f_s is the contact resonance frequency of the sample, k_s^* is the effective tip-sample contact stiffness, k is the spring constant of the cantilever and m is the equivalent mass in point mass model. AFAM measurements on a sample with known contact stiffness (k_s^*) and CRF (f_s), allows to calculate the contact stiffness on a given sample by

$$\boldsymbol{k_s^*} = \boldsymbol{k_{ref}^*}\left(\frac{\boldsymbol{f_s^2} - \boldsymbol{f_0^2}}{\boldsymbol{f_{ref}^2} - \boldsymbol{f_0^2}}\right) \qquad (2.5)$$

Where k_s^* and k_{ref}^* are the contact stiffness of the unknown sample and reference material respectively. The f_s , f_{ref} and f_0 are the resonance frequency of the cantilever in contact with sample, reference material and free vibrations in air respectively. The relation between elastic modulus and contact stiff is represented as [9, 11]

$$\boldsymbol{E_s^*} = \boldsymbol{E_{ref}^*}\left(\frac{\boldsymbol{k_s^*}}{\boldsymbol{k_{ref}^*}}\right)^{\boldsymbol{n}} \qquad (2.6)$$

where n=1 for flat surface. After calculating stiffness constant on reference and unknown sample, elastic modulus on the unknown sample can be calculated using equation 5 by assuming the elastic modulus of reference sample. For the present study, we take Si (100) as reference sample and its modulus value of 170 GPa was used for calculation.

2.2.3 Raman spectroscopy

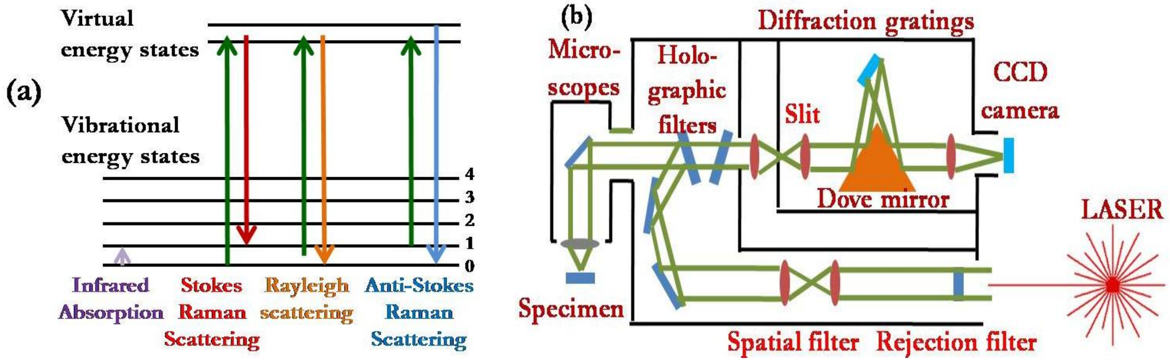

Figure 2.5 Schematic view of a) excitation process and b) instrumentation setup

Laser Raman spectroscopy is an unique non destructive technique to investigate the chemical structure of materials. It is also use to analyze defect and disorder in the materials.[13-16] Raman spectroscopy works on the principle of interaction of light with materials. When an incident light beam with an energy of $h\nu_0$ (h = plank constant, ν_0 = frequency of light) interacted with a material surface, it gets scattered either by elastic or inelastic manner, as shown in Fig. **2.5 a)**. Where the elastic scattering is known as Rayleigh scattering and it has the highest probability of occurring. On other hand inelastic scatterring with a difference in vibrational energy by $\pm h\upsilon_s$. The Raman scattering with loss of energy $h\nu_0 - h\upsilon_s$ known as Stokes line and gain in energy $h\nu_0 + h\upsilon_s$ known as Anti Stokes. For being a Raman active, the molecules should undergo change in polarizability during the vibration. A schematic representation of Raman Spectroscope is given Fig. **2.5 b)**. Raman spectroscopy has been extensively used to analyze the carbon based materials both crystalline such as graphite, diamond and a-C.[13] It is known the a-C is a mixture of disorder sp^2 (graphitic) and sp^3 (diamond like) bonding states and properties of this material varies with the ratio of sp^2/sp^3 bonding. Numerous studies are available on Raman spectroscopy investigations of DLC films to find out the amount of a-C, graphitic (sp^2) or diamond (sp^3) phase existing in the films A detailed Raman analysis of various DLC films has been discussed in subsequent chapters. In this study inVia micro-Raman spectrometer (Renishaw, UK) was used. Major components of this instrument is given below

- Excitation Source: Ar^+ laser with 514.5 and 488 nm excitation wavelengths
- Sample illumination through Leica microscope equipped with 10×, 20×, 50× and 100× objective lenses.
- Diffraction gratings: 1800 grooves/mm for the monochromatization of scattered signal
- Thermoelectric cooled CCD for detecting the signal in backscattering configuration

Throughout the thesis work Raman spectroscopy analysis was carried out with the laser power of 3 mW to avoid any heating and further damage of the samples. WIRE 3.2 software is utilized for fitting and extracting the data from Raman spectra. The Raman bands are fitted with both Gaussian and Lorentzian peaks after background subtraction.

2.2.4 X-ray Photo Electron Spectroscopy (XPS)

X-ray Photo Electron Spectroscopy (XPS) also known as Electron Spectroscopy for Chemical Analysis (ESCA) is a powerful quantitative spectroscopic technique to analyze elemental composition, chemcial bonding state and electronic state of the materials. It is highly surface sensitive with an average depth resolution upto 5 nm. It can be applied to characterize all variety of materials such as inorganic compounds, metal alloys, semi conductors, polymers, glass and bio materials. XPS is capable to detect all the elements starting from lithium (Li) with atomic number 3 and above. Detection limits up to parts per million (ppm) is possible. XPS analysis carried out by exciting the sample by a mono chromatic X-ray source (Al Kα) and an electron analyzer is used to measure the energy of the emitted photo electrons. XPS plot comprised of number of photo electron detected (on y axis) and binding energy (eV) (on x axis). Each element gives it characteristic XPS peaks at characterstic binding energy values. The schematic given in Fig. **2.6** illustrates emission process of the photo electron with a kinetic energy of E_k is given by

$$\boldsymbol{E_k = h\vartheta - E_b - w} \qquad (2.7)$$

Where h_ϑ is the energy of photons, E_b is the binding energy of the atomic orbital from which photoelectron emitted and W is the spectrometer work function.

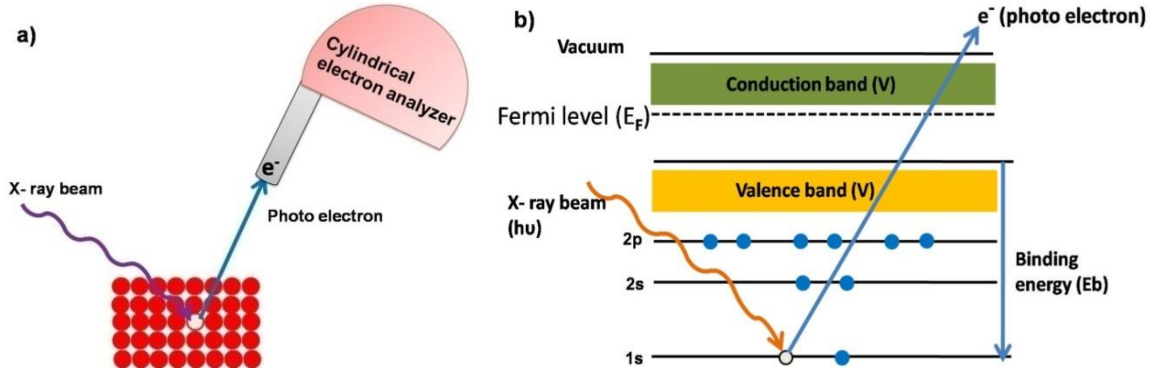

Figure 2.6 Schematic representation of XPS a) instrumental setup and b) Photo electron emission process

The chemical state of the materials is identified by the chemical shifts arise due to the difference in chemical potential and polarizability. In this thesis work XPS (M/s SPECS, Germany) system with a monochromatic Al $K\alpha$ (1.4866 keV) source was used. Curve fitting analysis was done using Gaussian–Lorentzian line shapes after careful subtraction of Shirley back-ground. A detailed XPS anaylsis of various DLC films was covered in subsequent chapters.

2.2.5 Auger Electron Spectroscopy (AES)

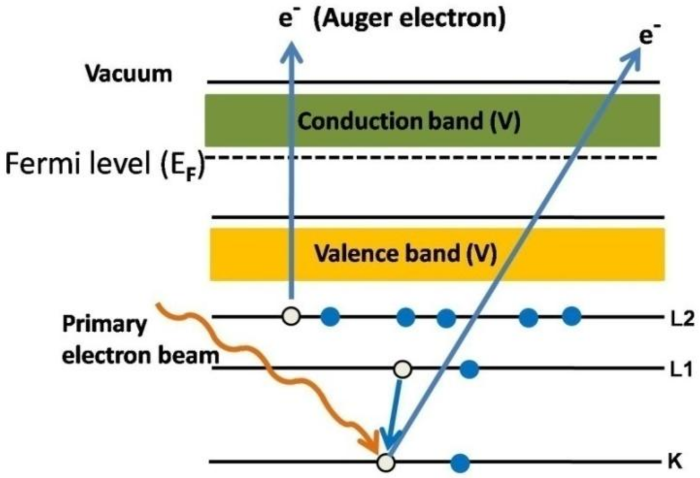

Figure 2.7 Schematic view of Auger electron emission process (KLL transition)

Auger electron spectroscopy gives quantitative elemental concentration and chemical state from the material surface. It is highly surface sensitive with a depth resolution of about 5 nm. Auger instruments are capable to obtain a lateral resolution of upto 8 to 10 nm by scanning the focused micro electron beam. The depth information can be explored by sputtering the layers. Auger spectroscopy is accomplished by using a focused micro electron beam onto the sample surface. Electron analyser is used to analyse the energy of Auger electrons emitted from material surface. A schematic representation of Auger spectroscopy is shown in Fig. **2.7**. The quantification of elemental analysis is carried out by measuring the kinetic energy and intensity of the Auger peak. In contrast to XPS, here a focused electron beam is used so it is mostly suitable for metals and semiconductors. However, it has a much smaller spatial resolution than the XPS. The systems works more similar to a SEM with an Energy dispersive spectroscope (EDS), it also uses a focused electron beam for elemental characterization.

2.2.6 Rutherford Back Scattering spectroscopy (RBS)

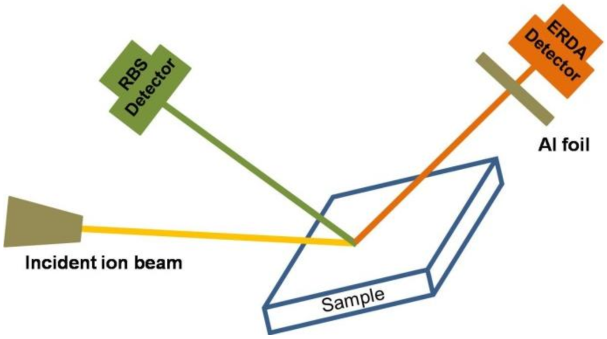

Figure 2.8 Schematic representation of the ion beam analysis setup with both RBS and ERDA detectors

Rutherfod back Scattering spectrometry is a widely used nuclear method to analyse surface layers of the solids. It works on the principle of change in energy due to an elastic collision. The test involves bombarding the target (test sample) with a beam of mono energetic alpha particles with energies in the range of MeV, the incident particles are scattered by the columbic field of the nuclei of the atoms comprising the target. Collection of back scattered particles at the backscattering angles (*i.e*, angles > 90^o with respect to the beam direction) is performed and hence the term Rutherford Backscattering Spectrometry. The relative yields of the scattered α-particles can be used to obtain information on depth dependent elemental concentration of the target. Superior mass resolution and ability to analyze thick targets are the strength of this technique. A schematic representation of RBS setup is shown in Fig. **2.8**. Kinematic factor is one of the important quantity in RBS measurements. It is the ratio of particle energies after the collision and energy of the incident ion.

$$\boldsymbol{k = E/E_o} \qquad (2.8)$$

The ratios are readily expressed by the conservation of energies and momentum in a two body collision, the kinematic factor K for the scattering of an incident ion of mass M_1 through an angle θ by a target atom of mass M_2 is obtained by

$$\boldsymbol{K} = \left(\frac{M_1 cos\theta + \sqrt{M_2^2 - M_1^2 sin^2\theta}}{M_1 + M_2}\right)^2 \qquad (2.9)$$

To increase the sensitivity of the method, it is important to choose experimental parameters such a way that the difference between kinematic factors K of the projectiles back scattered from different kinds of target elements in the target should be as large as possible. In the present thesis work RBS measurements were carried out using helium ions to obtain the film density. He^+ ions are accelerated to typically 2 - 3 MeV energy and are incident normal to the target mounted in a scattering chamber operating at a vacuum level of ~ 1×10^{-7} mbar. A surface barrier detector is used for detecting the backscattered ions and it is mounted at 165^o with respect to the incident beams.

2.2.7 Elastic Recoil Detection Analysis (ERDA)

Elastic Recoil Detection Analysis is a powerful ion beam technique to analyze depth resolution and concentration of lighter elements (1< Z <8) in materials. Moreover it gives the quantitative elemental concentration. This is quite similar to the RBS technique except in this method the probing ions are the ones ejected from the target after hitting by the high energy ion beam. Recoiling of the target atom is due to the columbic interaction of the incident ions with the atomic nucleus of the target material. The sensitivity of the ERDA increased at lower recoil angles and it is advantages to keep M1>>M2. The Kinematic factor for ERDA measurements is given by the following expression

$$k = \frac{4M_2/M_1}{(1+M_2/M_1)^2} \cos^2 \varphi \qquad (2.10)$$

2.2.8 Tribometer

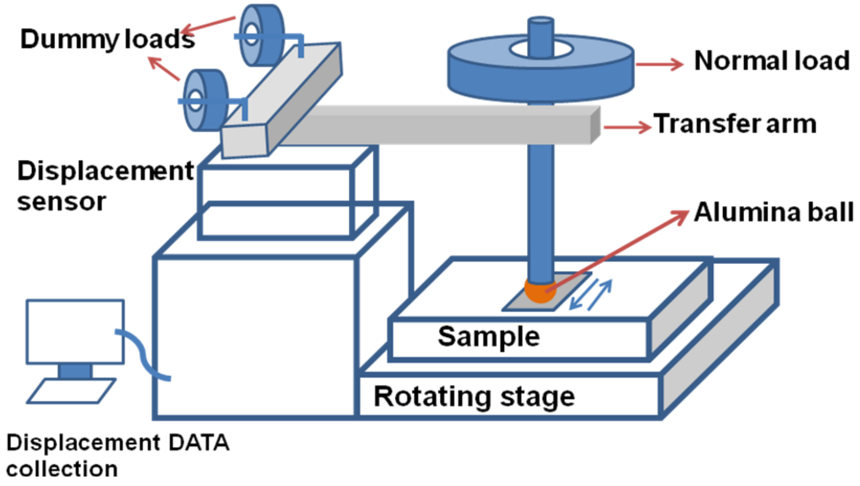

Figure 2.9 A schemcatic representation of tribometer setup

The word tribology derived from a Greek word “tribos” means rubbing, so literally it is the science of rubbing. By definition it is the science and technology of interacting surfaces in relative motion. It is a combination of three independent fields such as friction, lubrication and wear. Tribology is of immense economic interest and a better understanding of this can enormously cut down the investment. Moreover the frictional loss is the foremost barrier in attaining conservation of energy towards achieving eco-friendly society. Novel materials minimizing friction in the machineries to make them economical and energy efficient are always in great demand. A tribometer or tribo tester is the test instrument used to measure the tribological parameters such as coefficient of friction and wear rate of the two mating surfaces. The tribology measurements are specific to a combination of mating parts as well as conditions under which the test is carried out. Friction and wear mainly depends on the physical properties of the individual materials and sliding induced chemical interactions between the mating surfaces. External parameters like surface roughness, test environment, normal load, sliding speed, sliding material and lubricant used are also highly influential in determining the friction and wear. The conventional tribo testers comprised of a Load cell, counter body, transfer arm with LVDT sensor and a rotating sample holder. Displacement of the arm during sliding is meaured by LVDT sensor. A standard weight used to be placed over the arm whose other holds the counter body. Transfer arm in surface normal to the flat surface of the test sample. A schematic representation of the tribometer used for these studies is given in Fig. **2.9**. Due to its weight of the counter body comes in contact with the sample surface. Either of the arm or the test material holder will be in rotation to creating sliding action between the mating surfaces. When the two surfaces are in relative motion under loading condition a force exerts tangential to the contact surface and it is in line with the sliding direction. The coefficient of friction measured by taking the ratio of tangential force by normal force as shown in simple equation.

$$\boldsymbol{F} = \boldsymbol{\mu} \, \boldsymbol{N} \qquad (2.11)$$

In general the tribo test is exposed to the atmospheric conditions. Some instruments comes with a provision to pass the desired gas medium close to the sliding contact or the whole setup will be placed under an encloser filled with the desired gas medium. Based on the contact geometry commercially available tribo testers are classified into 1) pin on disc and 2) ball on disc. In the Pin on disc setup the contact is a sharp point contact whereas ball on disc is a shallow contact.

In this study, CSM make standard ball on disc tribometer was used. This works in linear reciprocating mode. Different normal loads sliding speeds were used for selecting an appropriate combination. A detailed discussion on the effect of normal load and sliding speed is given chapter 4. We chosen 6 mm dia Al_2O_3 ball as the counter body for this thesis work. The detailed testing conditions and procedure for different films are given in respective chapters.

2.2.9 Surface profilometer

Surface profilometer consists of diamond stylus or probe, which scans across the sample surface to measure the roughness. It can also be used to measure the dimension (width and depth) of craters or tracks. The vertical moment of the stylus due to force exerted by the sample is measured to obtain the surface roughness or dimension of the tracks. Profilometer is capable to scan larger areas over the length scales of few mm. In this study we used the stylus profoilometer to measure the dimensions of the wear tracks required to calculate the wear rate.

2.2.10 Contact Angle Measurements

Recently, a lot of attention is drawn towards wetting characteristics of the DLC materials. This is useful for bio-medicine, oil recovery, lubrication, automobile and textile industry applications. In general water is the commonly used liquid to obtain wettability characteristics of many materials. Consider a drop of liquid on a horizontal flat surface, the contact angle is defined as the angle between the liquid-solid and liquid-vapor interface. Geometrically it is measured by drawing a tangent starting from the liquid-solid contact along the liquid –vapor interface. Depending on the value of contact angle, the wetting nature surface further sub classified into four categories: hydrophilic, superhydrophilic, hydrophobic and super hydrophobic. When the water spreads over the surface (contact angle <<90°) then the contact angle is very small and these surfaces are pronounced as hydrophilic. On the other hand where water drop beads over the surface (contact angle >>90°) results in higher contact angle are pronounced as hydrophobic surfaces. The shape of the water drop is determined by interaction forces exerted by the contact surface onto the water drop. Adhesive forces acting between the liquid-solid interface favors spreading and cohesive forces within the liquid that counteract the spreading. The balance, is described by Young's equation (2.12), relates the contact angle to the surface free energies of a system containing solid (S), liquid (L), and vapor (V) phases, as shown in Fig. **2.10 a)**,

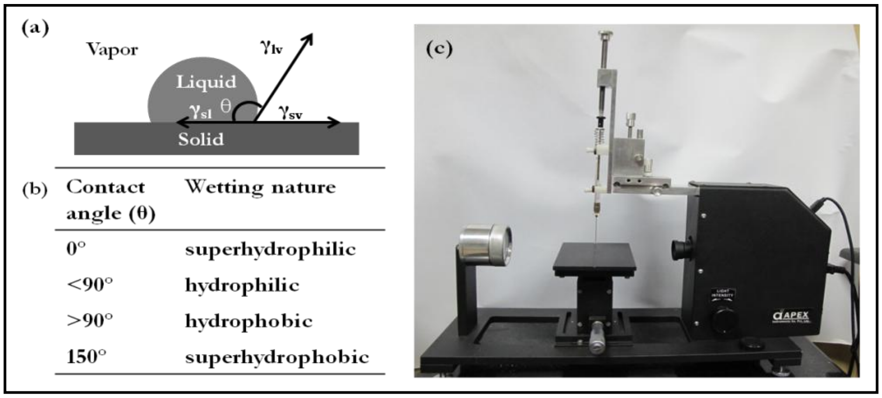

Contact angle (θ)	Wetting nature
0°	superhydrophilic
<90°	hydrophilic
>90°	hydrophobic
150°	superhydrophobic

Figure 2.10 (a) Schematic of contact angles (CA) formed by sessile liquid drops on smooth homogeneous solid surface, (b) table of CA with wetting property and (c) Contact angle measurement set up in our lab.

$$\gamma_{sv} - \gamma_{sl} = \gamma_{lv} cos\theta \qquad (2.12)$$

Where, γ_{sv},γ_{sl} and γ_{lv} represent the surface free energy of solid, solid-liquid interface and liquid, respectively. The contact angle measurement set up is shown in Fig **2.10 c)**. The major components of the set up are a Light source, micro syringe connected with screw gauge to put a droplet with constant volume and a CCD camera interfaced with computer to capture the images used for measuring contact angle. In addition to wettability nature one can get the surface energy of the materials surface by measuring the contact angle using different liquids simultaneously. In this thesis work contact angle for variety of DLC films was measured and it is correlated with physical and structural properties. The details of measurement and film surfaces are discussed in the respective sections of the thesis.

2.3 References

1. R. Geller, *Rev. Sci. Instrum.* **1990**, 61, 659.
2. A. Girard and G. Melin, *Nuc. Instrum. Meth. Phys. Res. A* **1996**, 382, 252.
3. A. Girard, *et al., Rev. Sci. Instrum.* **2004**, 75 (5), 1381.
4. H. Conrads and M. Schmidt, *Plasma Sources Sci. Technol.* **2000**, 9, 441.
5. A. Ganguli and R. D. Tarey, *Curr. Sci.* **2002**, 83(3), 279.
6. K. D. Vernon-Parry, *III-Vs Review* **2000**, 13 (4), 40.
7. G. Binnig, *et al.*, *Phys. Rev. Lett.* **1986**, 56 (9), 930.
8. Y. Seo and W. Jhe, *Rep. Prog. Phys.* 2008, 71, 16101.
9. U. Rabe, *et al., Ultrasonics* **2000**, 38, 430.
10. U. Rabe , *et al., Ultrasonics* **2002**, 40, 49.
11. F. Marinello, *et al., Wear* **2011**, 271, 534.
12. D. Passeri, *et al., Ultramicroscopy* **2013**, 128, 32.
13. P. K.Chu, *et al., Mater. Chem. Phys.* **2006**, 96 (2), 253.
14. A. C Ferrari and Robertson, *J. Phil. Trans. R. Soc. London, Ser. A* **2004**, 362 (1824), 2477.
15. A. C. Ferrari and J. Robertson, *Phys. Rev. B* **2000**, 61(20), 14095.
16. Y. Wang, et al., *Chem. Mater.* **1990**, 2, 557.

Chapter 3: Effect of gas composition and pulse DC biasing on structural and mechanical properties of DLC films

3.1 Introduction

DLC films are ingeneral classified as tetrahedral amorphous carbon (ta-C), amorphous carbon (a-C), and their hydrogenated counterparts as ta-C:H, a-C:H.[1-3] The tetrahedral amorphous carbon (ta-C) films are nothing but the DLC films with higher sp^3 bonding (more than 70%). On the other hand, amorphous carbon (a-C) films have less sp^3 bonding and their mechanical, electronic, optical properties can be tuned by controlling the sp^2/sp^3 ratio. This is one of the important factors behind promoting this material for various technological applications.[4-7] Additionally, the presence of hydrogen also plays a major role in stabilizing the sp^3/sp^2 ratio in amorphous carbon films. Physical and chemical deposition methods allow growth of DLC film with desired sp^2/sp^3 bonding state and hydrogen concentration.[1, 8] Various deposition and growth processes were adapted for controlling chemistry and phase fraction of the DLC film. A careful literature survey on DLC films highlighted that ion energy, ion flux density and source gas composition are crucial in controlling the bonding of DLC films.[9-13] Many studies are focused on the effect of feed stock gas composition in controlling bonding (sp^2/sp^3 ratio) as well as hydrogen content on mechanical properties.[12-14] The Ar and H_2 are most commonly used gases for the purpose of dilution in DLC growth. Earlier studies show that dilution with both these gases has significant influence on growth rate, hydrogen content and bonding. It is reported that substrate biasing helps in stabilizing the sp^3 bonding and improves the mechanical properties of DLC films. In addition to the structural properties the surface chemistry is also a strong contender for controlling friction behavior of DLC films. DLC films are known for their altering friction behavior with respect to the testing environment. Many studies in recent times proved that the absorbed oxygen plays a crucial role in deciding friction coefficient of DLC films.

This chapter focuses modification of structural and mechanical properties of DLC films-via change in gaseous composition and substrate bias parameters (voltage, duty cycle and frequency). Correlation between film density and hydrogen content is established. Extensive analysis on the surface chemistry of DLC films is also carried out. The role of bonding and surface chemistry is described to modify the elastic and tribological properties of DLC films.

3.2. Experimental section

3.2.1 Film growth

The DLC films were deposited in three different set of conditions by varying namely 1) Gas composition, 2) substrate bias voltages and 3) duty cycle and pulsing frequency. Feed stock gas composition variation was studied by changing Ar:CH_4 ratio. The growth was carried out by changing flow rate of one gas at a time. Each time flow rate of either one was varied as 5, 10, 15 and 20 sccm, by keeping flow rate of other gas constantly at 10 sccm. These films are denoted as Ar series (Ar flow rate was variable) and CH_4 series (CH_4 flow rate was variable). In the second set, the substrate bias was varied as -50, -100, -150 and -200 V while keeping other growth parameters constant. These samples were designated as B_1, B_2, B_3 and B_4 throughout the thesis. In the third set, the pulse frequency and duty cycle were varied by keeping gas composition and bias voltage constantly. Duty cycles were varied as 50, 70 and 90 % where pulse frequency was set at 10 kHz. On the other hand pulse frequency was varied as 10, 25, 50 and 75 kHz while the duty cycle kept constant at 70%.

3.2.2 Characterization

Topography and film thickness were measured using AFM and FESEM. Chemical structure of these films was analyzed by laser Raman spectroscopy. RBS and ERDA were employed to obtain elemental composition, density and hydrogen content. The tribology studies were carried out to get the value of friction coefficient and wear rate. AFAM measurements were carried out to analyze the elastic properties of the films.

3.3. Results and discussion

3.3.1 Effect of gas composition

a) Film thickness

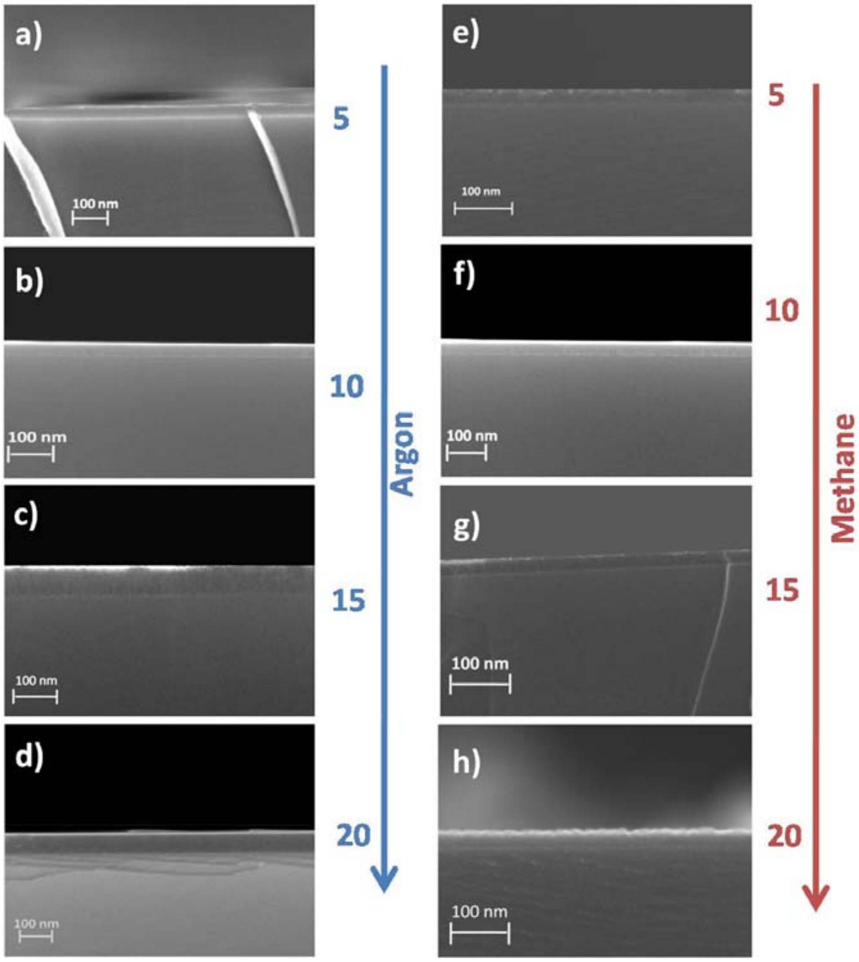

Figure 3.1 FESEM cross section images of DLC films grown under different gas concentrations, (a-d) Ar series and (e-h) methane series (the numbers in figure indicates the flow rate in sccm)

The cross section FESEM imaging was carried out to obtain the growth rate as a function of source gas composition. Fig. **3.1 (a-h)** illustrates the cross section of FESEM images of films corresponds to both Ar and CH_4 series. In the former case where Ar flow rate was varied, upto 15 sccm the film thickness observed to increase and then decrease. Dilution with Ar gas helps in dissociation of CH_4 gas and it increases with the Ar concentration.[11, 15] Dissociation of methane liberates the carbon ions needed for the DLC film growth.

Table 3.1 Film thickness, density and H content of Ar and CH_4 series DLC films

sample		Film thickness (nm)	Film density (g/cc)	H content (%)
Ar series	5 sccm	25	1.4	40
	10 sccm	37	1.7	30
	15 sccm	75	2.2	26
	20 sccm	50	1.3	46
CH4 series	5 sccm	18	1.8	28
	10 sccm	35	1.6	30
	15 sccm	38	1.3	27
	20 sccm	30	1.1	23

The carbon ion concentration goes up with increase in dissociation rate and this leads to higher growth rate. In addition, the energetic Ar^+ ions also physically bombard the film surface throughout the growth. This causes re-sputtering of the film due to the heavier mass of Ar^+ ions.[15, 16] Increase in Ar concentration reduces concentration of C^+ ions due to fixed gas flow.[11, 16] Reduction in C^+ ions and physical sputtering by Ar^+ reduces film thickness at higher Ar concentration. On the other hand when CH_4 flow rate increased up to 10 sccm, the film thickness observed to increase and decrease thereafter. Upon dissociation, CH_4 liberates both C^+ and H^+ ions. The C^+ ions are major constituents for the growth, whereas H^+ ions cause chemical etching of DLC films. Increase in CH_4 concentration in feed stock gas liberates higher H^+ ions upon dissociation. Thus, the reduction in film thickness with increase in CH_4 concentration.[1, 15] The values of film thickness for both Ar and CH4 series are given in table 3.1.

b) Raman studies

Laser Raman spectroscopy is used to analyze the chemical structure of the DLC films grown under different gas composition. The broad spectra between 1000 to 1800 cm^{-1} seen in Fig. **3.2 a) (**Ar series) and **3.2 b)** (CH_4 series) are typical signature of DLC films. Two major peaks at around 1300 and 1500 cm^{-1} correspond to D and G peaks of sp^2 bonded carbon, respectively. These two peaks are associated to the zone centre vibration modes of A_{1g} and $E_{2g,}$ respectively. The Raman spectra belong to Ar 5 sccm in Fig. **3.2 a)** does not show any peak and it showed high luminescence back ground which is a usual feature of low density and highly defected DLC films. From Fig. **3.2 a)** it is also clear that with increase in Ar content the intensity of the spectra increased upto 15 sccm and reduced thereafter. This is attributed to difference in growth rate as evident from Fig. **3.1.** The Fig. **3.2 b)** showed an increase in peak intensity upto 10 sccm which gets reduced on further increase in flow. It is also reflected in the growth rate. However, the quality of the DLC films cannot be judged by Raman spectra it requires other information like film density and hydrogen content.

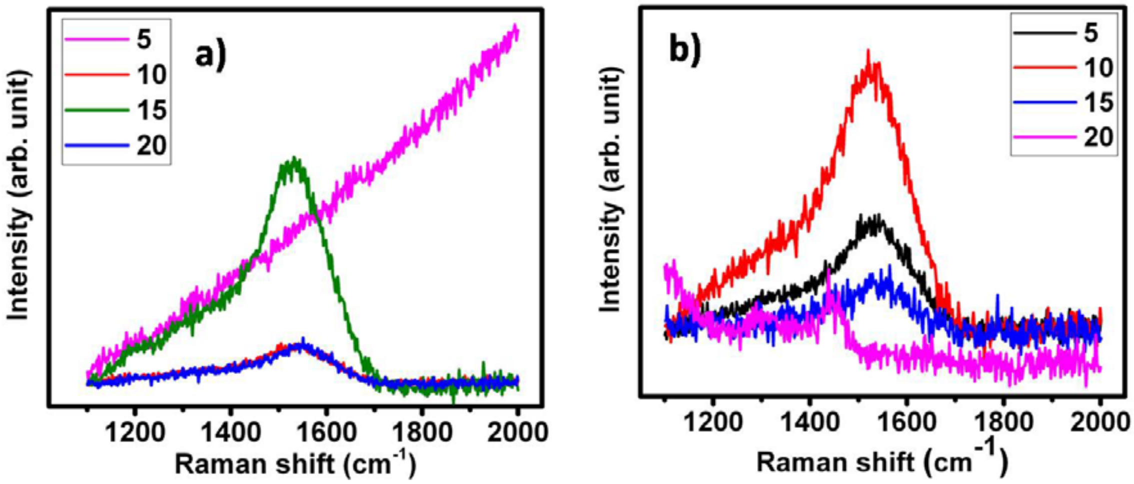

Figure 3.2 Raman spectra of DLC films grown under different gas concentration a) Ar and b) CH_4 series (the numbers in figure indicates the flow rate in sccm)

c) Film density and hydrogen content

RBS and ERDA were employed to obtain the film density and hydrogen content. Fig. **3.3 a)** and **b)** depict the film density and hydrogen content of DLC films belonging to Ar and CH_4 series, respectively. It is evident from Fig. **3.3a)** that the film density increased with Ar concentration up to 15 sccm and reduced thereafter. This is attributed to the Ar^+ ion bombardment during the growth.[16] It also resulted in reduction of hydrogen content by displacing the lighter hydrogen atoms from the DLC network as explained by the sub-implantation growth model.[1] However, density is reduced with further increase in Ar content. Because higher Ar ion flux per carbon atom results in higher ion bombardment of film which enhances the sp^2 bonding.[11] Whereas the increase in hydrogen content is because Ar dilution increases dissociation efficiency of CH_4 which also leads to higher hydrogen incorporation in the films.[15, 16] On the other hand increase in CH_4 content resulted in lower density as well as lesser hydrogen content. As the methane content increases the chances of Ar ion bombardment comes down, thus the reduction in film density with increase in CH_4

content.[17] Higher CH_4 content gives higher hydrogen species. Higher hydrogen content involves breaking the C-H bonds and formation of H_2 which escapes from the film easily. In general, hydrogen saturates the dangling bonds and shields the DLC network from forming sp^2 C=C bonding. Removal of hydrogen from DLC networks encourages the sp^2 C=C bonding which possess lower film density.[1] This could be the plausible reason for the poor density of films grown under high CH_4 content. From the above finding it is evident that the DLC films grown with Ar:CH_4 at 15:10 sccm gives dense films and this optimized ratio is maintained for rest of the work in this thesis.

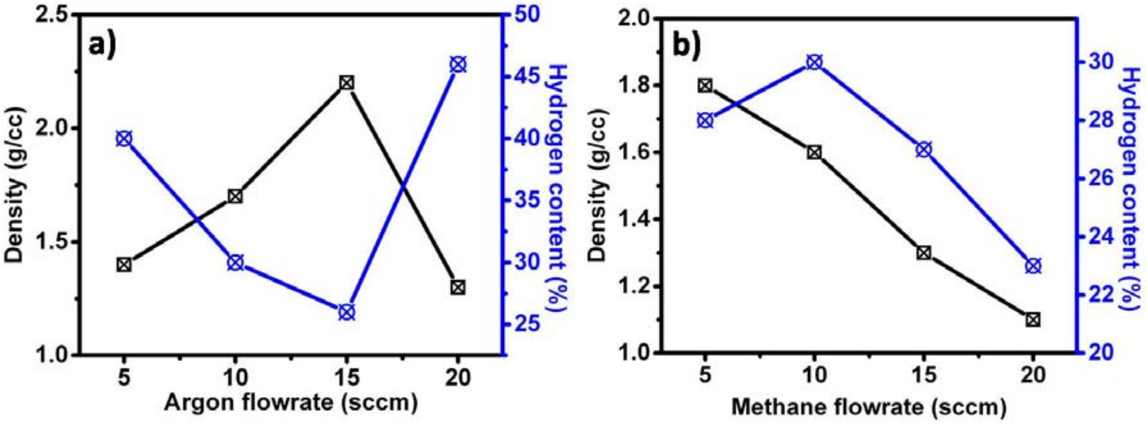

Figure 3.3 Film density and hydrogen content of DLC films grown under different gas concentration a) Ar and b) CH_4 series

3.3.2 Effect of duty cycle and frequency of pulsed DC bias

The study was extended to vary the duty cycle and pulse frequency to get DLC films with improved density.

a) Film density and hydrogen content

The variation in film density and hydrogen content of DLC films *vs* duty cycle pulse frequency is shown in Fig. **3.4 (a and b)**. It is evident that film density initially increased with the duty cycle and reduced thereafter. At lower duty cycles the pulse off time is around half the deposition time during which the Ar^+ ion bombardment is absent. This leads to lower ion fluxes.[18] But, still the growth continues by the neutral hydrocarbon species sticking on the film surface resulting in lower film density. Since the Ar^+ ion bombardment is crucial to improve DLC film density its absence results in poor density.[1] As the duty cycle increases, the time for Ar^+ ion bombardment increases which further improves the film density. Because, pulsing bias helps in increases the ion current and density, it also increases with the duty cycle and frequency.[19]

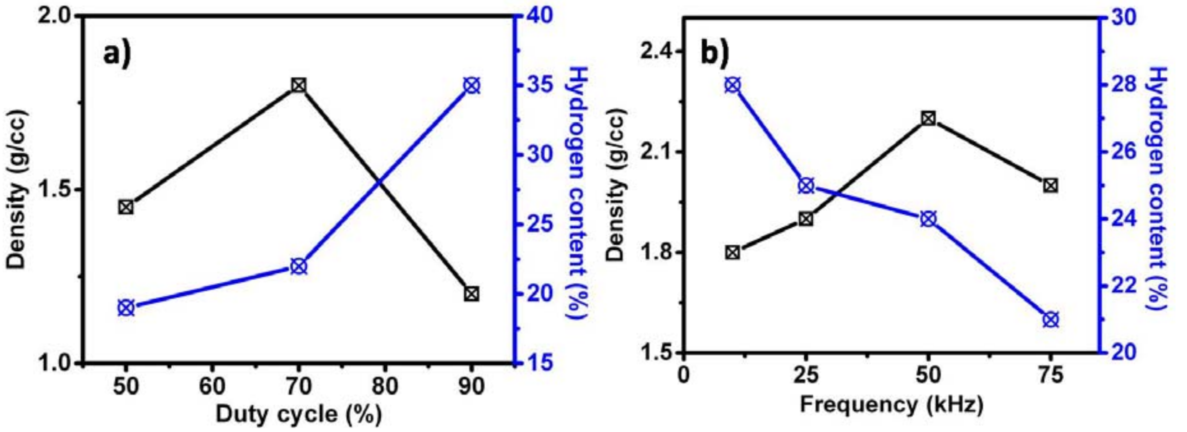

Figure 3.4 Variations in film density and hydrogen content of DLC films grown as a function of a) duty cycle and b) pulsing frequency of pulse bias

However, at higher duty cycles the film density is decreased. This is due to charge accumulation at the film surface because of the insulating nature of DLC structure. It in-turn repulses the Ar^+ ions and avoids the ion bombardment, thus the reduction in film density. Whereas, hydrogen content continuously increased with duty cycle. At higher duty cycles, the growth rate was higher. This was related to increase in ion flux/ density which result incorporation of hydrogen into the film.

However, the film density increased with pulse frequency upto 50 kHz and then reduced thereafter. This is due to increase in flipping rate of polarity with pulsing frequency. This avoids buildup of surface charge and results in higher Ar^+ ion bombardment. Moreover, the increase in pulsing frequency also increases the ion current and density at the substrate which improves the film density.[19, 20] However, at very high pulsing frequency the sluggish movement of heavy Ar^+ ion reduces ion bombardment thus reduction in film density at higher frequency.[19] On the other hand, the hydrogen content is found to be continuously reduced. The plausible reasons are the reduction in growth rate and increase in Ar^+ ion bombardment. Higher Ar^+ ion bombardment can easily displace the lighter hydrogen atom from the DLC network. However, complete removal of hydrogen content is difficult due to high affinity of the carbon atoms towards hydrogen.

b) Elastic properties

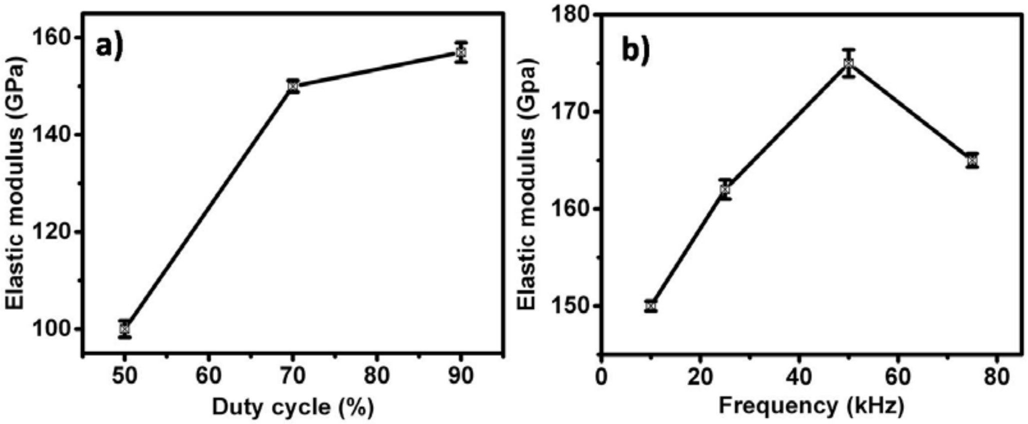

Figure 3.5 Elastic modulus of DLC films grown as a function of a) duty cycle and b) frequency of pulse bias

Elastic modulus of DLC films were calculated using contact resonance frequency (CRF) spectra measured in point spectra mode of AFAM. The CRF values are an averaged value of 5 measurements on each film. Fig. **3.5 (a & b)** depict the variation in elastic modulus of DLC films grown as a function of duty cycle and pulse frequency. Elastic modulus increased with increase in duty cycle. On the other hand elastic modulus increased with pulse frequency upto 50 kHz and then reduced. It is attributed to the variation in film density.

c) Tribological properties

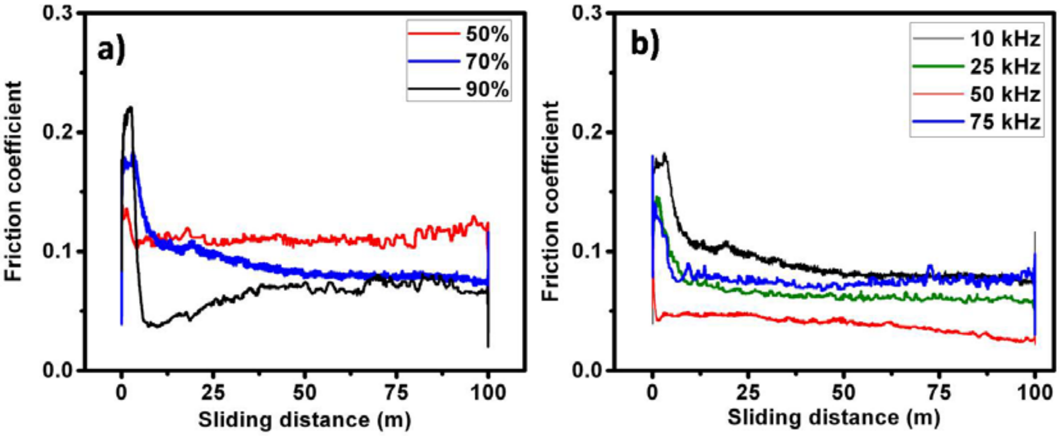

Figure 3.6 Friction coefficient of DLC films grown as a function of a) duty cycle and b) frequency of pulsing bias

The effect of duty cycle and pulse frequency on friction coefficient is depicted in Fig. **3.6 a) and b)**, respectively. The friction coefficient reduced with increase in duty cycle. This is attributed to the higher film density at higher duty cycle. On the other hand with increase in frequency the friction coefficient reduced upto 50 kHz and increased up on further increase in pulse frequency. The friction coefficient showed a direct correlation with the film density and it followed similar trend as it is observed in case of elastic properties. A clear inter dependence of structural, elastic and tribological properties is observed.

3.3.3 Effect of substrate biasing

It is well established that substrate biasing is a crucial parameter to grow sp^3 dominant DLC films. The widely accepted sub implantation growth model of DLC films proved that ion energy around 100 eV is optimum to obtain maximum sp^3 content. Various studies already existed on the effect of substrate biasing on the properties of DLC films. However, effect of bias voltage on elastic properties and tribological properties of DLC films is so far not reported. In this chapter, microscopic evidence of sub implantation growth model is described. It is linked with structural properties of DLC film as a function of substrate bias to explain the friction behavior.

a) Film thickness

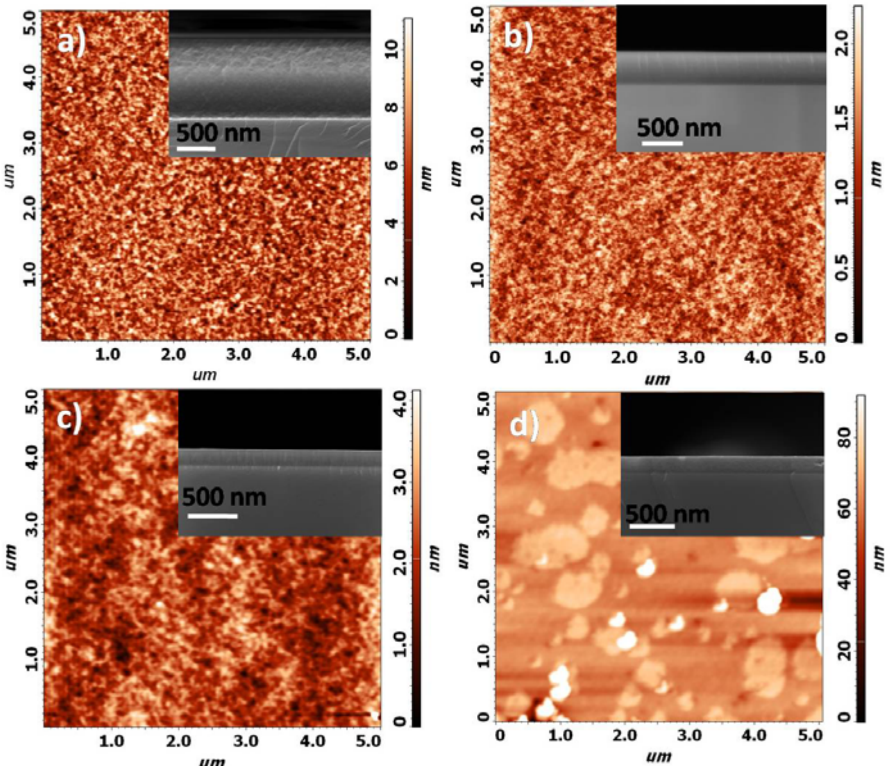

Figure 3.7 AFM topography of DLC films grown at substrate bias of (a) -50, (b) -100, (c) -150 and (d) -200 V. FESEM cross sectional micrograph are given in inset

Fig. **3.7** shows topography of films grown at different substrate bias. The inset shows corresponding cross section FESEM images. It is evident from the topography that the films are uniform. The RMS roughness was measured over an area of 5 × 5 μm^2 for B_1, B_2, B_3 and B_4 films and the values are found to be 0.5, 0.14, 0.25 and 4.5 nm, respectively. The film B_2 is found to have the lowest roughness of 0.14 nm. Such a low roughness value is explained using the subimplantation growth model.[1] Film B_4 deposited at higher biasing of -200V showed coexistence of two different phases over the film surface (Fig. **3.7 d)**). Such second phase evolution might be attributed to the high energy ion induced local heating caused by high substrate bias.[21] The cross sectional FESEM images shown in Fig **3.7** of these films reveal significant reduction in film thickness with increase in substrate bias. Thickness of the films is found to decrease from 850 to 240 nm when the bias was changed from -50 to -200V, respectively. The reduction in the film thickness is due to the re-sputtering of the film with increased biasing.[22] Further increase in substrate biasing raises the local temperature of the film and thereby enhances the etching of film surface through hydrogen ions.[21, 22]

b) Raman studies

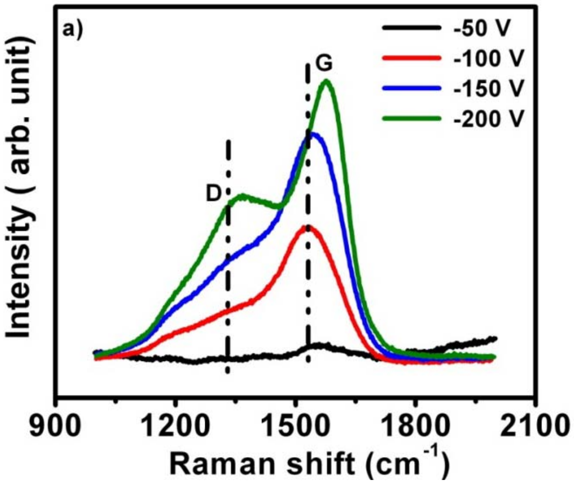

Figure 3.8 Raman spectra of DLC films grown as a function of substrate bias

The chemical nature of the DLC film was analyzed by Raman spectroscopy. These films possess a broad Raman spectra spread over the range 1000 to 2000 cm^{-1} as shown in Fig. **3.8**. It was further deconvoluted and fitted with three peaks using combination of Gaussian and Lorentzian line profiles. The spectra comprise of major peaks located at 1350 and 1560 cm^{-1} corresponding to D and G bands, respectively.[23] The additional peak around 1200 cm^{-1} corresponds to trans-poly acetylene (TPA).[24] With increase in biasing, blue shift in G peak position, noticeable increase in D band intensity and increase in I_D/I_G ratio were observed. Moreover, the reduction in FWHM of G band is observed with increasing bias. Such observations strongly indicate ordering of sp^2 clusters in ring/chain and the film undergoes graphitization.[1, 23] A noticeable increase in D band of hydrogenated (h) -DLC films is associated with oxidation of the surface.[8] In addition the reduction in FWHM of G peak confirms the formation of large ring like sp^2 structures. Such reduction is aided by the oxidation in *h*-DLC films.[8] Thus, the second phase seen in the topography of the B_4 film in Fig. **3.7 d)** is constituted by large aromatic rings of sp^2 clusters.

These films are further characterized by RBS and ERDA analysis to obtain film density and hydrogen content, respectively. These values are given in table-3.2. The film density is found to increase from 0.7 to 2.2 g/cc with the bias voltage. In contrast, hydrogen content in the film reduced from 37 to 16 %. This shows that the film B_1 is highly hydrogenated (C-H-sp^3) and polymer like which results in poor density. The density estimation from RBS and ERDA provide a direct support to Raman observations of increase in sp^2 concentration in DLC films. The increase in sp^2 content and variation of density in these DLC films as a function of substrate bias can be explained by invoking an established growth mechanism called sub-implantation model.[25] According to the sub-implantation model, the ion energy of C radicals decides the type of C-C bonding in the DLC films. The ion energy mainly depends on the applied substrate bias during growth. At low substrate biases, the C ion energy is lower than the penetration threshold energy (Ep) (~30 eV) and hence, C ions just stay on surface and relax to minimum energy state by forming sp^2 bond with glassy structure. However, H is also incorporated in the growing film as the energy required to form C-H bonding is minimum.[1, 26]

Table-3.2: Properties of DLC films grown as a function of substrate biasing

Sample	Surface roughness (nm)	Film thickness (nm)	Film density (g/cc)	H_2 content (%)	I_D/I_G ratio	G peak position (cm^{-1})	G peak width (cm^{-1})	Wear rate (mm^3/Nm)
B_1	0.5	850	0.7	37	0.357	1530.5	175.6	5.0×10^{-6}
B_2	0.14	475	2.2	22	0.404	1541.6	158.8	1.6×10^{-7}
B_3	0.25	290	1.8	19	0.55	1555.2	146.7	1.0×10^{-6}
B_4	4.5	240	1.5	16	0.764	1579.4	113.3	2.2×10^{-6}

The H incorporation in the glassy carbon favors C-H sp^3 bonding but the film density remains very low.[1] At -50V bias, the C^+ ions gain enough energy to penetrate into the sub-surface and occupies the interstitial sites. During sub-implantation growth process the locally altered bonding around the penetrated atoms reforms itself to become bulk bonding of the film with appropriate hybridization i.e. the atomic hybridization will adjust easily to change according to the local density under high energy ion bombardments.[25] Hence, the DLC film becomes sp^2 dominant if the local density is low and sp^3 dominant if the local density is high.[25] At -100V bias, a large amount of C^+ ions enter sub-surface of the growing film since the C^+ ions have sufficient energy. Since larger C^+ ions occupy interstitial sites the C-C sp^3 bonding is energetically favored and this in-turn increases the film density. In the meantime, H is also removed from the growing film since the C-H bonds get easily broken at high energy ion bombardments. At substrate bias greater than -100V, C ions gain much higher energy and it penetrates deeper into the film. The excess energy of C^+ ions get dissipated in different processes viz. a) penetration into the subsurface, b) atomic displacements along the penetration track and c) release of phonons which results in thermal spikes at sub-pico second time scale.[27] This thermal spike allows the atoms to diffuse back to the surface and relax the density locally to stabilize with sp^2 bonding.[1, 28, 29] The size of the sp^2 clusters further increase with bias. Thus, the film density is high at substrate bias of -100 V and it reduces with increase in bias. In addition, the increase in ion energy also causes preferential sputtering of the lighter hydrogen atoms from the DLC films.[1] Thus, reduction in hydrogen content also occurs with increase in substrate bias.[1, 26]

c) AFAM anlaysis

Fig. **3.9 a)-e)** illustrates the CRF mapping of DLC films corresponding to (b) B_1, (c) B_2, (d) B_3, and (e) B_4, respectively. The CRF mapping of the B_1 and B_2 films are very smooth with a variation in frequencies from 675 to 680 and 762 to 765 kHz, respectively. This indicates that these films possess homogenous elastic properties. Similarly, the sample B_3 also exhibits a smooth CRF mapping but several isolated nanoclusters of 50 nm diameter with low CRF values are observed over the homogeneous background Fig. **3.9 d)**. Thus, it is inferred from the CRF mapping that the nanoclustered regions have lower elastic modulus than the matrix. Fig. **3.9 e)** shows the AFAM mapping of the sample B_4 which varies from 705 to 750 kHz. As similar to the topography, the CRF mapping is also highly inhomogeneous with mixture of low and high frequency regimes indicating presence of soft and hard modulus phases. Based on the CRF mapping, statistical analysis was carried out to extract the CRF for a particular sample. In order to avoid tip induced error in elastic modulus due to wear, the tip was always scanned over reference silicon before and after AFAM measurements on actual DLC films. Fig. **3.10** shows the variation in elastic modulus (E) of the DLC films as a function bias. The elastic modulus of sample B_1 is found to be 110 GPa which is much lower than the reference Si.

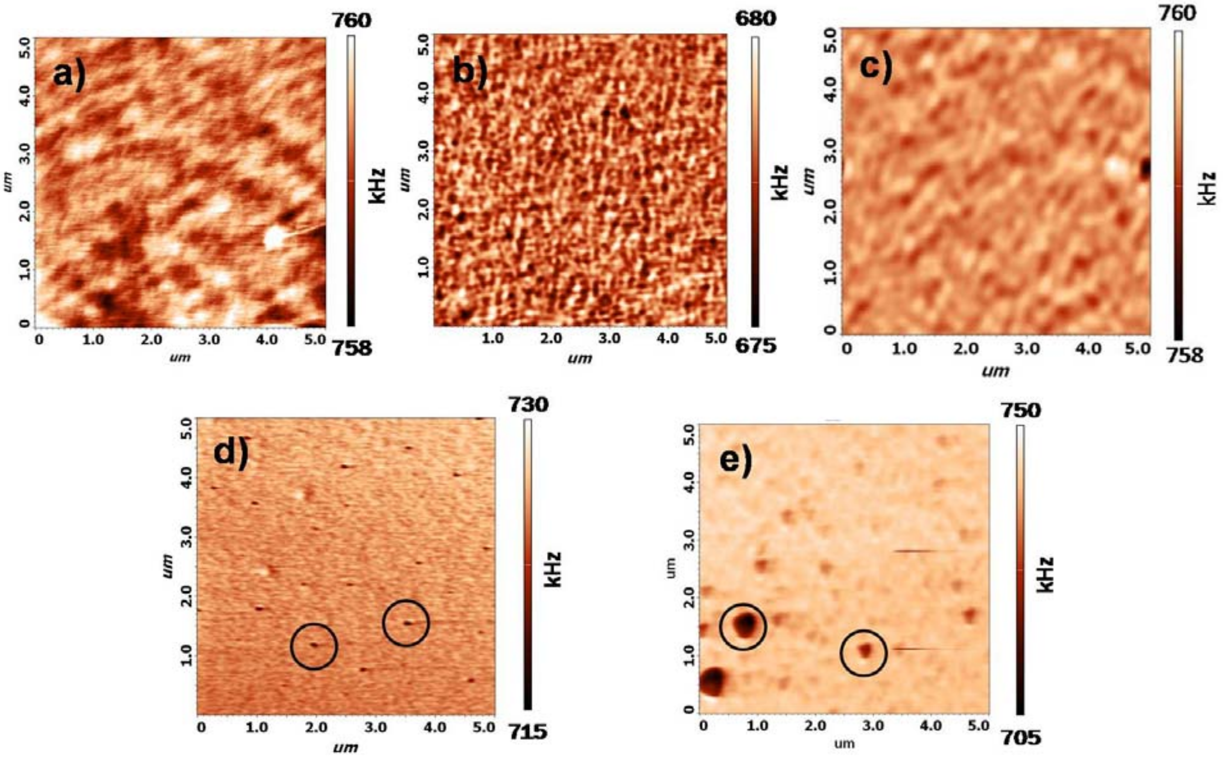

Figure 3.9 Contact resonance frequency mapping of DLC films grown at different substrate bias of (a) Si (100), b) -50, (c) -100, (d) -150 and (e) -200V, respectively

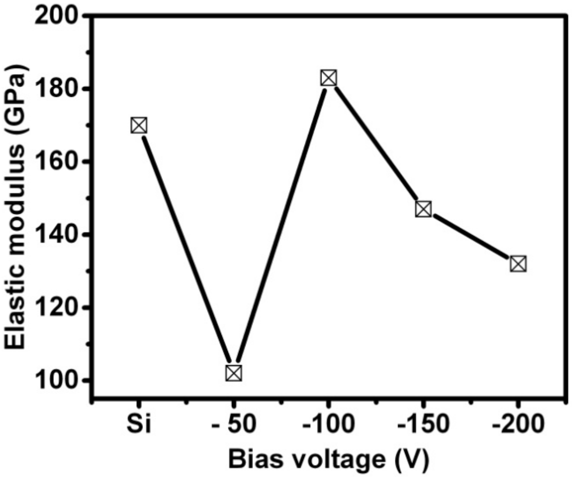

Figure 3.10 The calculated elastic modulii of the DLC films grown at different bias

As the bias increases to -100V, E of the sample B_2 enhanced to 185 GPa which is higher than the reference Si. However, further increase in substrate bias to -150 and -200V, lead to decrease in E to 145 and 130 GPa, respectively. The variation in elastic modulus with biasing exhibited the similar trend as observed by the film density. The reduction in elastic modulus is directly correlated to the enhancement of *sp*^{2} bonding and lower density observed by Raman spectroscopic analysis and film density, respectively. This study provides a direct microscopic evidence for evolution of soft second phases in DLC matrix under high substrate bias.

d) XPS Analysis

Fig. **3.11** shows the XPS survey and corresponding C1s spectra of DLC films deposited as a function of substrate biasing. The C1s peaks of these films were deconvoluted into five peaks centered at 284.6, 285.5, 286.7, 287.9 and 289.1 eV corresponding to *sp*^{2} C=C, *sp*^{3} C-C, C=O, C-O and O=C-OH, respectively. Film B_1 exhibited high surface charging and to counter the charge, the neutralizer (low energy electron gun/flood gun) was used, which resulted in an additional peak at 283.8 eV shown in Fig. **3.11**. The intensity of the chemical shift around 284.6 eV is high for all the films. This implies that the film surfaces are dominated by *sp*^{2} bonding. However, with increase in biasing, the intensity of *sp*^{2} peak decreases and intensity of *sp*^{3} peak increases. It is known that the substrate biasing helps in stabilizing *sp*^{3} bonding in DLC film.[30] XPS analysis is surface sensitive; hence the results of surface chemical shift cannot be compared to the bulk property. On the other hand, intensity of the deconvoluted peak corresponding to C=O, C-O and O=C-OH decreased with bias in B_1 to B_3 film. However, it increased for the film B_4, indicating chemical reconstruction of the surface.

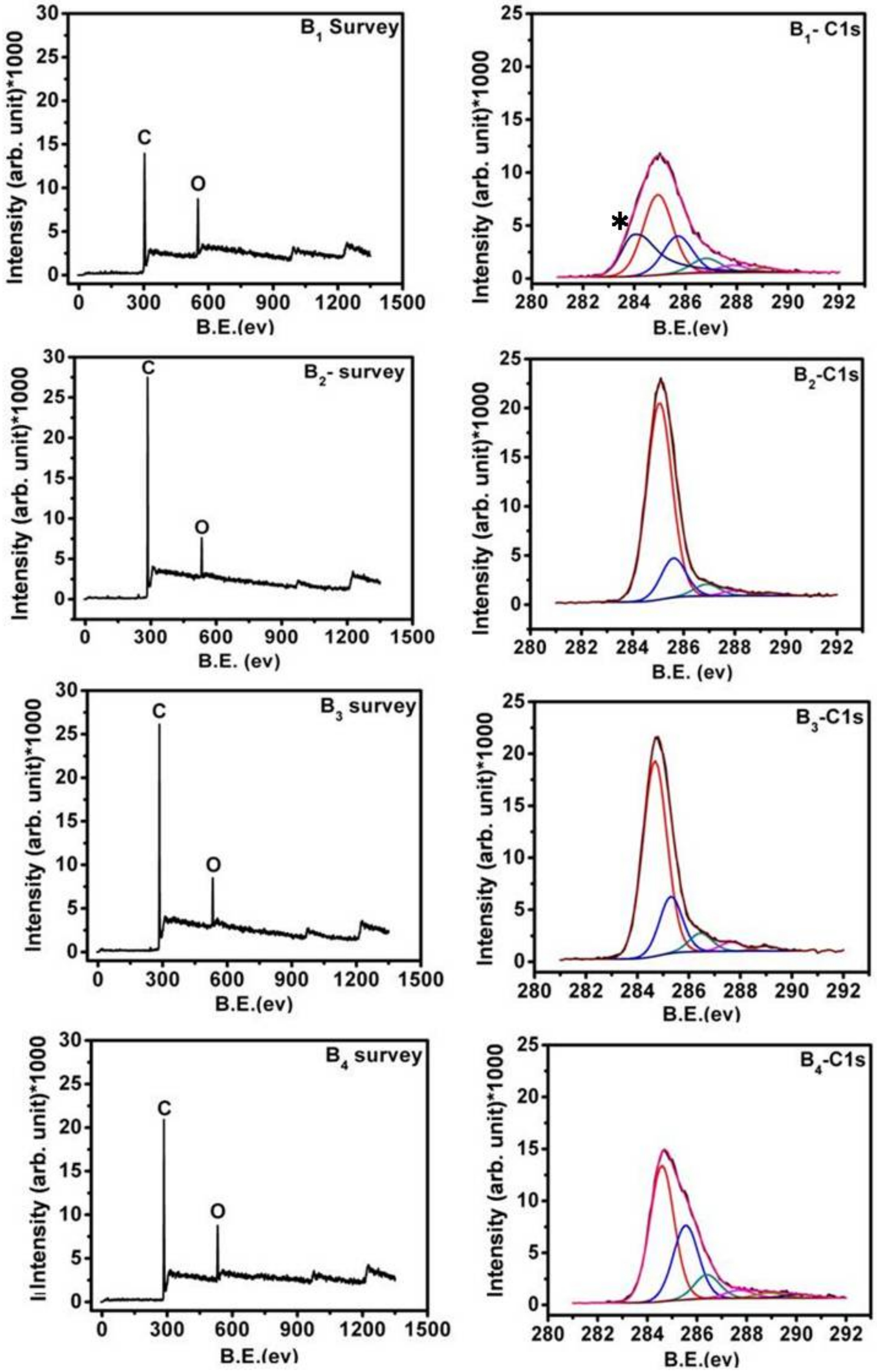

Figure 3.11 XPS survey spectra and deconvoluted high resolution C1s spectra of DLC films grown at different substrate bias (peak with symbol ‘*’ denotes charging in B_1 sample)

Detailed analysis of C/O ratio of the film was obtained from the fitting of the C1*s* and O1*s* peaks. From the XPS survey spectra shown in Fig **3.11,** it is clear that C/O ratio reduces with increase in biasing. It is an indication of the increase in oxygen adsorption. Potential energy of sp^3 terminated surface is high when it consist dangling bonds. This possesses high polarity as compared to sp^2 terminated surface.[31] This is well corroborated with the increase in intensity of C=O, C-O and O=C-OH peaks as shown in C1*s* spectra of the film (Fig. **3.11)**. In addition to this, the film B_4 possesses a second phase which results in formation of fresh dangling bonds at the edges. This in turn aids further oxygen adsorption. On the other hand, the film B_1 also possesses significant amount of adsorbed oxygen. This can be attributed to the presence of defects resulting from the lower film density. A defect laden film is more susceptible to oxygen/moisture adsorption.[32]

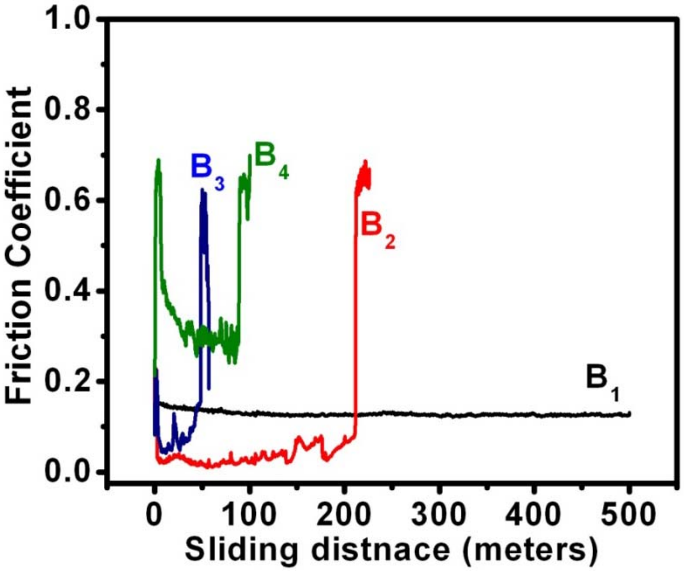

Figure 3.12 Friction coefficient of DLC films grown at different substrate bias

The variation of friction coefficient as a function of sliding distance for the film grown at various biasing voltages is shown in Fig. **3.12**. It is observed that the friction coefficient abruptly increases within 100 meters of sliding distance for the film deposited at higher bias

(B_3 and B_4). This is possibly caused due to reduction in film thickness. However, the friction coefficient also relies on sp^2/sp^3 bonding fraction and film density. Substrate bias introduces residual stresses into the films which would have caused the early failure in B_3 and B_4.[33] Thus, it is difficult to figure out the exact parameter which causes abrupt change in friction coefficient. The friction coefficient of the film B_4 is found to be high from beginning of the sliding. Adsorbed layer of oxygen impurities is likely to be a contributing factor in further raising the friction coefficient. The high friction behavior prolonged for longer sliding distances, if the quantity of adsorbed oxygen is high. In case of less adsorption, the oxide layer abruptly fails after a few sliding cycles, bringing the ball directly into contact with the film and further sliding continues between them. In ambient conditions, fresh oxygen gets trapped between the deformed surfaces and forms chemically instable C=O bond. It is a self-sustained reaction and continues to exist throughout the sliding. In this case, the friction coefficient initially falls and saturates at a different value. On the other hand, the film B_1 appears to be stable. But, the friction coefficient of the film is higher than films B_2 and B_3. The higher friction coefficient can be related to reduced sp^2/sp^3 ratio in the B_1 film.[26] Furthermore, the role of adsorbed oxygen influencing friction and wear behavior cannot be ignored. Oxygen in the film produces structural and chemical defects which deteriorate surface mechanical properties resulting in high friction and wear.[34, 35] Both the films B_1 and B_4 contains larger concentration of adsorbed oxygen on the surface and exhibit higher friction coefficient. Therefore, this aspect confirms the role of adsorbed oxygen in influencing friction coefficient. Furthermore, surface roughness could be one of the most useful reasons to explain the friction behavior.[36] Roughness is highest for B_4 film (4.5 nm) and it leads to high value of friction coefficient from the beginning of sliding cycles.

However, B_2 film is smoothest (rms value 0.14) and showed lowest value of friction coefficient up to the failure point. Early failure of B_2, B_3 and B_4 films in comparison to B_1 is certainly not related to gradual wear, as it is evident from the film density. B_1 is less dense compared to other three films (table -3.2). Residual stresses of film and interface may increase with biasing.[33] Basically, quantification of residual stress in interface is described by film stress. This is evident from the systematic increase in density of film with biasing. Interfacial stress relaxes when tribo stress overcomes the residual stress in interfaces and this may lead to abrupt film failure. For thinner film, the stress in the interface could be higher because the distance between the contact and interface is small. This might be possible reason for early failure of thinner film compare to thicker one. Therefore, both residual stress of the film/interface and film thickness t together caused the film failure.

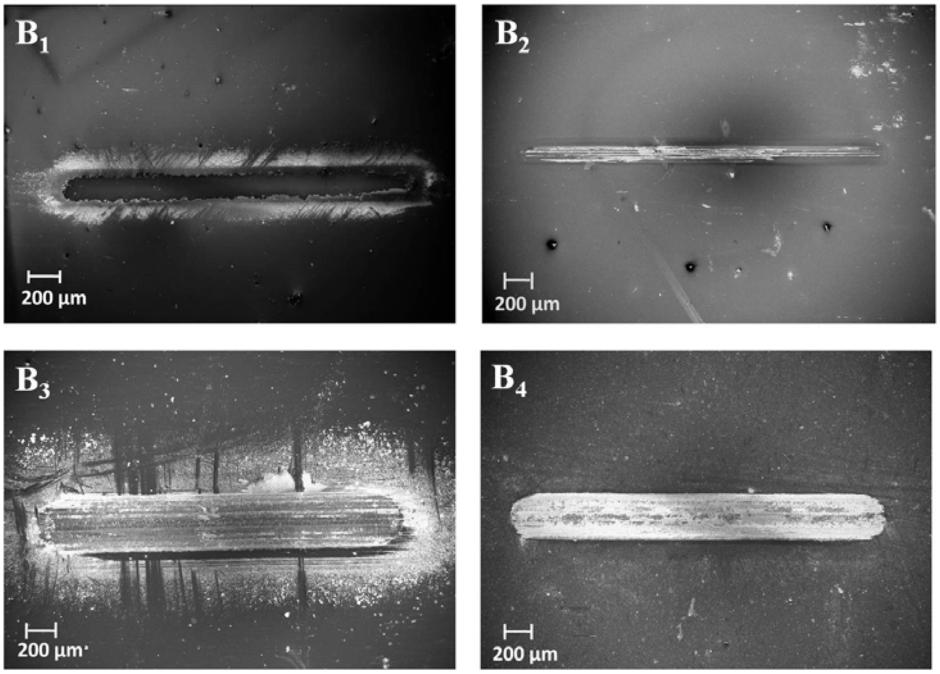

Figure 3.13 FESEM images of wear tracks on DLC films grown at different substrate bias

The FESEM images of the wear tracks showed that the film B_1 is completely deformed (Fig. **3.13**). As mentioned earlier, the film B_1 is more of polymer like and has low film density.

This film is poorly adhering to substrate which causes easy deformation and formation of stable and sustainable deformed layer. This is the reason that this film not showed abrupt failure (Fig. **3.12**). Except B_2, all other films wear out and depict larger wear track width. The wear rate measurements show that the film B_2 is highly wear resistant and it is attributed to the less adsorbed oxygen and smoother surface. Considering all the three parameters, such as friction coefficient, wear life and wear resistance the film B_2 turns out to be superior compared to others. Therefore, to further improve the friction stability, the film $B_2$was selected for nitrogen doping.

3.4 Conclusions

The Ar dilution of feedstock gas resulted in high growth rate and lower hydrogen content in DLC films. It also helped in increasing the film density. On the other hand increase in CH_4 concentration caused reduction in the film density as well as hydrogen content. Both high duty cycle and pulse frequency increased the film density. It is attributed to the Ar^+ ion bombardment. Substrate bias voltage showed a significant influence on the microstructure and chemical bonding of the DLC films. Higher bias enhanced the sp^2 C=C bonding and leads to clustering of the graphitic phase. Elastic modulus mapping confirmed the evolution of graphitic second phase. The elastic modulus of the second phase is lower than the matrix. An increase in friction coefficient with increase in biasing was observed. It is correlated with the absorbed oxygen layer on the surface of DLC films. This study brought out the significance of surface chemistry and chemical bonding in deciding the friction coefficient and wear rate.

3.5 References

1. J. Robertson, *Mat. Sci. Engg.* **2002**, R 37, 129.
2. A. Grill, *Diamond Relat. Mater.* **1999**, 8, 428.
3. Y. Lifshitz, *Diamond Relat. Mater.* **1999**, 8, 1659.
4. W. S. Choi, *et al., Mater. Lett.* **2008**, 62, 577.
5. N. Dwivedi, *et al., J. Appl. Phys.* **2012**, 111, 014908.
6. D. S. da Silva, *et al., J. Appl. Phys.* **2011**, 110, 043510.
7. E. Rismani, *et al., J. Appl. Phys.* **2012**, 111, 084902.
8. A. A. Al-Azizi, *et al., Langmuir* **2015**, 31, 1711.
9. J. Zhou, *et al., Plasma Sources Sci. Technol.* **2006**, 15, 714.
10. N. V. Mantzaris, *et al., J. Appl. Phys.* **1996**, 79, 3718.
11. Y. H. Liu, *et al., Surf. Coat. Technol.* **2006**, 200, 5819.
12. D. Caschera, *et al., Thin Solid Films* **2011**, 519, 4087.
13. Y. Jeng, *et al., Thin Solid Films* **2013**, 529, 301.
14. J. Libardi, *et al., Thin Solid Films* **2004**, 459, 282.
15. G. Cicala, *et al., Surf. Coat. Technol.* **2004**, 180 –181, 222.
16. G. Capote, *et al., Diamond Relat. Mater.***2004**, 13, 1454.
17. G. A. Viana, *et al., Diamond Relat. Mater.***2010**, 19, 756.
18. H. Nakazawa, *et al., Thin Solid Films* **2013**, 539, 134.
19. P.J. Kelly, *et al., Vacuum* **2000**, 56, 159.
20. H. Nakazawa, *et al., Thin Solid Films* **2015**, 574, 93.
21. A. V. Keudell *et al., J. Appl. Phys.* **1997**, 81, 1531.
22. P. Wang, *et al., Appl. Surf. Sci.* **2007**, 253**,** 3722.

23. A. C. Ferrari *et al., Phil. Trans. R. Soc. Lond. A* **2004**, 362, 2477.

24. F. Piazza, *et al., Appl. Phys. Lett.* **2003**, 82 (3), 358.

25. Y. N. Chen, *et al., J. Phys. Chem. C* **2015**, 119, 16148.

26. A. C. Y. Liu, *et al., Phys. Rev. B* **2007**, 75, 205402.

27. S. Bai, *et al., J. Phys. Chem. C* **2012**, 116, 12559

28. K. Hayashi, *et al., J. Phys. Chem. C* **2011**, 115, 22981.

29. J. D. Schall, *et al., J. Phys. Chem. C* **2010**, 114, 5321.

30. D. W. M. Lau, *et al., Phys. Rev. Lett.* **2008**, 100, 176101.

31. R. Paul, *et al., J. Phys. D: Appl. Phys.* **2008**, 41, 55309.

32. N. Paik, *Surf. Coat. Technol.* **2005**, 200, 2170.

33. W. Zhang, *et al., Diamond Relat. Mater.***2002**, 11, 1837.

34. H. I. Kim, *et al., Tribo. Lett.* **2006**, 1, 53.

35. J. Andersson, *et al., Surf. Coat. Technol.* **2003**, 163-164, 535.

36. P. K. Shaha, *et al., Thin Solid films* **2010**, 519, 1618.

Chapter 4: Effect of sliding speed and normal load on the tribological properties of DLC films

4.1 Introduction

A large amount of energy and material are lost due to high friction between sliding components and this considerably reduces the lifetime of components. Owing to high thermal conductivity, high hardness, low friction and high wear resistance, DLC films has emerged as promising material for several tribological applications.[1–4] In real time applications, a tribological coating operates at high temperature, high loads and higher sliding speeds. In such conditions, films with phase stability and deformation resistance are essential. However, DLC films are tribologically sensitive to test atmospheres due to presence of chemically susceptible carbon atoms which easily interact with oxygen, hydrogen and moisture present in the atmosphere.[5, 6] Depending upon the chemical nature of DLC films and test conditions, these interactions may either enhance or degrade the tribological properties. They are also influenced by sliding counter bodies, applied load and sliding speed.[7–16] The results show significance of chemical and mechanical nature of sliding interfaces which influence friction behavior of DLC films.[17] Mainly, at high sliding speeds, the chemical stability of the film degrades due to surface oxidation and this causes deformation in sliding interfaces resulting in less wear resistance.[14] Chemical stability of a DLC film is governed by two parameters, namely shear induced graphitization due to mechanical energy and passivation of the dangling bonds caused by hydrogen and oxygen atoms/molecules.[10, 12, 13, 18] Most of the work describes that low friction in DLC film is contributed by graphitization.[10–13] However, this matter is largely debated and discussed whether graphitization or passivation is dominating factor to explain low friction behavior in DLC film.[13,14] On the other hand, in view of contact mechanics, applied normal load would be a crucial parameter for tribological behavior. Recent reports on friction and wear properties in the context of deformation governed by normal load emphasis its significance. [14, 15, 19, 20]

In this aspect, this chapter deals with tribological studies of DLC films at different sliding speeds and normal loads. Change in sliding speeds is an important criterion for graphitization due to mechanical energy generated at tribo-contact; it further influences the wear resistance. Chemical and structural changes inside wear tracks due to sliding are analyze by Raman spectroscopy and AFAM. On the basis of the above characterizations, the sliding speed and normal load dependent tribological mechanism of DLC films and their chemical and physical transformation are proposed.

4.2 Experimental details

Friction and wear behavior of DLC films were measured by a ball-on-disk tribometer (CSM, Switzerland) operating in a linear reciprocating mode. The Al_2O_3 ball of 6 mm diameter was used as a sliding counter body against DLC films. Here, selection of ball was based on the chemically inertness and thermal stability and during the tribology test. Moreover, Al_2O_3 ball is hard (18 GPa) and generally comparable to the hardness of DLC film. The surface roughness of the ball was approximately 30 nm. A stroke length of 3 mm was used in linear reciprocating sliding motion. Tribology tests were carried out in two set of conditions: 1) normal load kept constantly at 1 N and sliding speeds were varied as 0.2, 0.5, 1 and 3 cm sec^{-1} and 2) sliding speed is kept constantly at 3 cm sec^{-1} and normal load varied as 1, 2, 5 and 8 N. The tests were carried out in ambient (dry and non-lubricated) conditions. All the measurements were repeated for three times on each sample and data was found to be reproducible. Wear track dimensions and wear rate were measured by a stylus profiler.

4.3 Results and discussion

4.3.1 Morphology, topography and chemical structure of DLC film

Fig. **4.1 a)** shows FESEM image of the DLC film, confirming that the film is uniform and ~500 nm thick. Surface rms roughness of the film is ~0.12 nm, determined from the AFM topography shown in Fig**. 4.1 b)**. Hardness (H) and elastic modulus (E) are measured by nano indentation technique and values are found to be 9.5 GPa and 112.3 GPa, respectively. The Load displacement curve is shown in Fig. **4.1c)**.

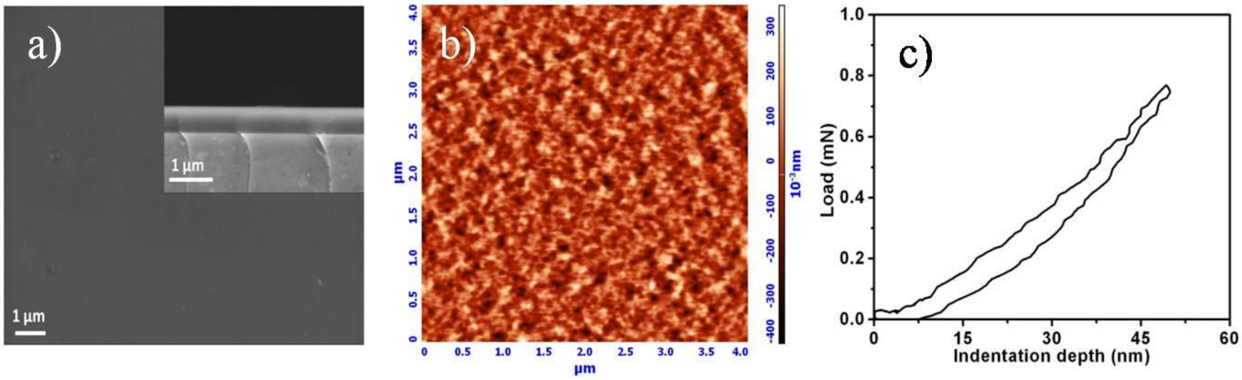

Figure 4.1 Typical (a) FESEM image of surface and cross-section (b) AFM topography and (c) nano indentation data of DLC film

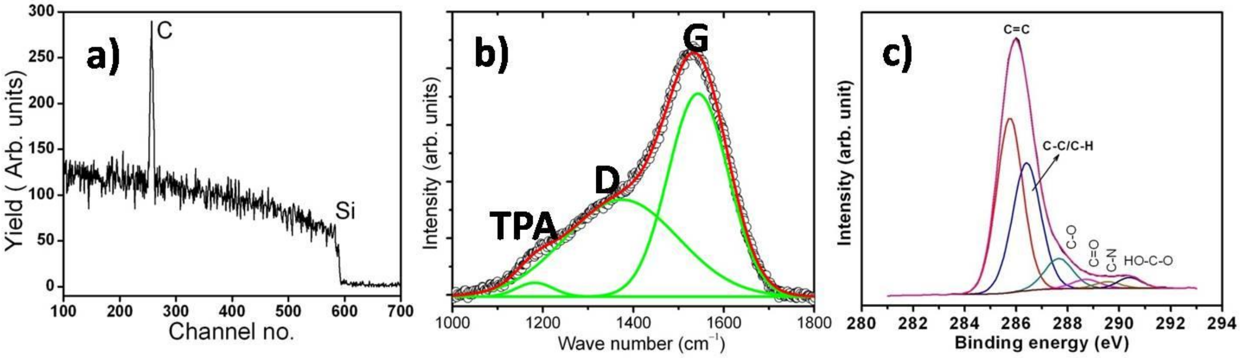

Figure 4.2 Typical (a) RBS spectra (b) Raman spectra and (c) XPS of the DLC film

ERDA measurement showed 25% amount of hydrogen in the film and film density was found to be 2.2g/cc. This fact suggests that DLC film is hydrogenated (Fig. **4.2a**). Low value of E and H (hardness) associated to large fraction of hydrogen content in the film. A detailed chemical structure analysis of DLC films was carried out using Raman spectroscopy (Fig.

4.2b). The broad Raman spectrum was deconvoluted into three segments using a Gaussian fitting method. Peaks around 1360 cm^{-1} and 1540 cm^{-1} correspond to D and G bands. [24] The additional peak centered around 1200 cm^{-1} indicates formation of TPA.[21] Details of the Raman spectra are given in chapter 3. The C 1*s* spectra are deconvoluted into five peaks (Fig. **4.2 c)**). Chemical shift at binding energy of 285.7 and 286.4 eV are designated to C=C (sp^2) and C-C/C-H (sp^3) bonding.[22] Chemical shift of these bands at higher binding energy is observed and this could be related to surface charging due to insulating nature of DLC film.[23] Based on XPS data, the sp^2 and sp^3 fraction in the film are found to be 55.6% and 44.7%, respectively. Large sp^2 fraction is described by large amount of hydrogen in the film. Other peaks at 287.65, 288.7 and 290.4 eV belong to oxygen functional groups, mostly arising due to atmospheric contamination and contributed by C-O, C=O and O-C-OH species, respectively.[22] Minute fraction of C-N peak is observed at 289.5 eV and that could be related to adsorption of atmospheric nitrogen. Physical and chemical properties of hydrogenated DLC film are presented in table-4.1.

Table- 4.1: Physical and chemical properties of hydrogenated DLC film

Film property	
Hardness	9.5 GPa
Elastic modulus	112.3 GPa
Hydrogen content	25%
Density	2.1 g/cc
sp^2/sp^3 ratio (XPS)	0.52

4.3.2 Tribological behavior of DLC films

Sliding speed dependent friction coefficient and wear track dimensions of the film is shown in Fig. **4.3** and Fig. **4.4**, respectively. Four sliding speeds 0.2, 0.5, 1 and 3 cm/s in linear reciprocating mode were selected. The range of the sliding speeds is sufficient to observe physical and chemical changes.[9] At sufficiently less sliding speed, mechanical energy of the sliding interfaces is not expected to change the DLC phase. The friction coefficient is found to decrease with sliding speed and an ultra- low value ~0.05 is measured at a sliding speed of 3 cm sec^{-1}. The average of friction coefficient along with standard deviation is shown in the inset of Fig. **4.3**. In contrast, high friction coefficient ~0.2 is observed at lower sliding speed of 0.2 cm sec^{-1}. Dimension of the wear track is significantly less (~ 10 nm) at a sliding speed of 0.2 cm s^{-1}. This value increases with sliding speed and reaches to approximately 130 nm at a sliding speed of 3 cm s^{-1}. Overall, the wear resistance of the film is found to be extremely high. The wear rates were calculated and given in table-4.2.

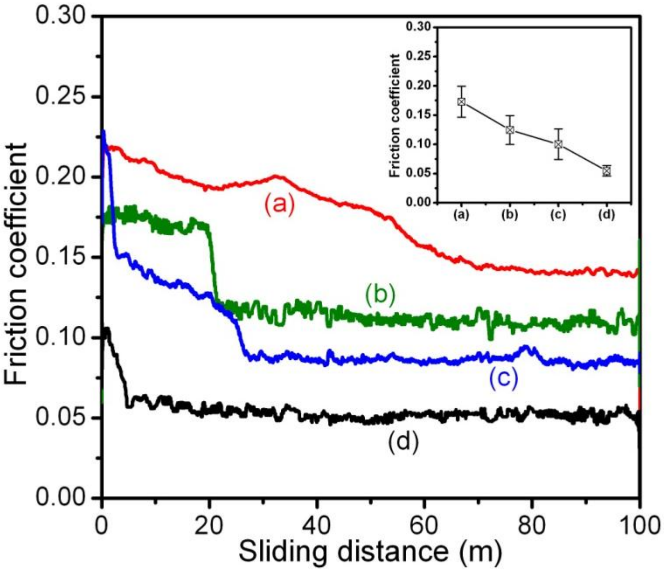

Figure 4.3 Friction behavior of DLC film at sliding speeds of (a) 0.2 (b) 0.5 (c) 1 and (d) 3 cm/s

Fig. **4.5** illustrates the friction coefficient of DLC films obtained at different normal loads such as 1, 2, 5 and 8 N. It is clear that the friction coefficient increased with normal load and finally film worn out at 8 N. The average value of friction coefficient along with standard deviation is shown in the inset of Fig. **4.5**. The load dependant friction behavior can be explained in terms of contact pressure generated due to the applied load.

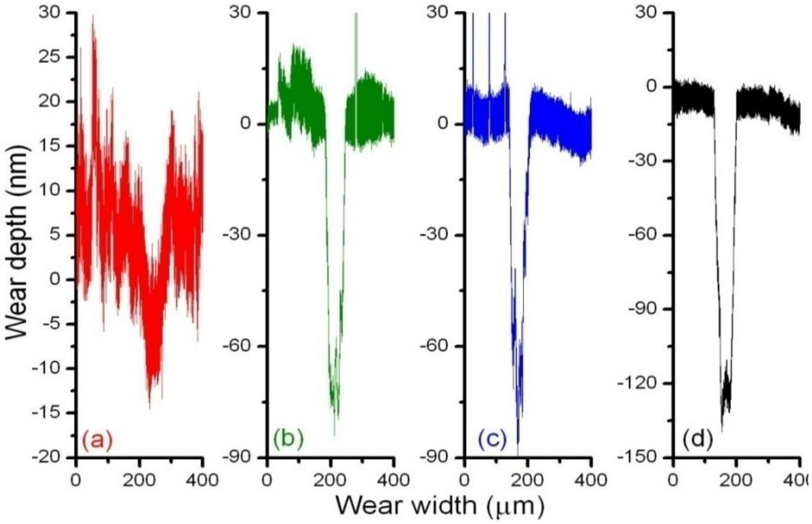

Figure 4.4 2D wear tack profiles at sliding speeds of (a) 0.2 (b) 0.5 (c) 1 and (d) 3 cm/s

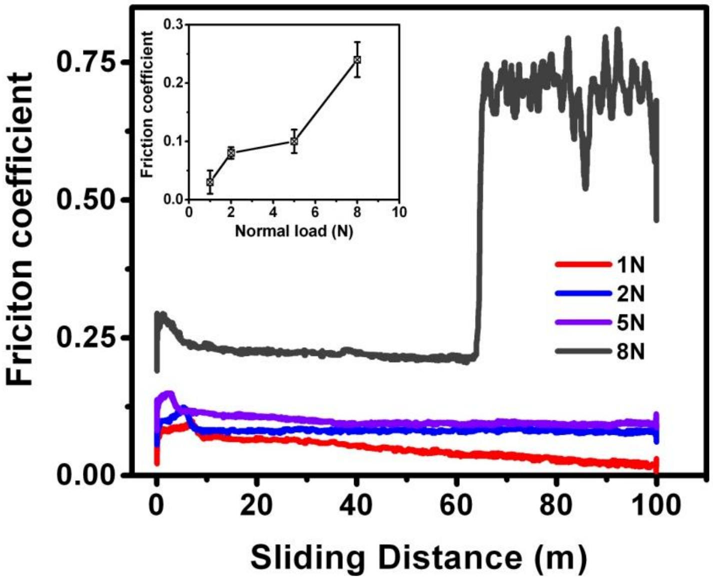

Figure 4.5 Friction coefficient of DLC films tested under different normal loads

It has been established that in the purview of Hertzian elastic contact, the relationship between friction coefficient and normal load is given by the following expression[19, 20]

$$\boldsymbol{\mu = S_0.\pi\left(\frac{3R}{4E^*}\right)^{2/3} F_n^{\;-1/3} + \propto} \quad \ldots\ldots\ldots\ldots\ (4.1)$$

where S_0 interfacial shear strength at zero, R is the radius of ball, E^* is the reduced modulus, F_n is the applied normal load and α is a constant for the pressure dependant contact. The equation 4.1 can be further simplified by replacing the applied load (Fn) with contact pressure (P), to the expression[20]

$$\mu = \frac{S_0}{P} + \propto \qquad \ldots\ldots\ldots\ldots\ldots\ (4.2)$$

From the above expressions it is clear that the friction coefficient should decrease with increase in normal load. However, beyond a threshold contact pressure the plastic deformation of substrate starts, which results in increase of friction coefficient. At very high contact pressure the substrate gets cracked and film worn out and cause abrupt increase in friction coefficient and is clearly seen in Fig. **4.5**.

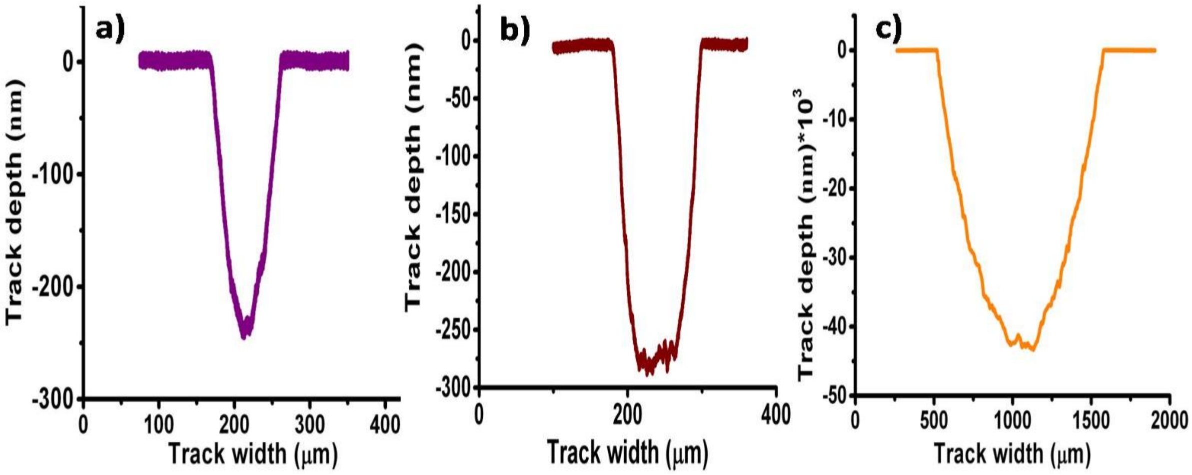

Figure 4.6 2D wear tack profiles at normal loads of (a) 2 (b) 5 and (c) 8 N

The 2D wear track dimensions of the tracks generated after testing at different normal loads are given in Fig. **4.6**. It is evident that the track depths shown in Fig. **4.6 a)**, **4.6 b)** for 2 N and 5 N are nearly twice than that of tracks formed at 1 N normal load (Fig. **4. 4d)**). Wear track corresponds to 8 N normal load shown in Fig. **4.6 c)** illustrates that the track is extended well into the substrate. This is a clear indication for severe plastic deformation. The wear rates are calculated and listed in table-4.2. At higher normal loads, wear rates increased by 2 to 3 orders. Hence, higher normal loads are detrimental for the tribology studies of DLC films.

Table-4.2: Wear rate of DLC film as a function of sliding speed and normal load

Sample	Wear rate (mm^3/Nm)
1N, 0.2 $cmsec^{-1}$	7.1×10^{-8}
1N, 0.5 $cmsec^{-1}$	2.4×10^{-7}
1N, 1 $cmsec^{-1}$	4.3×10^{-7}
1N, 3 $cmsec^{-1}$	6.8×10^{-7}
2 N, 3 $cmsec^{-1}$	5.5×10^{-6}
5N, 3 $cmsec^{-1}$	8×10^{-6}
8N, 3 $cmsec^{-1}$	1.1×10^{-3}

4.3.3 Raman analysis of wear track

Raman spectra mapping across the wear tracks were carried out in order to study the chemical/structural changes. The mapping is carried out in the total area of 150 μm^2, with spatial step size of 0.5 μm.[25] This involves collection of Raman spectra in a pre-defined area with a given spatial step size. In the post analysis, intensity mapping is carried out with particular peak intensity providing distribution of the corresponding peak. The I_D/I_G ratio is obtained by analyzing the Raman mapping and the corresponding spectra is shown in Fig. **4.7**. Furthermore, three selected locations namely (a), (b) and (c) of each wear tracks as indicated in Fig. **4.7** were used to calculate the change in I_D/I_G ratio and FWHM of G peak with respect to the sliding speed. These results are shown in Fig. **4.8** and Fig. **4.9**, respectively.

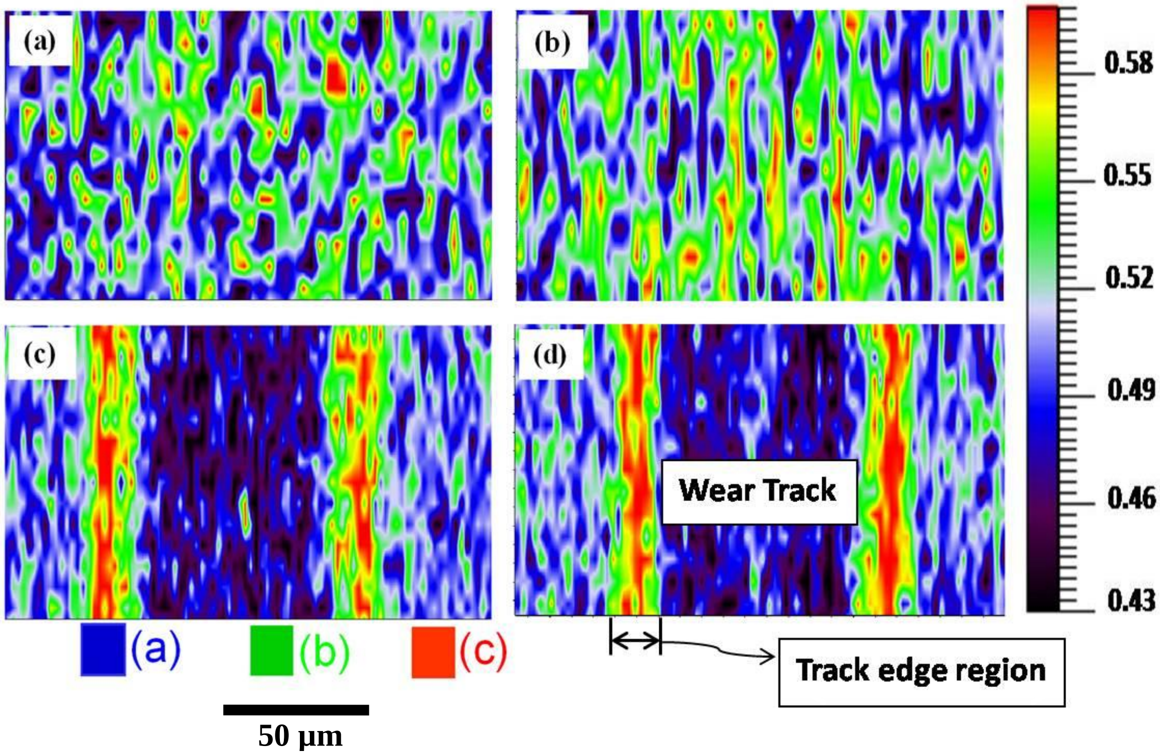

Figure 4.7 I_D/I_G ratio mapping of wear tracks formed at sliding speeds of (a) 0.2 (b) 0.5 (c) 1 and (d) 3 cm/s at load 1 N.

From these results, it is clearly seen that the I_D/I_G ratio is less at the centre of the wear track (Fig. **4.8 a)**). This corresponds to the mapping location **(a)** of wear track indicated in Fig. **4.7**. Moreover, the I_D/I_G ratio is found to decrease with increase in sliding speed. Since, the I_D/I_G ratio is also proportional to sp^2/sp^3 ratio; i.e reduction in I_D/I_G ratio indicates increase in sp^3 bonding.[1] In this location, the FWHM of G peak also increases with sliding speed (Fig. **4.9 a)**) and it is a measure of disordered phase.[24] In contrast, slightly away from the centre of the wear track, the I_D/I_G ratio further increases with sliding speed (Fig. **4.8 b)**). The FWHM of G peak corresponding to this location is found to decrease (Fig. **4.9 b)**). Furthermore, increase in I_D/I_G ratio and decrease in FWHM of G peak is prominent at the location **(c)** of wear track (Fig. **4.8 c)** and **4.9 c)**).

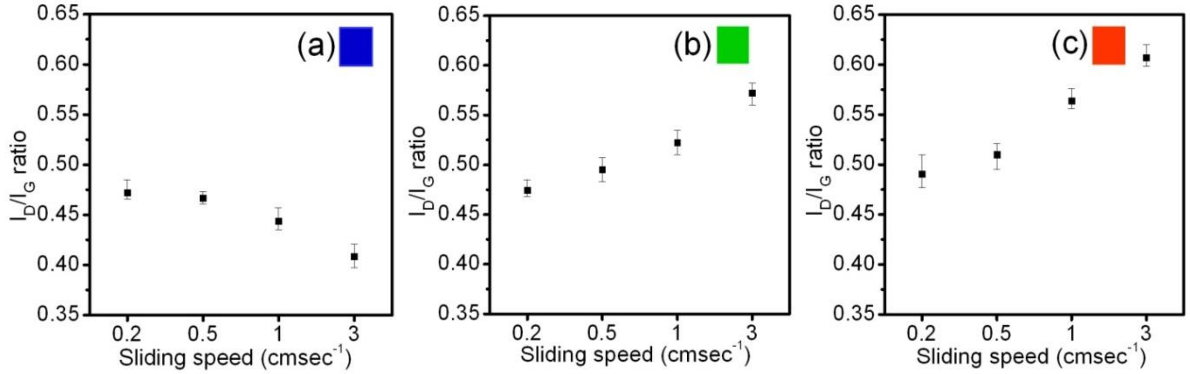

Figure 4.8 Sliding speed dependent I_D/I_G ratio in wear track of DLC film at locations (a), (b), and (c) indicated in Fig. 4.7.

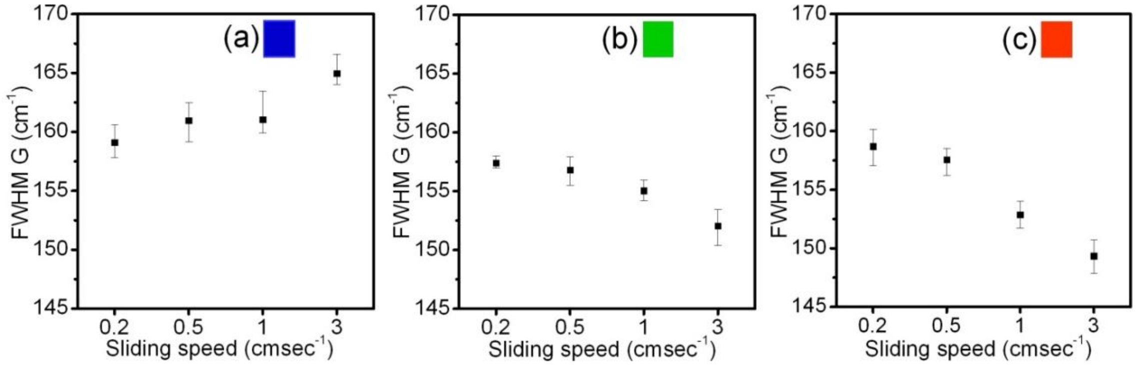

Figure 4.9 Sliding speed dependent FWHM of G band in wear track of DLC film at locations (a), (b), and (c) indicated in Fig. 4.7.

This indicates that the combination of mechanical, frictional and thermal energies result in formation of graphitized debris, which worn out from the DLC film. Layered sp^2 phase easily migrates away from the centre of wear track which is highly stressed region compared to the edge of the track where the contact stress is less.[12, 14] Surface energy of the wear debris is supposed to be high due to higher surface to volume ratio. In this condition, the wear debris is chemically active and easily reacts with ambient atmospheric contamination. This process results in further graphitization/amorphization. It is noticed from the I_D/I_G ratio and FWHM of G peak that chemical transformation is significant when the sliding speed is more than 1 cm sec^{-1}. However, only a small extent of graphitization/amorphization is observed at sliding speeds of 0.2 and 0.5 cm sec^{-1}. At higher sliding speeds, thermal energy at the microscopic asperity contacts becomes high enough to transform *sp*^{3} phase into graphitized *sp*^{2} phase. These chemical changes affect the physio-mechanical properties of the wear tracks in a microscopic scale which in turn influences friction and wear behavior.

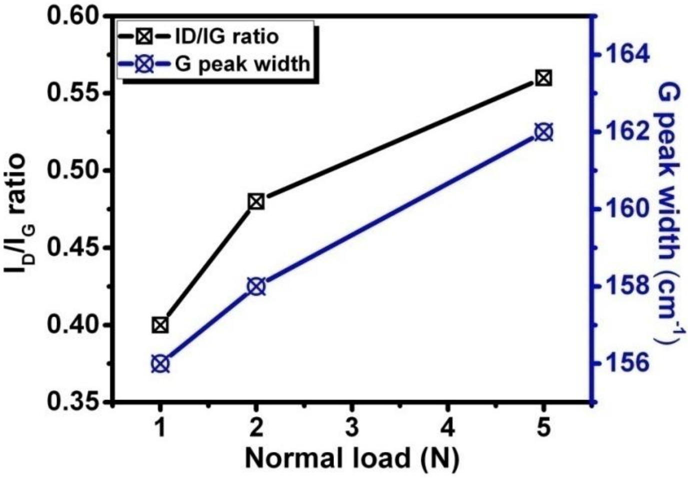

Figure 4.10 I_D/I_G ratio and FWHM of G peak inside wear tracks formed at different normal loads

Similar studies are extended to the wear tracks obtained in the tribology tests carried out at different normal loads. However, in this condition, Raman mapping of wear track is not possible due to difficulties in maintaining optical focus constantly at higher track depths. To overcome this difficulty, individual Raman spectra at centre of the wear track was collected. The Raman spectra were further deconvoluted to obtain the I_D/I_G ratio and FWHM of G peak. The measured values are plotted and shown in Fig. **4.10**. The I_D/I_G ratio increased with increase in normal load, indicating graphitization. This might be due to the severe deformation caused by the higher contact pressures. Increase in wear track depth indicates high wear of the film. Raman spectra results of the wear track obtained at 8N are not obtained because the film is completely worn out. This resulted in the Raman spectra dominated by substrate (Si) signal itself.

4.3.4 AFAM analysis of wear tracks

Raman mapping across the wear track of h-DLC film shows chemical changes and these changes are largely dependent on sliding speed. AFAM mapping of the wear tracks was carried out to substantiate physical and chemical transformations occurred in the DLC films due to wear. This was used to obtain the local variation of elastic properties across the wear track. For these studies, wear track obtained at 1 N load with different sliding speeds was considered. It is understood that the nature of local bonding in DLC is coupled to its structural and elastic properties. Hence, the elastic modulus measurements by AFAM would provide valuable information about the nature of local bonding. Several cursory CRF measurements were performed with different loads applied at various locations on the films. Fig. **4.11** shows the CRF measured over a pristine DLC surface with applied loads varied between 2 and 12 μN.

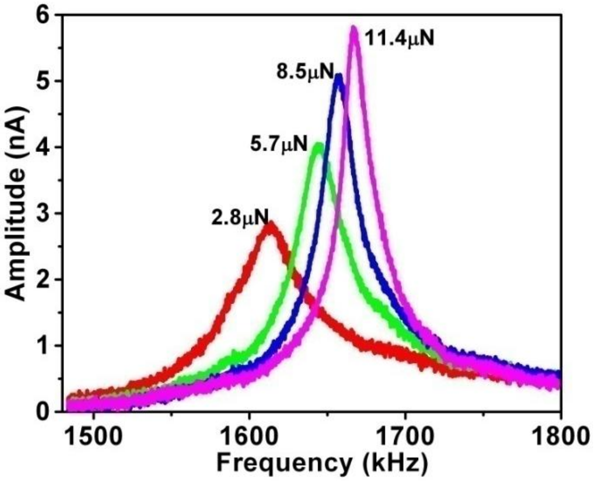

Figure 4.11 First order contact resonance frequency spectra of the cantilever on pristine DLC film at different loads

The peak position and amplitude of the CRF increase with load as expected. This behavior indicates interaction between the tip and the sample which could be explained in the framework of Hertzian contact mechanical model. [26, 27] Based on the CRF spectroscopy, AFAM imaging was carried out with an applied load of 4μN. The topography and AFAM amplitude images were simultaneously acquired at two different frequencies in which one is kept above the CRF and the other is placed below CRF. When the excitation frequency is decreased below the resonance, contrast inversion is observed and the softer region becomes bright. The intermediate contrast indicates no significant change in elastic modulus with respect to the pristine DLC film surface. Elevated height around the rim of the wear track and several bands aligned along the wear direction having different heights are seen in the topography (Fig. **4.12 a)**).

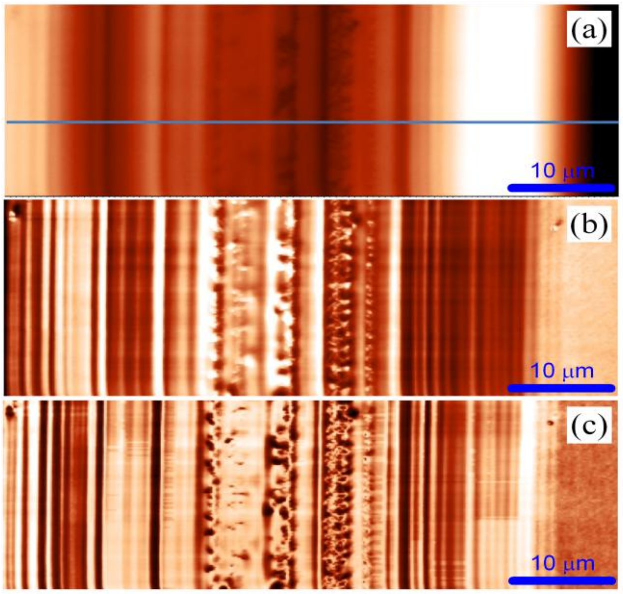

Figure 4.12 Simultaneously measured (a) topography (b) AFAM amplitude images at two different frequencies in which one is above the contact resonance frequency and (c) other is below the CRF

AFAM images also contain corresponding bright and dark bands aligned along the track direction as observed in topography. These bands with a range of contrasts in topography and AFAM images are attributed to inhomogeneous distribution of stress around the sliding interfaces. This is due to surface roughness of the ball. However, the observed contrast is found to be inversed when the imaging frequency is changed from the higher to lower CRF (Fig. **4.12b)**, **c)**). The rim of the wear track is found to be darker (brighter) when measured at frequency higher (lower) to CRF. This indicates that the wear track rim is softer than the pristine DLC and it could be related to the migration of a-C/*sp*^{2} clusters towards the rim of the track during sliding.[12]

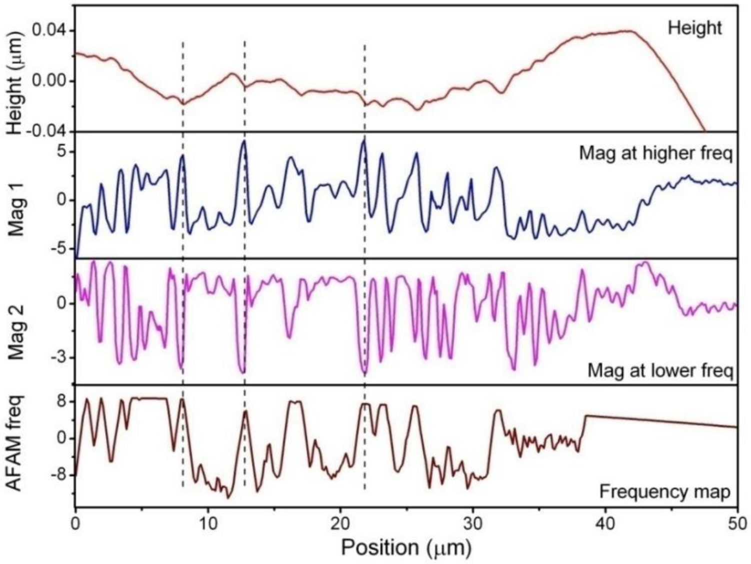

Figure 4.13 Line profile topography of (a) AFAM amplitude at higher to contact resonance frequency (CRF) (b) at lower CRF (c) and CRF for the wear track with sliding speed of 3 cm/s

To have a clear picture over the correlation between the topography and AFAM images, a line profile was measured along the line shown in topography (Fig. **4.13**). The CRF profile, which is directly proportional to the elastic modulus of the sample, is also shown in this plot. The plot contains vertical dotted lines to provide guideline to compare the different parameters at the same position. It clearly indicates that the valley features in topography exhibits higher AFAM amplitude. This means that the valley features possess higher CRF values. It is known that stress profile varies across tribo track due to deformation by shearing occurred between tribo-contact interfaces. The valleys in topography attributed to highly deformed zones. In the highly deformed region, the *sp*^{3} phase dominates which is evident from the Raman analysis and corresponds to stiffer regions of AFAM image.

4.3.5 Friction and wear mechanism

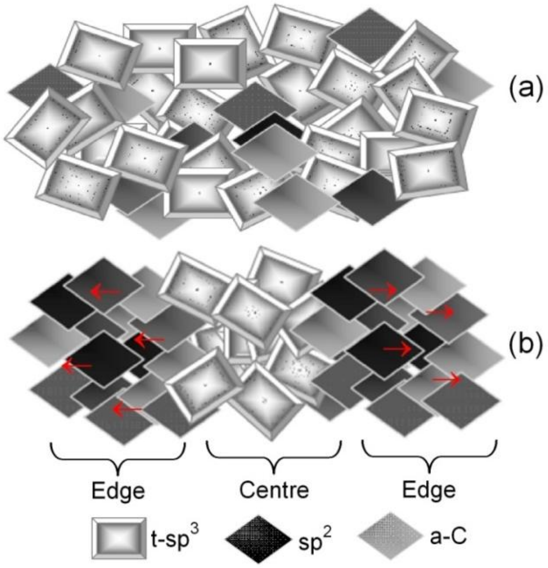

Figure 4.14 Schematic representation of sp^3 and sp^2 phase across the wear track at (a) less and (b) high sliding speed

Friction coefficient is found to decrease with increasing sliding speed and the average value reduces to ~0.05 at a maximum sliding speed of 3 cm sec^{-1}. In contrast, wear loss increases with the sliding speed. The results can be explained by chemical transformation of DLC phase which is influenced by the sliding speed. It is seen from the Raman spectroscopic results that I_D/I_G ratio does not increase very much at lower sliding speeds, which indicates insignificant conversion of sp^3 to sp^2 phase. This is clearly shown in Raman mapping image (Fig. **4.7**) and the results are presented in Fig. **4.8** and Fig. **4.9**. From the Raman analysis, it is shown that at lower sliding speeds, friction is mediated through sp^3 dominated phase. Based on the above analysis and inference a possible mechanism is shown in schematic (Fig. **4.14 a)**)).

Thus, the wear loss is small due to presence of stiffer sp^3 phase. However, at higher sliding speeds, sufficient thermal and kinetic energies are provided on the microscopic contact asperities leading to conversion of sp^3 into sp^2 phase.[9] Structural symmetry of sp^3 phase breaks down due to surface oxidation which is activated by thermal and kinetic energies. Broken symmetry tends to get minimum free energy states in order to form sp^2 phase. The sp^2 phase shear easily along the weakly interacting *c*-axis and gets removed layer by layer from the sliding zone and thus increasing the wear track dimensions (Fig. **4.4**). Surprisingly, at high sliding speeds, sp^2 phase does not exist in the centre of wear track and get relocated at the edge of the wear track leaving the central region of the wear track to be dominated by sp^3 phase. However, it does not mean that sp^2 phase is converted into stiffer sp^3 phase. It is understood that such a conversion needs extremely high activation energy, which is impossible in a tribo-sliding system used in the present study.[28] Assume the case if sp^2 phase is converted into the sp^3 at the centre of the wear track, then its accumulation at the edge of the wear track would not have appeared. Hence, it is clear that sp^3 phase converted into sp^2 in the centre of the wear track and migrated towards the edge during sliding (Fig. **4.14(b)**).[9] Here, the question can be raised that how the sp^2 phase is migrated to the edge of the wear track and how this migration process results in lower value of friction coefficient. First, the migration of the layered sp^2 phase is governed by stress and it normally moves from higher to lower stress region. It occupies the edge region of wear track where contact stress is less. Secondly, layered graphitized phase slides easily along the *c*-axis over each other thus the dissipation of frictional energy is less. However, at lower sliding speeds, the conversion of sp^3 to sp^2 phase is small as evident from I_D/I_G ratio. This phase is intact with sp^3 phase and does not find enough energy to slip and further restricted to migrate across the wear track. To check the role of transfer layer properties, a typical Raman spectrum was obtained from the Al_2O_3 ball scar (Fig. **4.15**).

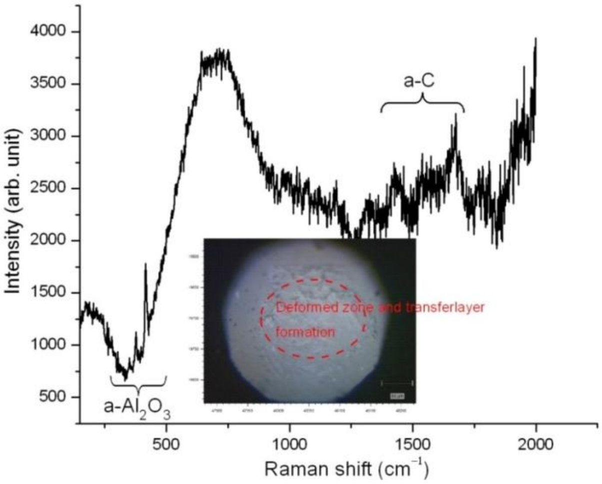

Figure 4.15 Raman spectra of ball scar showing evidence of a-C. In inset optical image of the scar is shown

For this analysis, the test condition was selected as given in Fig. **4.3 d)**. Raman spectra obtained from the ball scar shows couple of peaks around 375 and 416 cm^{-1} and these peaks are assigned to Al_2O_3 phase.[29] At high wave number region weak signature of a-C peaks are observed, indicating transfer layer formation.[1] This representing that scar developed on the ball contact is self deformation of Al_2O_3 ball and carbon transfer layer formation. This is shown in optical image of Fig. **4.15**.

4.4 Conclusions

Hydrogenated DLC films were grown on silicon (100) substrates by ECR-CVD technique. These films are a mixture of sp^2 and sp^3 bonding as evident from Raman and XPS analysis. Sliding speed dependent friction and wear properties of this film were investigated in ambient atmospheric and inert condition. In ambient condition, at lower sliding speeds, the friction coefficient was high while wear resistance was extremely high. In contrast, ultra-low friction coefficient and less wear resistance were observed at higher sliding speeds. This anomalous behavior of friction and wear was investigated using Raman and AFAM mapping across the wear tracks. At lower sliding speeds, sp^3 phase remains unaffected in the wear track and friction/wear is dominated by this phase. The harder sp^3 phase is the driving factor for extremely high wear resistance. However, at high sliding speeds, conversion of sp^3 to sp^2 is observed and this phase accumulated at the edge of the wear track due to stress driven migration. The layered sp^2 structure possesses ultra- low friction coefficient of ~0.05. However, wear loss is high because of the softness of the sp^2 phase, which is prone to easy attrition. Friction coefficient further decreased to 0.03 and 0.02. On the other hand the higher normal loads resulted in higher friction coefficient. This is due to the plastic deformation of the substrate occurs at higher contact pressures. Finally the film worn out at 8 N because the substrate gets cracked due to severe plastic deformation, it in turn caused the abrupt increase in friction coefficient. Moreover, the wear rate also increased by 2 to 3 orders with higher normal loads. This study brought out the significance of sliding speed and normal load and further correlated them with the physical and chemical transformations in controlling the friction behavior of DLC films.

4.5 References

1. J. Robertson, *Mater. Sci. Eng.* **2002**, R 37, 129.
2. A. Erdemir and C Donnet, *J. Phys. D Appl. Phys.* **2006**, 39, R 311.
3. C.A. Charitidis, *Int. J. Refr. Met Hard Mater.* **2010**, 28, 51.
4. J.W. Suk, *et al.*, *Carbon* **2012**, 50, 2220.
5. J. A. Heimberg, *et al.*, *Appl. Phys. Lett.* **2001**, 78, 2449.
6. J. Anderson, *et al.*, *Wear* **2003**, 254, 1070.
7. H. Meerkamm, *et al.*, *Int. J. Refr. Met Hard Mater.* **1999**, 17, 201.
8. A. M. Pfupfu, *et al.*, *Diamond Relat. Mater.* **2011**, 20, 1143.
9. H. Ronkainen, *et al.*, *Wear* **2001**, 249, 260.
10. Y. Liu, *et al.*, *Surf. Coat. Technol.* **1996**, 86–87, 564.
11. Y. Liu, *et al.*, *Surf. Coat. Technol.* **1996**, 82, 48.
12. A. A. Voevodin, *et al.*, *Diamond Relat. Mater.* **1996**, 5, 1264.
13. L. Cui, *et al.*, *Carbon* **2014**, 66, 259.
14. D. W. Kim and K. W. Kim, *Wear* **2013**, 297, 722.
15. L. Cui, *et al.*, *Tribol. Inter.* **2015**, 82, 195.
16. M. T. Bao, *et al.*, *Sci. Rep.* **2014**, 4: 3662.
17. B. Lichun, *et al.*, *J. Appl. Phys.* **2011**, 110, 33521.
18. A. Erdemir, *Surf. Coat. Technol.* **2001**, 146 –147, 292.
19. T. W. Scharf, *et al.*, *J. Appl. Phys.* **2007**, 101, 063521.
20. J.M. Jungk, *et al.*, *Acta Mat.* **2008**, 56, 1956.
21. F. Piazza, *et al.*, *Appl. Phys. Lett.* **2003**, 82 (3), 358.
22. X B Yan, *et al.*, *J. Phys. D: Appl. Phys.* **2004**, 37, 2416.

23. S. Kaciulis, *Surf. Interface Anal.* **2012**, 44, 1155.

24. A. C. Ferrari and J. Robertson, *Phil. Trans. R. Soc. Lond.* A **2004**, 362, 2477.

25. K. K. Madapu, *et al.*, *J. Raman Spectrosc.* **2013**, 44, 791.

26. U. Rabe, *et al.*, *Surf. Interface Anal.* **2002**; 33, 65.

27. U. Rabe, *et al.*, *Ultrasonics* **2000**, 38, 430.

28. W. Jian-Tao, *et al.*, *Phys. Rev. B* **2011**, 84, 12102.

29. M. Kadleikova, *et al.*, *Microelect. J.* **2001**, 32, 955.

5.1 Introduction

Chapter 5 details the *in-situ* doping of nitrogen into DLC films and its influence on mechanical and tribological properties of DLC films. Owing to its superior mechanical and wear resistance, DLC films are obvious choice of material for protective coating applications.[1-5] As discussed in chapter 3, ion energy and gas composition are the major components required to grow dense DLC films with high sp^3 content.[6] Almost all the growth methods adopted for synthesis of DLC films involve either high energy species or the ion energy increased by external means (substrate biasing).[1-3] High kinetic energies of the species during growth develops compressive stresses into DLC films.[6] These intrinsic stresses lead to catastrophic failure of these films in both cohesive and adhesive manner during their lifetime. Moreover, high residual stress limits the achievable film thickness. Above the threshold thickness, film buckles and ultimately delaminates from the substrate which further curtails its usage in various applications.[7]

Various approaches have been adopted to grow DLC films for reducing the residual stresses. Among which the most popular ones are thermal annealing and doping/alloying.[8-13] However, thermal annealing is proved to alter the chemical bonding as well as micro structure and thereby deteriorate the physical properties of the films.[8-11] Incorporation of metal or non metals into DLC matrix is found to be the right choice to achieve lower residual stresses and thus improving the film adhesion. Incorporation of wide range of heavy metallic elements namely, Ti, Cr, V, Nb, W, Cu, Al, Ag and Mo and lighter elements Si, S, P, F, O, N and B have been extensively studied.[12-22] Doped /alloyed DLC films exhibited improved properties like thermal stability, bio compatibility, electrical conductivity, wear resistance and ultra low friction coefficient. Among all the non-metallic dopants, nitrogen draws more attention because of its easy availability in ultra high pure gaseous state. Nitrogen doping is an effective way to modify the DLC film chemically due to its electronic structure. It forms C-N bonds and improves their mechanical properties, toughness and film-substrate adhesion.[12- 15] Nitrogen found to reduce the intrinsic compressive stresses in DLC films. In addition, electrical conductivity of DLC films also improved with nitrogen incorporation.[12-15] In this chapter, nitrogen dopant was incorporated into the DLC matrix. Influence of this incorporation on mechanical and tribological properties was studied.

5.2 In-situ nitrogen doping

In-situ nitrogen doping of the DLC films in this study were carried out by admitting high pure (99.999%) N_2 gas at flow rates of 0.5, 1.0 and 2.5 sccm into the process chamber along with the ultra high pure Ar (dilution gas) and CH_4 (source gas). During doping all other growth conditions were maintained constant as described in chapter 3. Doping of the films was carried out at a substrate biasing of -100V with a pulse frequency of 50 kHz. These films are designated as $B_{2-0.5}$, $B_{2-1.0}$ and $B_{2-2.5,}$ respectively.

5.3 Results

5.3.1 Topography and film thickness

Fig. **5.1 (a-d)** illustrates the AFM topography of nitrogen doped DLC films. It is evident that the films are uniform and smooth. The topography shows these films are featureless; it is a typical signature of the amorphous carbon network. The measured rms roughnesses of the films are found to be in the sub-nanometer range varying between 0.2 to 0.13 nm. The rms roughness of the DLC films reduced after nitrogen doping. However, the reduction is only 0.1 nm which is not very significant, but it confirms that ultra smoothness of DLC films is maintained even after incorporation of nitrogen into the DLC matrix.

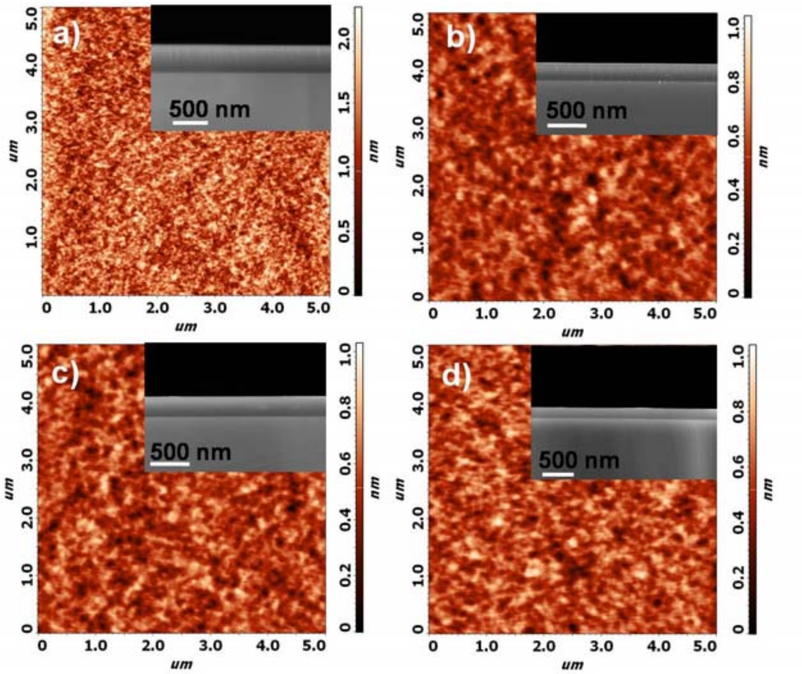

Figure 5.1 AFM topography of as grown and nitrogen doped DLC films at various nitrogen flow rates of (a) 0, (b) 0.5, (c) 1 and (d) 2.5 sccm

To evaluate the growth/etching rate of DLC films with nitrogen doping, the film thickness was measured using FESEM. Inset of Fig. **5.1** depicts the cross-section FESEM images of nitrogen doped DLC films. Cross- section FESEM imaging is carried out on the freshly cleaved surface of N-DLC/Si to obtain the film thickness. A significant decrease in film thickness from 475 to 200 nm upon nitrogen-doping is observed. This is attributed to the etching of DLC film by nitrogen ions/radicals during growth process.[12]

5.3.3 Raman spectroscopy

Fig. **5.2** shows the Raman spectra of nitrogen doped DLC films. A broad spectra spread over the range of 1000 to 1800 cm^{-1} in the Raman spectra is a typical signature of amorphous carbon materials.[23-25] The vibrational frequencies of solid carbon nitride are expected to lay very close to the modes of the analogous unsaturated CN molecules, which fall in the regime of 1000 – 1800 cm^{-1}. Thus, it is extremely difficult to assess from D and G bands whether an aromatic ring contains nitrogen.[24]

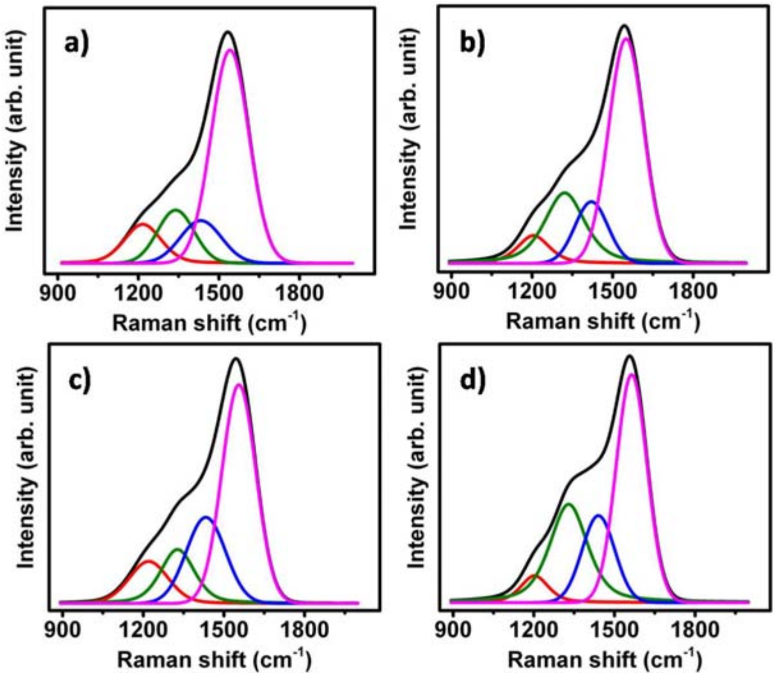

Figure 5.2 Raman spectra of nitrogen doped DLC films at various nitrogen flow rates of (a) 0, (b) 0.5, (c) 1 and (d) 2.5 sccm

Hence, both as grown and nitrogen doped DLC films possess similar features in Raman spectra over the range of 1000 to 1800 cm^{-1}. It is observed that Raman spectra consists of 4 major peaks around 1200, 1330, 1420 and 1550 cm^{-1}, respectively. The Raman peaks at 1330 and 1550 cm^{-1} correspond to the D and G modes of the graphitic carbon.[23-25] The D band is a zone edge A_{1g} mode activated by disorder and is due to breathing mode of sp^2 atoms in rings. Whereas the G band has E_{2g} symmetry and is due to bond stretching of pairs of C sp^2 atoms in both rings and chains.[23] Whereas other two peaks at 1200 and 1420 cm^{-1} correspond to TPA segment.[26, 27] Additionally, a noticeable raise in D peak intensity is evident from the Raman spectra. A detailed analysis of Raman spectra is carried out to obtain the most important structural parameters such as peak position, intensity and FWHM of G band and I_D/I_G ratios. Variations in all these parameters are illustrated in Fig. **5.3**. Nitrogen doping results a blue shift of G peak and its intensity also increased.

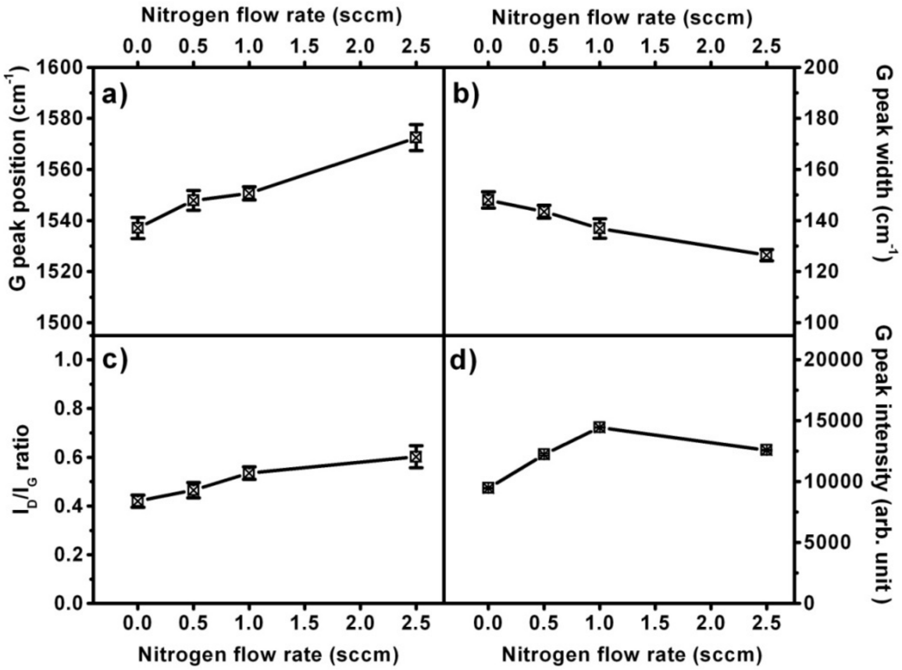

Figure 5.3 Raman parameter with N_2 flow rate (a) G peak position, (b) FWHM of G band, (c) I_D/I_G ratio and (d) intensity of G band

Both are related to the increase in graphitic phase in the system.[2] On the other hand, FWHM of G peak declines with nitrogen doping and it showed the clustering or ordering. The FWHM of G peak is the measure of ordering/disordering in graphite structure. Lower the FWHM higher the ordering or clustering.[23] In addition to this the I_D/I_G ratio also increased with nitrogen doping. It is also an indication for graphitization. All the observed facts are the signature of graphitization of DLC films resulted due to transformation of sp^3 into sp^2 bonding.

5.3.4 X-ray photoelectron spectroscopy

To confirm the doping and quantification of nitrogen in DLC films, XPS measurements were carried out. Fig. **5.4** depicts the XPS survey and deconvoluted C1*s* peaks corresponding to the nitrogen doped DLC films.

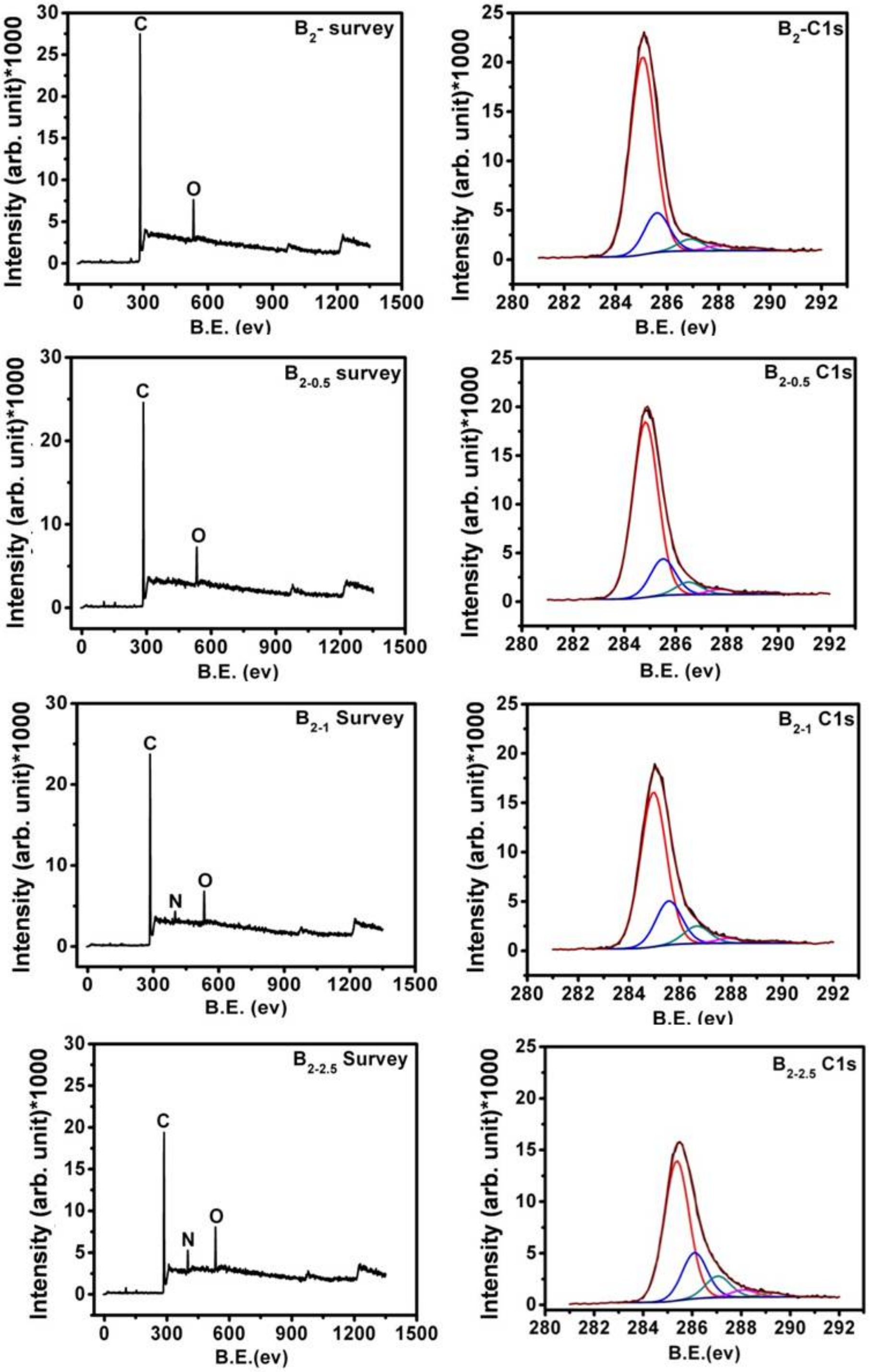

Figure 5.4 XPS survey spectra and C1s spectra of DLC films with different nitrogen concentrations such as 0, 0.5, 1 and 2.5 sccm, respectively

The survey spectra of the films showed that the film surface contains oxygen and nitrogen in B_{2-1} and $B_{2-2.5}$ film. The $C1_s$ peaks of the films were deconvoluted into five peaks ~284.8, 285.7, 286.6, 287.5 and 289.6 eV corresponding to sp^2, sp^3, C-O, C-N and OH-C=O, respectively.[14, 28] The analysis shows that the highest C-N bonding fraction is present in $B_{2\text{-}2.5}$ film. This corroborates well with N_2 flow rate which is highest in $B_{2\text{-}2.5}$ film and therefore, it is plausible to form C-N bonding. In fitting, peak width and position of low intensity peaks are tentative. C1s spectra showed that the surface of all the films is dominated by sp^2 bonding. However, the area under the curve corresponding to binding energy of 285.6 eV increases with nitrogen incorporation, which indicates an increase in sp^3 fraction.

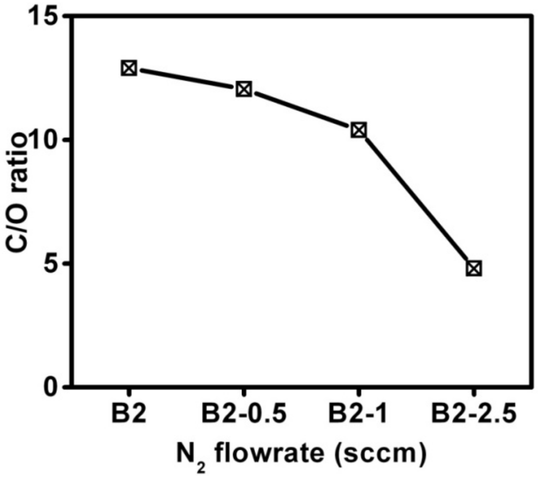

Figure 5.5 C/O ratio of nitrogen doped DLC films

Carbon to oxygen ratio was obtained from the area ratios of C1*s* to O1*s* peaks. The C/O ratio *vs* nitrogen flow rate is shown in Fig. **5.5**, which clearly showed that oxygen concentration increases with the incorporation of nitrogen into the film. It is discussed earlier that increase in dangling bonds in sp^3 network at the surface enhances oxygen absorption. From the Raman analysis, it is clear that the film become more disordered with the incorporation of nitrogen. The disordered sites are highly energetic and absorb oxygen easily. Small fraction of oxygen impurities in nitrogen gas is the other possibility for introduction of oxygen into film. Surface adsorption of atmospheric oxygen and water vapor cannot be neglected.

5.3.5 Film density and hydrogen content

Film density and hydrogen content of the DLC films are crucial in determining its physical properties. RBS is used to obtain the film density after the nitrogen doping. RBS measurements shown in Fig. **5.6 a)** confirm the continuous reduction in film density with nitrogen doping. The measured values of film density are fallen from 2.1 to 1.4 g/cc for pristine to highly doped film. The reduction in film density is attributed to the structural changes as observed in Raman spectroscopy analysis.[13]

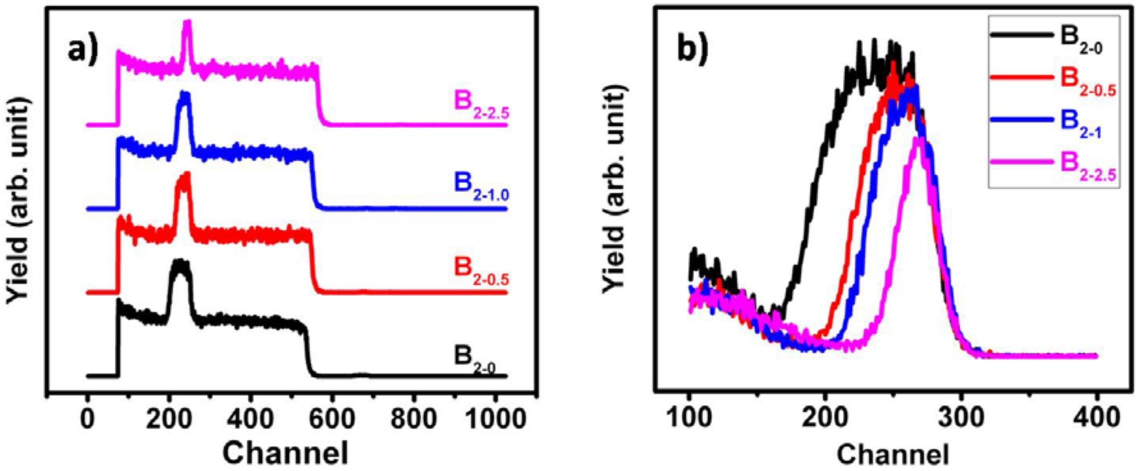

Figure 5.6 a) RBS and b) ERDA spectra of nitrogen doped DLC films

On the other hand hydrogen content of the films monotonically reduces with nitrogen incorporation as shown in Fig. **5.6 b)**. The values are tabulated in table-5.1. This is attributed to the structural transformations occurring due to nitrogen incorporation. Nitrogen replaces the H in C-H and form C-N bonding. It further causes reduction in hydrogen content.[13]

5.3.6 AFAM analysis

In general doping of metal or nonmetal of DLC films causes structural transformations which can lead to elastic inhomogenity in the films. AFAM was employed to check elastic inhomogenity and change in elastic modulus of the DLC films caused by nitrogen doping.

Fig. **5.7 a) to e)** show the CRF mapping of standard Si (100) as grown and nitrogen doped DLC films at different flow rates.

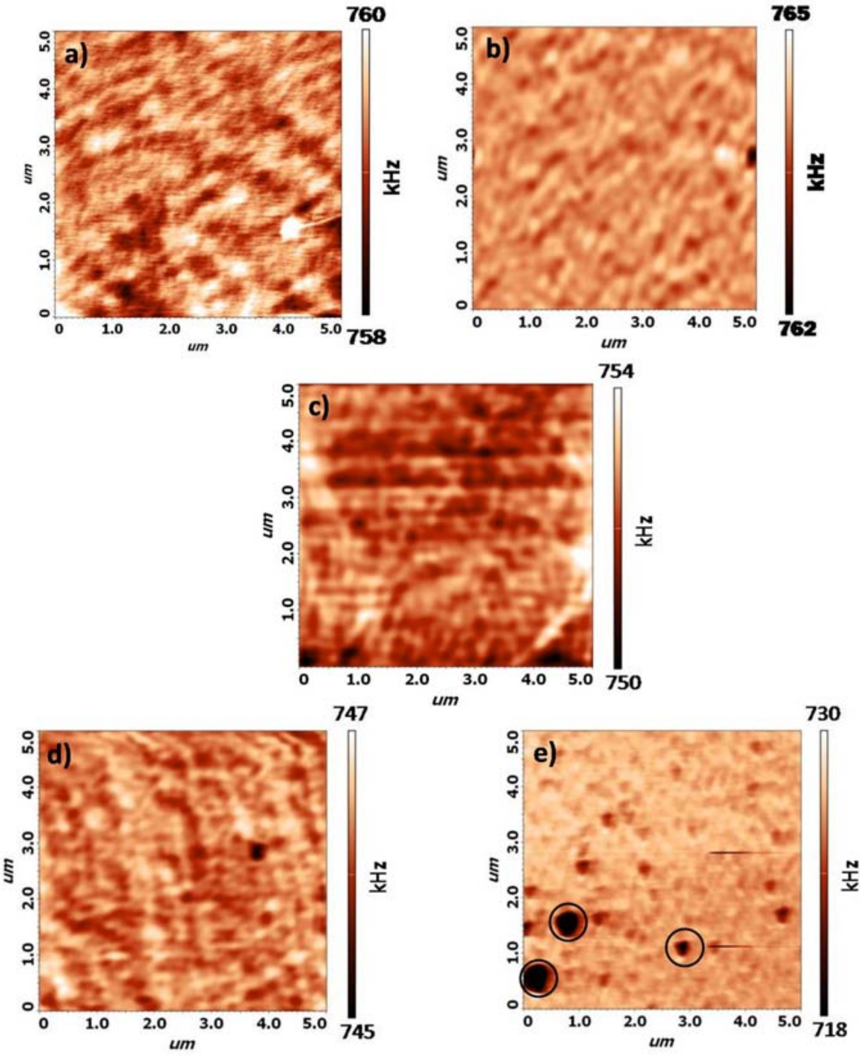

Figure 5.7 CRF mapping of various sample surfaces a) Si (100) substrate, b) as grown B_{2-0}, c) $B_{2-0.5}$, d) $B_{2-1.0}$ and e) $B_{2-2.5}$

The CRF mapping shows that the doped samples have homogeneous elastic modulus. As the nitrogen concentration increases, an evolution of second phase is evident. Further, increase in nitrogen concentration increases the clusters size in lateral dimension and also aerial density. The black circles drawn in Fig. **5.7 e)** indicate second phase in nitrogen doped DLC films. These observations indicate that the increase in nitrogen concentration in DLC film leads to formation of second phase. The corresponding CRF mapping of these samples revealed that elastic modulus of second phase is lower than the matrix and it is clear from the Fig. **5.7**. The CRF value of standard Si (100) substrate is 760 kHZ. The as grown DLC films possessed CRF value higher than that of the Si substrate. This indicates that as grown DLC film is harder than the Si substrate. On the other hand the CRF values continuously reduced with the nitrogen concentration confirms softening of DLC films with nitrogen incorporation. This is attributed to the structural transformation or graphitization observed in Raman spectroscopy studies. Based on the CRF mapping, statistical analysis is carried out to extract the CRF for a particular sample.

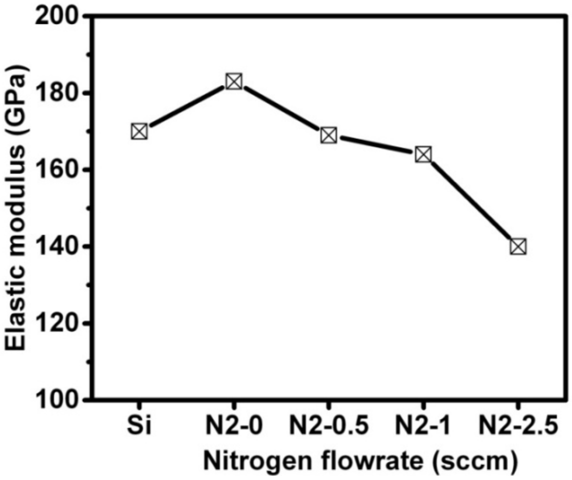

Figure 5.8 Calculated elastic modulus of nitrogen doped DLC films

The CRF values are converted into elastic modulus using equations given in AFAM part of the chapter 2. The E of Si (100) is taken as 170 GPa for the calculations. Fig. **5.8** shows the variation of elastic Modulus of the DLC films as a function of nitrogen flow rate. The reduction in E can be attributed to the increase in C=C *sp*^{2} bonding in the films with N concentration as evidenced from Raman, RBS and ERDA measurements.

5.3.7 Tribology studies

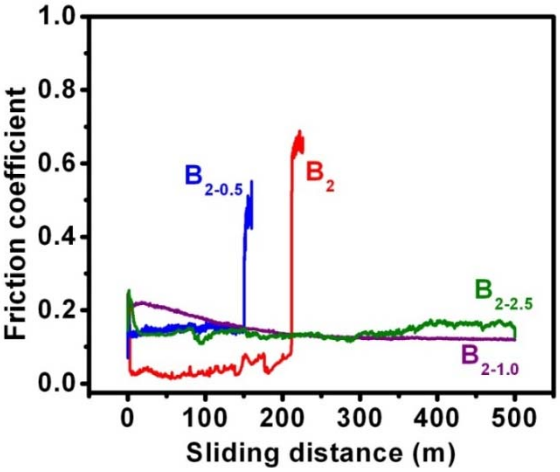

Figure 5.9 Friction coefficient of nitrogen doped DLC films

The influence of nitrogen doping on the DLC films on its tribological properties is evaluated by measuring the friction coefficient and wear rate by using ball on disc tribo meter. Details of the measurement are given in the chapter 2. These measurements were carried out with a 6 mm Al_2O_3 ball under 1 N normal load and 3 cm/sec sliding speed for a length of 500 meters. These tests were conducted in ambient atmosphere with relative humidity of 72%. Fig. **5.9** shows the variation in friction coefficient of nitrogen doped DLC films. The as grown film B_2 shows very low friction coefficient but it fails after sliding distance of ~ 200 m. The $B_{2-0.5}$ film shows an increase in friction coefficient and this value abruptly increased after sliding distance of ~150 m. This is due to reduction in film thickness which occurs with the nitrogen incorporation. On the other hand the films B_{2-1} and $B_{2-2.5}$ did not showed any abrupt change in friction coefficient even up to 500 m of sliding distance though the film thickness is much less. It is reported that nitrogen incorporation into DLC enhances its toughness which delays the failure. Therefore, even with lower film thickness these films could withstand for longer sliding distances. However, they exhibited higher coefficient of friction. This is attributed to decrease in sp^2/sp^3 fraction and increase in oxygen concentration. Continuously reduction in C/O ratio, as shown in Fig. **5.8,** confirms the increase in absorbed oxygen content at the surface with nitrogen concentration. The previous results with change in bias discussed in chapter 3 established the effect of absorbed oxygen concentration on the friction coefficient. The XPS survey spectra also shows that the C/O ratio decreases with increase in nitrogen doping as shown in Fig. **5.8**. It shows that oxygen absorption increased with nitrogen concentration. Even though film thickness reduces, resistance to wear improved significantly with nitrogen incorporation as shown in Fig. **5.10**. Considerably lower wear rate of $B_{2\text{-}2.5}$ film was observed despite less thickness and lower density. Nitrogen induced hardening and enhanced compressive stress causing improvement in toughness of the film. This is one of the possible reasons which has been suggested in other reports.[12] The growth of N doped DLC films can also be explained by the sub-implantation model as in case of substrate biasing discussed in chapter 3. Since the films were grown at optimum bias -100 V they expected to attain the maximum density and higher sp^3 content. In general N makes bond with carbon in either σ (sp^3) or π (sp^2) configuration.[24] However, the C-N sp^2 bonding is more favorable than the former.[24] Incorporation of N forms C-N bonds by removing H from the C-H bonds. It further encourages formation of C=C sp^2 bonding, because H is required for cross linking of C to stabilize the sp^3 bonding state.[14, 25]

Once local C-N sp^2 bond is formed, it further grows as sp^2 cluster of larger size. Thus the amount of sp^2 content also increases with nitrogen concentration. Nitrogen also acts as a bridge for sp^2 domains and results in enlargement of sp^2 cluster size.[29] These facts clearly explains the significant raise of D peak in Raman spectra of nitrogen doped DLC films, which in turn related to the graphitization and *sp*^{2} clustering with nitrogen doping. In addition, N radicals usually chemically etch the growing film and thus reduction in film thickness with N concentration as shown in table-5.1.

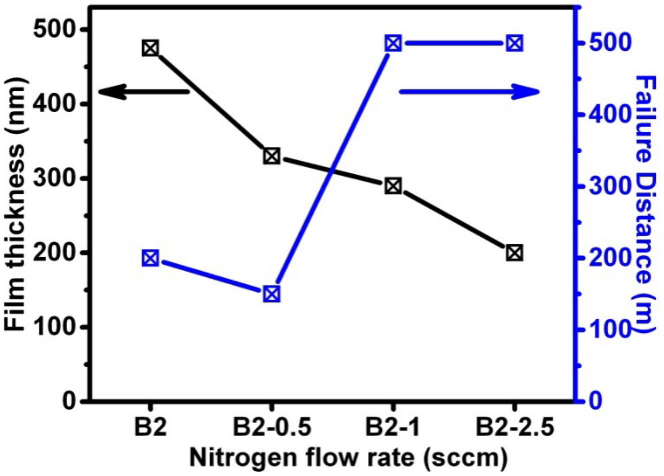

Figure 5.10 Film thickness and failure distance vs nitrogen flow rate

Table-5.1: Properties of nitrogen doped DLC films

Sample	Surface roughness (nm)	Film thickness (nm)	Film density (g/cc)	H_2 content (%)	ID/IG ratio	G peak position (cm^{-1})	G peak width (cm^{-1})	Wear rate (mm^3/Nm)
B_2	0.14	475	2.1	22	0.404	1541.6	158.8	1.6×10^{-7}
B_2-0.5	0.12	330	1.9	19	0.465	1547.9	143.46	3.0×10^{-8}
B_2-1	0.12	290	1.6	17	0.535	1550.6	136.92	5.6×10^{-9}
B_2-2.5	0.13	200	1.4	15	0.602	1573.1	126.46	3.0×10^{-7}

Thus, the film density and H concentration decrease with increase in N concentration in the films. This observation is consistent with the sub-implantation growth model. The changes in the structural properties due to nitrogen doping are also reflected by the formation of secondary phase shown in Fig. **5.7**. Generally, the film with higher C-C sp^3 bonding has higher resistance to deform in the elastic limit. The contact stiffness of the cantilever increases enormously for the films with higher elastic modulus. The local density and the type of C-C bonding decide the elastic modulus of the films. The observed elastic modulus of the films follows a direct correlation with the density and C-C bonding nature of the films. Moreover, chemical bonding, film density, hydrogen content significantly influenced the friction coefficient and wear resistance.

5.4 Conclusions

In-situ nitrogen doping of DLC films was carried out at by introducing nitrogen gas at different flow rates along with diluents Ar and CH4 gases. The quantitative XPS measurements showed that the nitrogen concentration varied with the flow rate. Raman spectroscopy and XPS results clearly show that nitrogen doping enhanced sp^2 bonding in the films. The film density and elastic modulus are found to be reduced with nitrogen concentration. It is corroborated well with the change in chemical bonding. N doping also encouraged the clustering of graphitic phase because nitrogen acts as bridge between sp^2 domains to coalesce as it is evident from both topography as well as elastic modulus mapping measurements. However, the graphitic clustering is taken place at lower voltages compared to the un-doped films. Although friction coefficient is observed to be increased with N doping but wear resistance increased by 2 orders.

5.5 References

1. J. Robertson, *Prog. Solid st. Chem.* **1991,** 21, 199.
2. J. Robertson, *Mat. Sci. Engg*. **2002,** *37*, 129.
3. A. Erdemir and C. Donnet, *J. Phys. D: Appl. Phys.* **2006**, *39*, 311.
4. J. Robertson, *Comp. Hard Mat.* **2014**, 3, 101.
5. A. Grill, *Diamond Relat. Mater.* **1999**, 8, 428.
6. Y. Pauleau, *et al., Springer*, **2008**, Chapter -4, 102.
7. B. K. Tay and P. Zhang, *Thin Solid Films*. **2002**, 420–421, 177.
8. H. Li, *et al., Thin Solid Films.* **2006**, 515, 2153.
9. A. C. Ferrari, *et al., J. Appl. Phys.* **1999**, 85(10), 7191.
10. T. A. Friedmann, *et al., Appl. Phys. Lett.* **1997**, 71 (26), 3820.
11. R. Kalish, *et al., Applied Physics Letters* **1999**, 74 (20), 2936.
12. D. Bootkul, *et al., Appl. Surf. Sci.* **2014,** *310*, 284.
13. M. K. Fung, *et al., Diamond Relat. Mater.* **1999**, 8, 472.
14. S. E. Rodil, *et al., Phys. stat. sol. A* **1999**, 174, 25.
15. M. Kaukonen, *et al., Phys. Rev. Lett.* **1999**, 83 (25), 5346.
16. L. Zhang, *et al., RSC Adv.* **2015**, *5*, 9635.
17. J. C. Sánchez-López, *et al., Springer*, **2008**, Chapter-12, 311.
18. M. Kaukonen, *et al., Appl. Phys. Lett.* **2005**, 87, 251918.
19. J. Vetter, *Surf. Coat. Technol.* **2014**, 257, 213-240.
20. Z. Wu, *et al., Appl. Surf. Sci.* **2012**, 258, 7918.
21. J. L. Endrino, *et al., Solid State Sci.* **2009**, 11, 1742.
22. P. Zhang, *et al., Diamond Relat. Mater.* **2004**, 13, 459.
23. A. C. Ferrari and J. Robertson, *Phil. Trans. R. Soc. Lond. A* **2004**, 362, 2477–2512.

24. A. C. Ferrari, *et al., Phys. Rev. B* **2003**, 67, 155306.

25. S. E. Rodil, *et al., J. Appl. Phys.* **2001**, 89 (10), 5425.

26. S. R. Polaki, et al., *Wear* **2015**, 338-339, 105.

27. F.Piazza, *et al., Appl. Phys. Lett.* **2003**, 82, 358.

28. P. K. Chu and L. Li, *Mat. Chem. Phys.* **2006**, 96, 253.

29. S.F. Yoon, *et al., Thin Solid Films* **1999**, 340, 62.

6.1 Introduction

This chapter deals with environmental effects on tribological characteristic of DLC films. The term DLC is a generalized name for a set of amorphous carbon structures such as a-C, ta-C and their hydrogenated counterparts a-C:H, ta-C:H. Moreover, it is found that no two types of DLC films have similar physical or chemical characteristics.[1-3] All the four variants differed by the amount of sp^3 bonding and hydrogen content. One of important properties of DLC includes extremely low friction coefficient and high wear resistance.[3,4] It is understood that friction coefficient and wear resistance of any material are related to chemical bonding, composition and microstructure. DLC is a mixture of sp^2 and sp^3 bonding and the ratio of these two carbon hybridized phases can be tuned by controlling the growth conditions. Moreover, the hydrogen content in DLC films inevitable when growth is carried out by chemical vapor deposition techniques.[3] The effect of sp^3/sp^2 ratio and hydrogen content on the tribology as well as other properties of DLC films is extensively studied.[5-10]

In addition to inherent parameters as discussed in previous chapters a research activity was carried out in the area of finding out the role of external factors influencing the tribological properties of DLC films. A few external factors such as surface chemistry, surface roughness, test environment and counter body are also found to be most influential on friction and wear rate of DLC films.[10-20] In general, DLC film surface either left with free dangling bonds or saturated with the hydrogen atoms/molecules depends on the type of DLC films and growth process.[6, 20] Due to unique covalency of carbon atoms in sp^2 and sp^3 hybridized state, the DLC films with dangling bonds easily interact with reactive gases and water vapor.[20] Thus the hydrogenated DLC film possess ultra low friction coefficient in vacuum and in inert atmosphere.[14] On the other hand, hydrogen free DLC film showed low friction in humid atmosphere.[14] Such differences are explained by the interaction of carbon with adsorbed atoms/molecules, hydrogen content and surface chemistry. Inert and reactive gaseous atmosphere significantly influence the tribological behavior of DLC films due to surfaces reactivity, adsorption of gases and dangling bonds. In this chapter, tribological properties of DLC films in inert and reactive gaseous mediums were investigated. Quantification of chemical structure of DLC films, surface chemical composition and adsorption of gases was investigated for meaningful correlation with friction and wear of DLC films.

6.2 Film preparation and measurements

For this study, two different types of DLC films were deposited. One is as-deposited DLC film designated as $B_{2\text{-}0}$ and other one is in-situ nitrogen doped DLC film designated as $B_{2\text{-}1}$ film. The details of synthesis and characterization results of these films were given in chapter 5. This study is carried out to evaluate the effect of oxygen as well as test environment on the friction and wear characteristics of DLC films. During the tribology test, the test chamber was purged with desired gases and flow rate was controlled to maintain the humidity level. In this study, friction and wear stabilities were evaluated under various tribology test atmospheres such as ambience, Ar, N_2, CH_4 and O_2. All the four gases used are ultra high pure (99.999%) to avoid any unwanted impurities. The mechanism of friction and wear in these atmospheres were extensively explored using surface analytical tools such as XPS and depth resolved AES. The sliding speeds and load were kept constant at 3 cm/s and 1 N, respectively. A stroke length of 3 mm was fixed for all the measurements. In ambient condition the relative humidity (RH) was approximately 75%. However, RH was kept below 25% during tribology test conducted amidst gaseous media (Ar, N_2, CH_4 and

O_2). We used mechanical stylus profilometer to obtain the wear volume. Wear rate was calculated based on wear volume analysis.

6.3 Results and discussion

6.3.1 Morphology of wear tracks

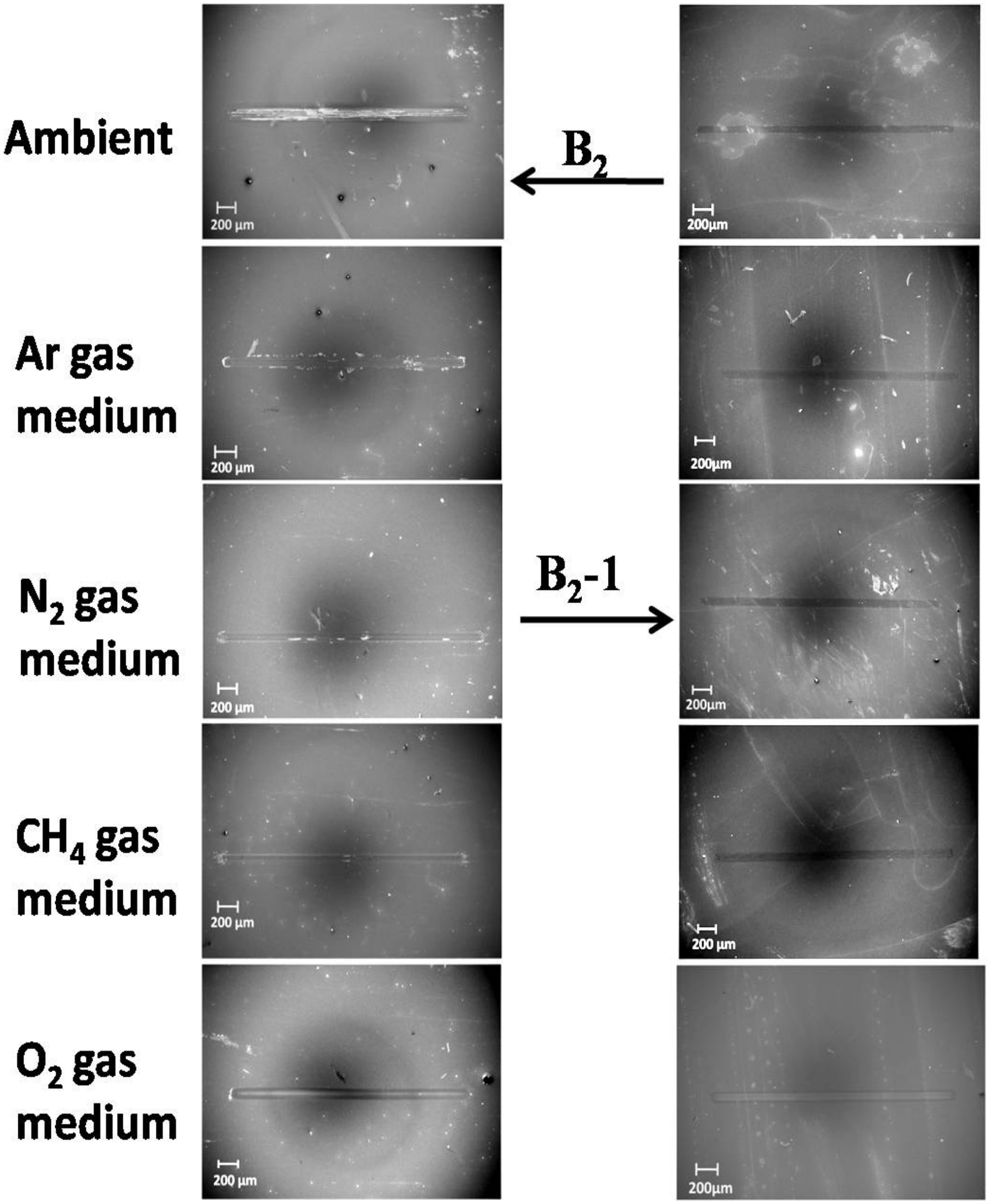

Figure 6.1 FESEM images of wear tracks on DLC film tested in various gaseous medium

The FESEM images of the wear tracks on as grown (B_{2-0}) and nitrogen doped (B_{2-1}) DLC films under different gaseous media are shown in Fig. **6.1**. The as grown (B_{2-0}) DLC film when tested in ambient conditions showed a significant damage, adhesive failure, large scale scratches and subsurface deformation. Interestingly, nitrogen doped film showed lowest wear and mechanical damage of DLC film while tested in ambient condition. Both the films showed inconspicuous deformation in nitrogen, methane and Ar atmospheres. In the presence of oxygen medium, wear and the damage of both these films seem to be increased, especially in case of B_{2-0} film. However, the nitrogen doped film seems to be more wear resistant with smaller wear track widths.

6.3.2 Raman spectroscopy studies

Fig. **6.2** illustrates the Raman spectra obtained inside the wear tracks on B_{2-0} and B_{2-1} tested under different gaseous medium. Raman spectra composed of broad spectra over 1000 to 1800 cm^{-1} as discussed in the previous chapter 3 and it confirms the growth of DLC films.

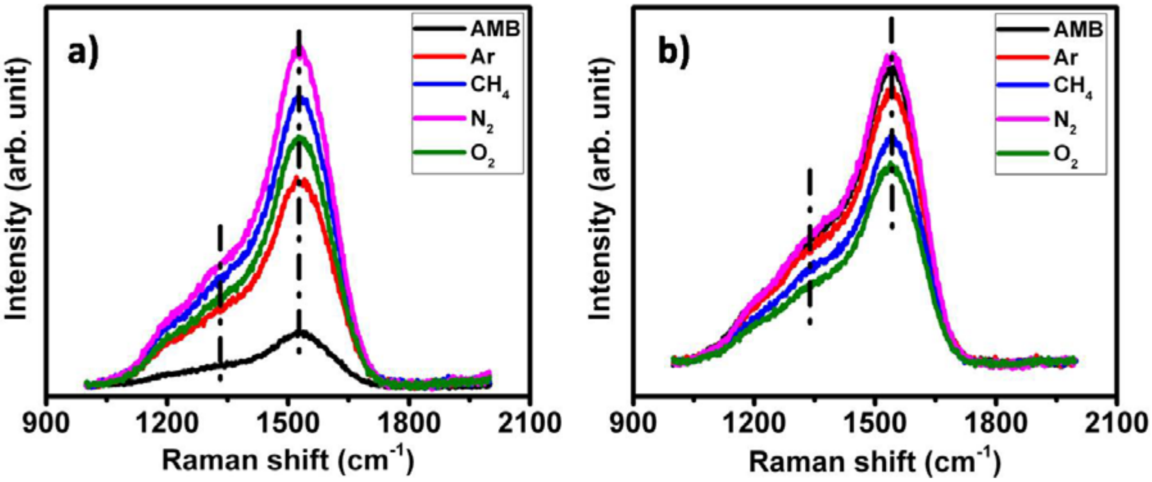

Figure 6.2 Raman spectra of wear tracks under different gas medium a) B_{2-0} b) B_{2-1}

To obtain the detailed information about chemical structure, the Raman spectra deconvoluted and fitted with four peaks. The Raman spectra acquired inside wear track does not show much difference with the bulk film surface showed in chapter 5. The I_D/I_G ratio and G peak position inside wear tracks of the films B_{2-0} and B_{2-1} tested in different gas medium are illustrated in Fig. **6.3**. The I_D/I_G ratio varied from 0.25 to 0.35 in B_{2-0} film with lowest and highest values correspond to Ar and O_2 medium, respectively. G peak position also varied but it is too small to draw any conclusion. On the other hand in case of B_{2-1}film, I_D/I_G ratio is between 0.3 to 0.35 and the G peak position varied from 1550 to 1555 cm^{-1}. The variations are too small to conclude significant changes in chemical structure. This shows that no significant change in chemical structure is observed due to change in gas medium during wear. However, significant variation in wear rate is evident from Fig. **6.1**.

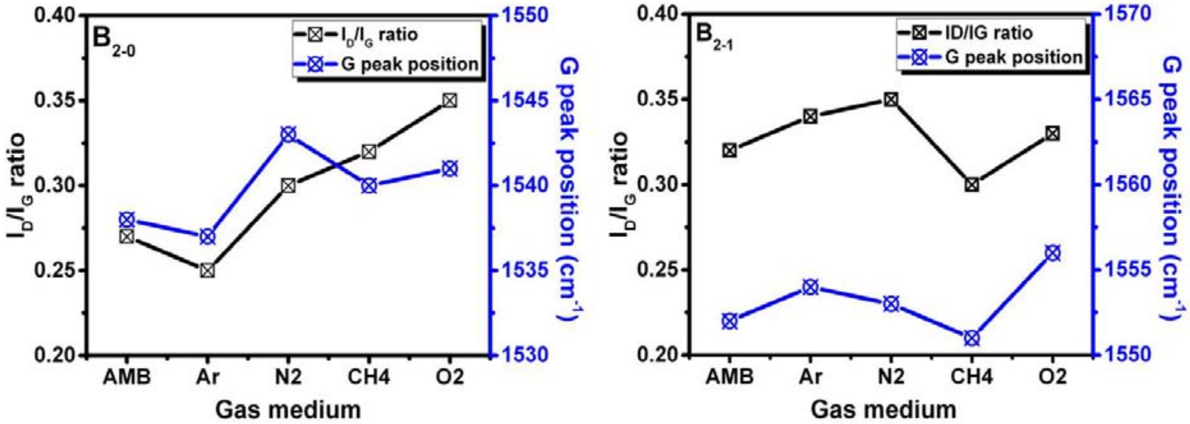

Figure 6.3 I_D/I_G ratio and G position inside wear track of B_{2-0} and B_{2-1} films tested in different gas medium

6.3.3 Tribology studies in different gas medium

As grown (B_{2-0}) and nitrogen doped DLC film (B_{2-1}) were selected for tribological tests under different gaseous atmosphere (Fig. **6.4**). A significant difference in friction coefficient is observed among these films and it is attributed to the difference in absorbed oxygen content. The details are discussed in chapter 5.

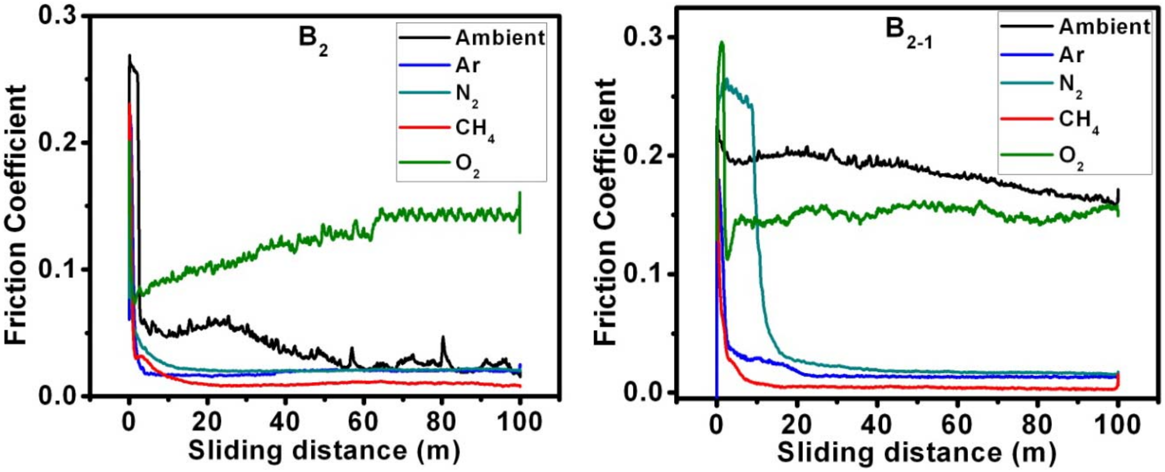

Figure 6.4 Friction coefficient of B_{2-0} and B_{2-1} films in different gas medium

Further reduction in friction coefficient is observed for both these films when the tribology tests were conducted in the presence of the gases such as argon, nitrogen and methane. Surprisingly both the films exhibited super low value of friction coefficient in methane gas medium. This is attributed to the passivation of the dangling bonds by the hydrogen, liberated due to the dissociation of methane at the contact interface.[21-23] Hydrogen passivation of dangling bonds interrupts the π-π* interaction and increases the electrostatic repulsion, dominated by weak van der Waals forces between the contact surfaces. These surface chemistry phenomenon of interfaces results in low friction coefficient.[24-26] Nitrogen and argon gases are inert but they prevent the exposure of the film surface to oxygen and moisture. Therefore, in these conditions, the low friction and wear is controlled by inherent chemical nature of hydrogenated DLC films where intrinsic hydrogen species provides contact passivation.[27]

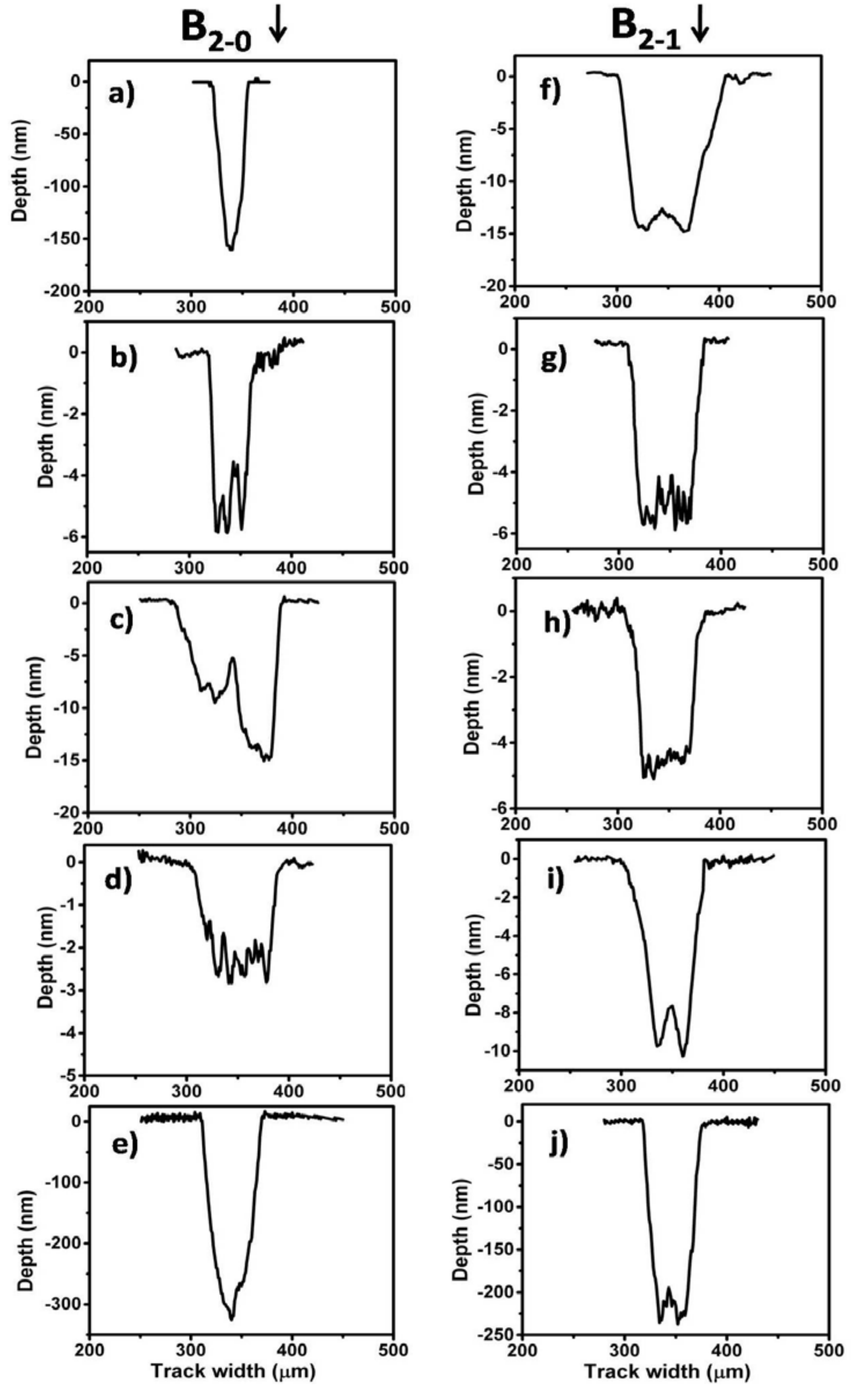

Figure 6.5 Wear track profiles of both B_{2-0} and B_{2-1} DLC films at different medium such as ambient (a, f), argon (b, g), nitrogen (c, h), methane (d, i) and oxygen (e, j)

In contrast, friction coefficient of both the films is high in the presence of oxygen. The oxygen is detrimental and destroys the ultra-low friction when DLC film is exposed to air and O_2 atmospheres.[28] Both these films exhibit reverse effect when tested in ambient atmosphere and this is due to the difference in C/O ratio. Reason behind the variation in friction coefficient with gas medium is described in the succeeding paragraph. The wear track dimensions measured by surface profilometer are illustrated in Fig. **6.5**. It is clear that the wear track depths significantly varied in both the films. Wear tracks corresponds to tests carried out in Ar, N_2 and CH_4 gases found too small with depths less than 10 nm implying that the wear is very small in these gas mediums for both the films. However, wear tracks corresponds to oxygen medium are high compared to all other. The wear track dimensions are well corroborated with the friction behavior shown in Fig. **6.4**.

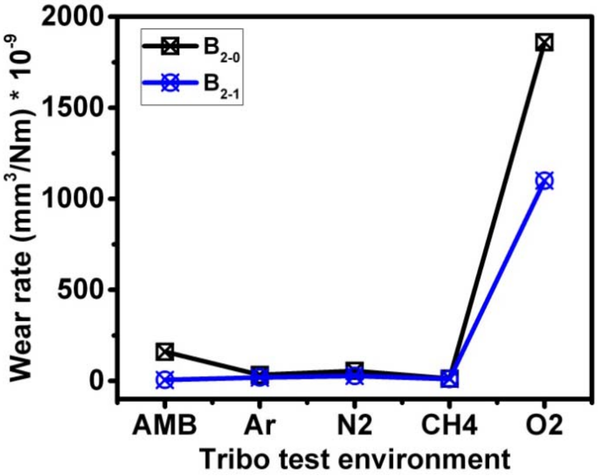

Figure 6.6 Wear rates of DLC films $B_{2\text{-}0}$, $B_{2\text{-}1}$ in different gas medium

The wear rates are calculated using the measured track dimensions and are showed in Fig. **6.6**. The wear rate measurements showed that the nitrogen doped DLC film has two orders lower wear rate than as grown one when tested in ambient conditions. This is attributed to the difference in absorbed substances at the film surface which has been discussed in chapter

5. It is clear that for both the films wear rates are reduced when tested in Ar, N_2 and CH_4 gas medium. On the other hand the O_2 medium enhanced the wear rate for both the films nearly ten times. This is attributed to the highly reactive nature of the carbon surfaces in oxygen environment.

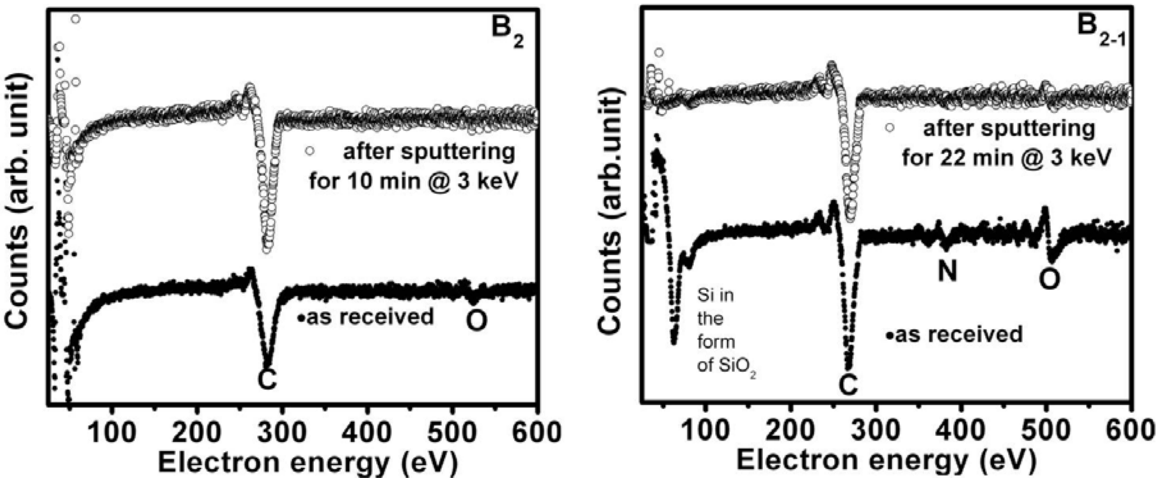

Figure 6.7 Auger spectra of the as grown ($B_{2\text{-}0}$) and nitrogen doped ($B_{2\text{-}1}$) DLC films

To define the contribution of oxygen contamination on friction and wear in DLC film, more realistic approach is needed. Therefore, depth resolved AES on the films $B_{2\text{-}0}$ and $B_{2\text{-}1}$ was carried out (Fig. **6.7**). In un-doped film, the oxygen was less on the surface and it was completely disappeared after 10 minutes of sputtering. However, the oxygen contamination is high on the nitrogen doped film and its presence persists even after sputtering for 22 mins. This is indicative of chemisorptive and diffusive ingress of oxygen into film matrix. The AES analysis confirms high oxygen adsorption in nitrogen doped film and it is well corroborated by XPS, which showed presence of high oxygen concentration on the surface of this film. Al peak is not observed in Auger electron spectroscopy, indicating absence of any physical contribution of Al_2O_3 into tribo-layer. Small amount of silicon in oxidized form is observed in nitrogen doped film and this must be originated from the substrate.

Fig. **6.8** shows schematic representation of the relaxation process of carbon networks in h-DLC film during wear test under different gaseous media. The as-grown films contain considerable amount of hydrogen as confirmed by ERDA. Film surface always has adsorbed oxygen and this is evident from XPS analysis. A representation of the surface bonding of the film in various gaseous media is also shown in the schematic (Fig. **6.8**). Under humid or oxygen medium, the absorbed oxygen react with C-H bonds and forms C-O-H and COOH under wear test condition.[20]

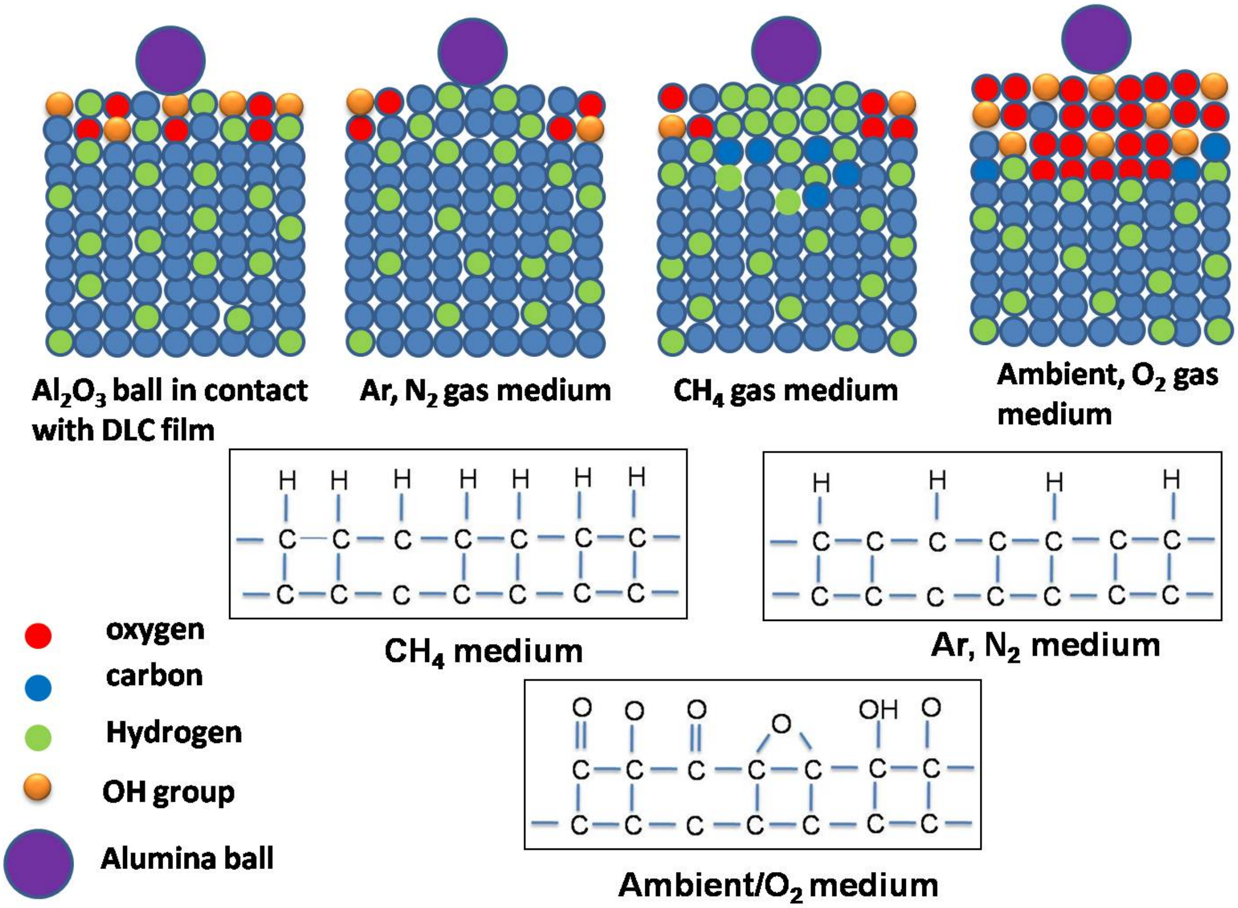

Figure 6.8 Schematic representation of bonding at the surface of the films

In such case, the surface becomes more electronegative due to the charge transfer from C and H to O atoms.[29] Hence, the increase in oxygen content decreases the electrostatic repulsive interaction between the surfaces which in turn destroy the low friction behavior. In contrast humidity enhances adhesion due to capillary force persists between the film surface and ball. This causes increase in friction coefficient. On the other hand, the friction coefficient of these films is found to be extremely low under inert gases such as Ar and N_2. Such inert gases eventually decrease the humidity in the system which could be correlated with the extremely low friction coefficient. Apart from humidity, the wear induced electrostatic charge on both film surface and alumna ball causes strong repulsion. The repulsive force reduces the shear strength of the contact that acts to lower the friction coefficient.[24]

6.4 Conclusions

Nearly vanishing friction coefficient (0.004) and ultra antiwear properties are observed in CH_4 atmosphere while friction coefficient slightly increased in Ar and nitrogen atmospheres. However, very high friction and high wear was observed in O_2 rich atmosphere and this effect was explained by segregation of oxygen species in contact interfaces. This was analyzed by depth resolved AES. The oxygen induces the defect in carbon network, destroying the low surface potential of sliding interfaces. However, super low friction coefficient in CH_4 atmosphere is attributed to surface reconstruction and passivation of carbon dangling bonds by hydrogen atom which is a dissociative species of CH_4 molecule. Investigations demonstrated the versatility of tribological properties of DLC films in various atmospheres and widened its range of applications.

6.5 References

1. A. C. Ferrari and J. Robertson, *Phil. Trans. R. Soc. Lond. A* **2004**, 362, 2477.
2. A. C. Ferrari and J. Robertson, *Phys. Rev. B* **2001**, 64, 075414.
3. J. Robertson, *Mat. Sci. Engg*. **2002,** 37, 129.
4. A. Erdemir and C. Donnet, *J. Phys. D: Appl. Phys.* **2006**, *39*, 311.
5. C. Donnet, *et al., Tribo. Lett.* **2001**, 9 (3), 137.
6. A. Erdemir, *Surf. Coat. Technol.* **2001**, 146 –147, 292.
7. J. Fontaine, *et al., Surf. Coat. Technol.* **2001**, 146 –147, 286.
8. A. Erdemir, *et al., Diamond Relat. Mater.* **2000**, 9, 632.
9. S. Yamamoto, *et al., Surf. Coat. Technol.* **2012**, 210, 1.
10. C. Donnet and A. Grill, *Surf. Coat. Technol.* **1997**, 94 – 95, 456.
11. H.I. Kim, *et al., Tribo. Lett.* **2006**, 21 (1), 53.
12. A. Erdemir, *Tribo. Int.* **2004**, 37, 1005.
13. J. Andersson, *et al., Surf. Coat. Technol.* **2003**, 163 – 164, 535.
14. H. Ronkainen, *et al., Wear* **2001**, 249, 260.
15. T. Le Huu, *et al., Wear* **1995**, 181 –183, 766.
16. C. Donnet, *et al., Surf. Coat. Technol.* **1994**, 68 – 69, 626.
17. Ala Alazizi, *et al., Langmuir* **2016**, 32, 1996.
18. J. Fontaine, *et al., Tribo. Int.* 2004, 37, 869.
19. S. J. Park, *et al., Diamond Relat. Mater.* **2003**, 12, 1517.
20. J. Andersson, *et al., Wear* **2003**, 254, 1070.
21. A. R. Konicek, *et al., Phys. Rev. B* **2012**, 85, 155448.
22. M.I. D. B. Bouchet, *et al., J. Phys. Chem. C* **2012**, 116, 6966.

23. Y. N. Chen, *et al., J. Phys. Chem. C* **2015**, 119, 16148.

24. L. Zhang, *et al., RSC Adv.* **2015**, 5, 9635.

25. S. Bai, *et al., J. Phys. Chem. C* **2012**, 116, 12559.

26. K. Hayashi, *et al., J. Phys. Chem. C* **2011**, 115, 22981.

27. J. D. Schall, *et al., J. Phys. Chem. C* **2010**, 114, 5321.

28. H. I. Kim, *et al., Tribo. lett.* **2006**, 21, 1, 53.

29. S. Dag and S. Ciraci, *Phys. Rev. B* **2004**, 70, 241401.

7.1 Introduction

Majority of research studies on DLC films are explored only for their mechanical properties.[1-3] Recently the focus has been shifted towards the surface modification methods for specialized applications such as self cleaning, super hydrophobic surface for anti fogging.[4-6] DLC films are ideal for bio transplants because of their mechanical stability, anti corrosion, anti wear in bio-aqueous medium makes it compatible to bio environments and that prevents side effect in cell growth.[7, 8] Increasing demand for DLC films in bio medical devices and bio sensors have grown due to its unique tunable wetting characteristics derived by surface chemical modification.[9-11] Developing DLC/diamond films with desired wettability characteristics in the range of hydrophilic to super hydrophobic is preferred for wide range of applications. Wettability is an essential property of materials and is influenced by both surface chemistry as well as surface topography.[12] It in turn alters the surface energy to achieve desirable wetting characteristics. Generally, the energy of diamond surfaces is tuned by hydrogenation, oxidation and surface termination by functional groups.[8, 13-15] This basically works on the principle of modified reconstruction and termination of dangling bonds. However, the long term sustainability of these surfaces in fluidic media is not reliable. Surface modification through doping is the other important method.[10, 13] Doping with atomic species alters bonding configurations and it reconstructs the surface chemistry.[8, 16] On the other hand, hierarchical structures created by micro or nano texturing on surface can also alter the wetting characteristics of the materials.[17] Advanced lithography to pattern the nanostructured surface is an useful technique. However, this is an expensive and involved complex processing method.[18] Plasma etching is another promising method to modify the surface both physically and chemically, which also creates hierarchical rough surface, suitable for functionalization.[13, 17 & 19] Mask less pattering array of nano rods or needle like structures on diamond surfaces by plasma etching is generated.[13] Wetting characteristics of plasma exposed films mainly depends on type of gas, plasma energy and time of exposure. Earlier studies showed that plasma exposed DLC films get functionalized with hydroxyl, carboxylic, carbonyl and nitrile groups which in turn influence the wetting characteristics.[19, 20]

The influence of surface chemistry on tribological properties of DLC films cannot be neglected. Tuning the surface chemistry and passivating unsaturated dangling bonds avoid strong adhesive interaction between mating parts and thus reduce the friction and wear. Recent studies showed that surface reactivity is mostly controlling the friction behavior and hydrogen terminated DLC films possessed ultra low friction coefficient.[21-24] Molecular dynamics and quantum chemical calculations carried out by Shandan Bai *et al.* showed that fluorine terminated DLC films results lower friction coefficient than the hydrogen terminated and it was explained by higher electronegativity of fluorine.[24] These studies showed the importance of surface chemistry in controlling friction behavior. However; controlled experimental studies are needed to support these theoretical models and to find out the practicality of such controlled studies.

In the present chapter, a novel post modification method of DLC film surface in hydrogen, oxygen and nitrogen plasma for various exposure time and energy (substrate biasing and microwave power) were investigated. Surface chemical reconstruction and physical changes of plasma exposed DLC surface was investigated by atomic force microscopy, Raman spectroscopy and X-ray photoelectron spectroscopy. Water contact angle of plasma exposed DLC film was correlated with modification of chemical and physical nature of surfaces. A model of contact angle variation of plasma exposed surface was proposed on the basis of chemical interaction of adsorbed chemical species and water droplet.

7.2 Plasma exposure and post exposure characterization of DLC surfaces

DLC films were exposed to hydrogen, oxygen and nitrogen microwave plasmas for surface modification. Plasma exposure studies were carried out in two set of conditions. In first case, the plasma exposure was carried out in 100 W microwave power with the variation of exposure time 10, 20 and 30 minutes. In second set of experiments, exposure time was fixed for 30 minutes and microwave power was varied as 100, 300 and 500 W. The films were designated as DX-1-1, DX-1-2, DX-1-3, DX-3-3, DX-5-3, where X indicates type of plasma i.e hydrogen (H), oxygen (O) and nitrogen (N). The first digit indicates microwave power (1-100 W, 3-300 W, 5-500 W) and the second digit indicates exposure time (1-10 minutes, 2-20 minutes, 3-30 minutes). Substrate bias assisted hydrogen plasma exposure of DLC films was also investigated. This has been carried out by applying substrate bias of -100 V during the exposure period for different exposure times such as 15, 30 and 60 mins. These samples are designated as S-15, S-30 and S-60, respectively.

The topography, surface roughness and film thickness were analyzed using AFM and FESEM, respectively. Chemical structure of plasma exposed films was investigated by laser Raman spectroscopy and XPS. Contact angle (CA) was measured and analysed by sessile drop method. Tribology studies were done as given in the previous chapters.

7.3 Results and discussion

7. 3.1 Topography and film thickness

Surface topography, chemical structure, and water contact angle of untreated DLC films are shown in Fig. **7.1**. It is evident that the untreated DLC film is uniform with rms roughness around 0.2 nm and thickness 450 nm. The influence of different plasma exposure on the topography of DLC film is illustrated in Fig. **7.2**. The vertically stacked images of DH, DO, DN refers to hydrogen, oxygen and nitrogen plasma with increasing exposure time and microwave power, respectively. At low microwave power, the topography shows fine feature of DLC surface which transforms into nano-granular morphology at higher microwave power and longer exposure time (Fig. **7.2**).

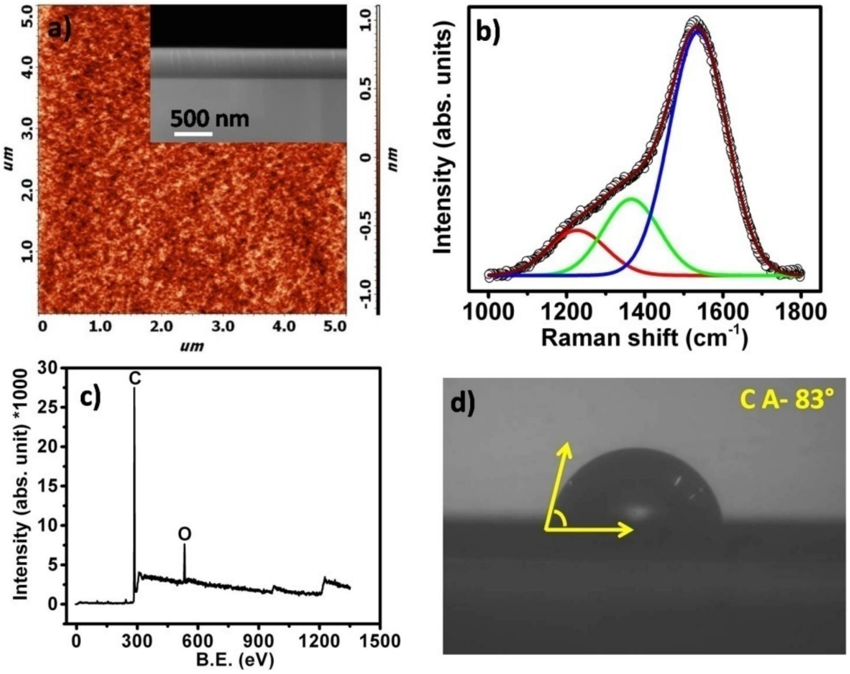

Figure 7.1 Surface topography, chemical structure and wetting characteristics of untreated DLC film: (a) AFM topography, (b) Raman spectra and (c) XPS survey spectra and (d) water contact angle

Moreover, morphological changes in oxygen and nitrogen plasma exposed films are significant at lower microwave power as illustrated in Fig. **7.2 (**DO) and Fig. **7.2 (**DN). This is attributed to the selective reactive plasma induced etching of the carbon network present in DLC films.[8, 20] The etching seems to be pronounced in case of oxygen in comparison to nitrogen and hydrogen plasmas. It is also evident that the change in surface topography becomes noteworthy feature upon plasma exposure at higher microwave power irrespective of the gaseous constituent present in plasma. At high power, chemical species present in microwave plasma diffuses further towards interior and interacts with subsurface region. Films exposed for 30 minutes in nitrogen plasma at 500 W power showed highest value of roughness. The corresponding cross section of FESEM image Fig **7.1** showed a reduction of film thickness with increase in exposure time and plasma power. Plasma exposure mainly involves recombination, etching and diffusion of atoms at the film surface.[19, 20] Surface diffusion reverses the surface roughness and it does not cause much reduction in film thickness. However, recombination and chemical etching alter the morphology, microstructure and bring about chemical transformation that causes significant reduction in film thickness.[19] Fig. **7.3** illustrates the reduction in film thickness with plasma exposure time and microwave energy. Film thickness reduces with exposure time as well as microwave energy irrespective of gas used. Reduction in film thickness is less in hydrogen plasma, moderate in nitrogen plasma and significant reduction is observed in oxygen plasma. This is attributed to the chemical etching caused by the plasma-surface interaction.[15, 19] Chemical etching is more severe in case of oxygen plasma than in hydrogen and nitrogen plasmas. This reduction follows the same trend as the topographical changes. At low microwave power and short exposure times the etching is insignificant. However, high energy leads to higher etching irrespective of the plasma gas used. At high microwave power, the ions are energetic so it causes re-sputtering from the film surface and in addition chemical etching exhibited by ion-surface recombination. Moreover, the chemical reactivity of energetic oxygen is always high and it easily adsorbs on film surface thereby initiating reaction with carbon atoms present at film surface. Therefore, reactivity of the gaseous ions and their energy determines the topography of the film surface upon plasma exposure.

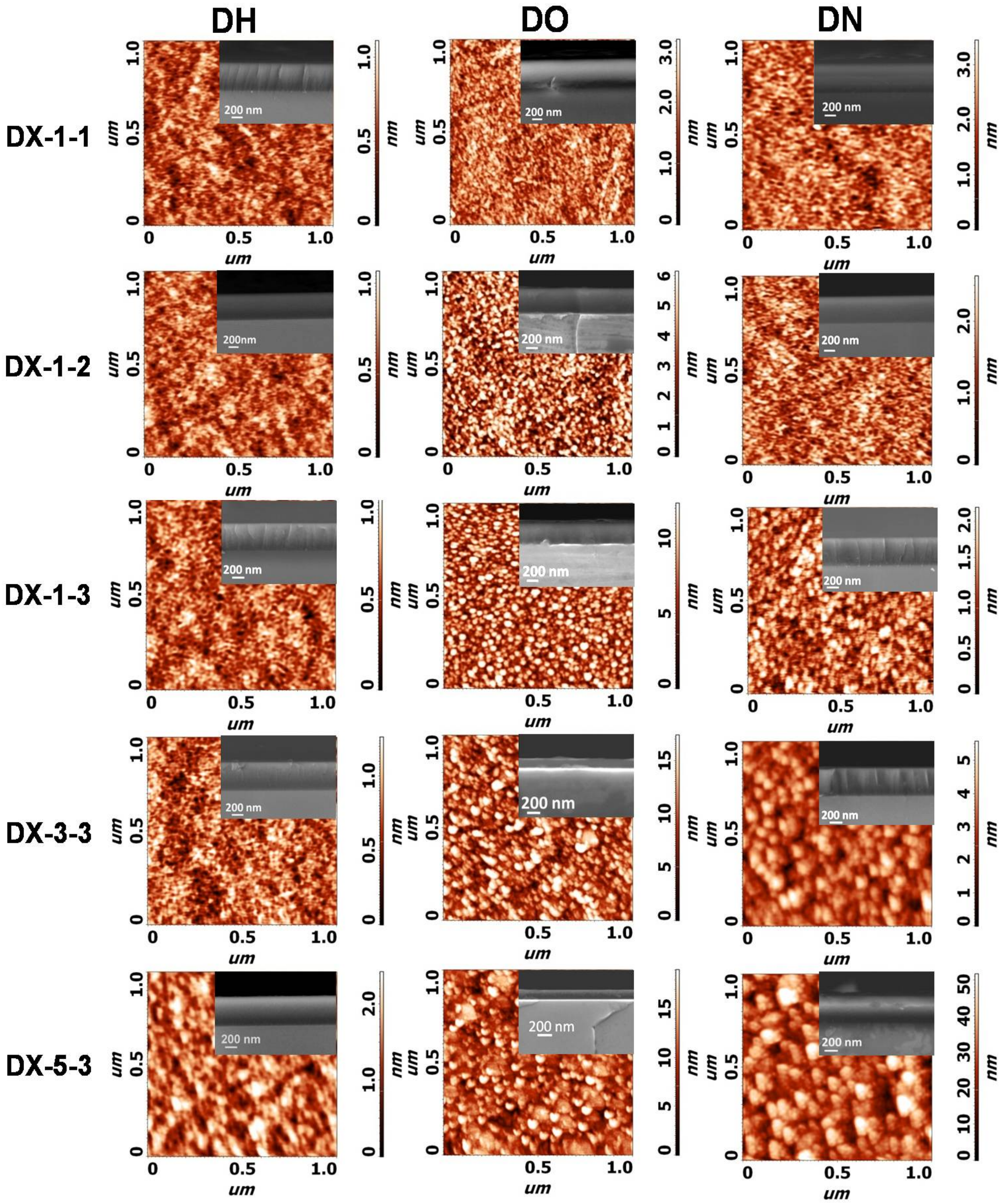

Figure 7.2 Surface topography of plasma exposed DLC films, inset in each image showed cross section of film thickness

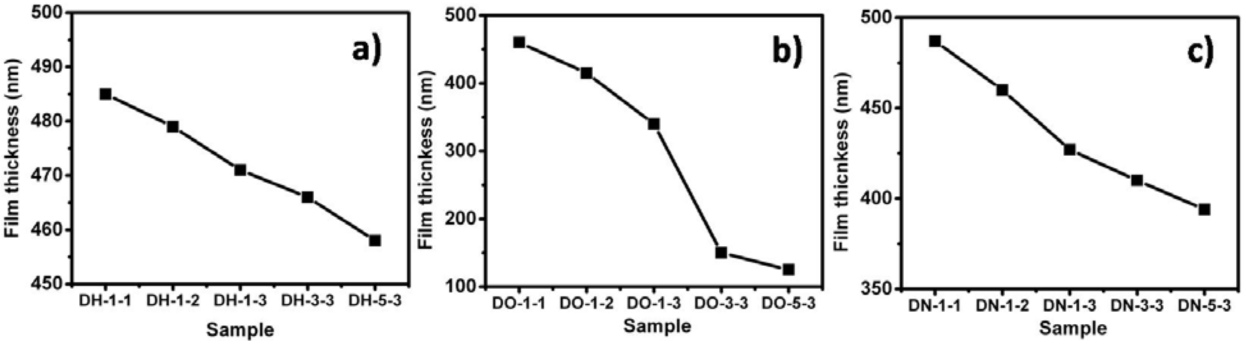

Figure 7.3 Film thickness of DLC films exposed to a) H_2, b) O_2 and c) N_2 plasmas

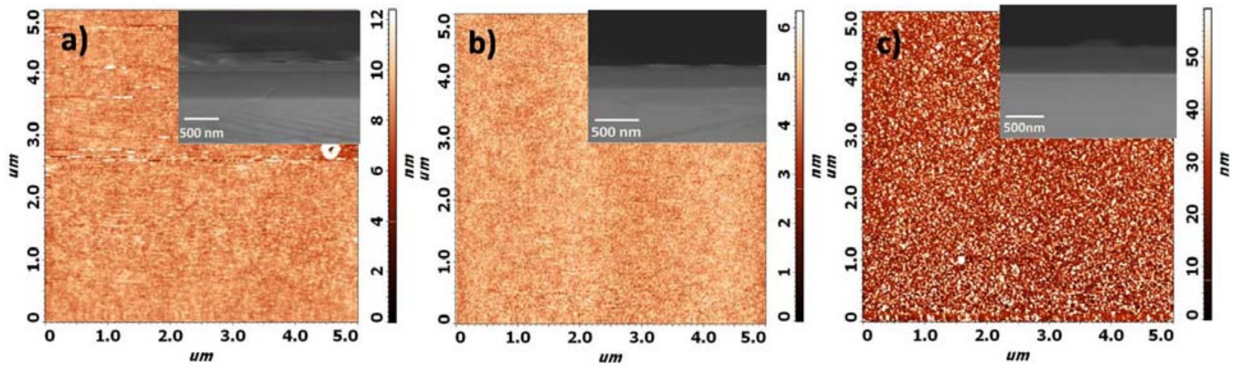

Figure 7.4 Surface topography of bias assisted hydrogen plasma exposed DCL films a) 15 b) 30 and c) 60 mins

The surface topography and corresponding cross section FESEM image of bias assisted hydrogen plasma exposed DLC films are given in Fig. **7.4**. It is clear that increase in surface roughness and reduction in film thickness occurred as the exposure time increases. Even with the substrate biasing the surface roughness at lower exposure times (15 and 30 mins) is insignificant. However, the reduction in film thickness seems to be significant it shows that the chemical etching is persisted might be at a lower rate. The values of roughness and film thickness are given in table-7.1.

7.3.2 Raman and X-ray photoelectron spectroscopy

Fig. **7.5** illustrates the Raman spectra of the plasma exposed films. The results show typical signature of the DLC. A broad band present in Raman spectra is deconvoluted into four major peaks positioned around 1200, 1320, 1430 and 1540 cm^{-1}. Two bands around 1200 and 1430 cm^{-1} correspond to TPA.[19] Peak shape and broadening of the curve is quite similar with no significant change in the Raman spectra of plasma exposed films. Fig. **7.6** depicts I_D/I_G ratio and G peak position of plasma exposed films. The I_D/I_G ratio of the DLC films exposed to hydrogen plasma continuously increased upto 0.37 against 0.24 for untreated film. This indicates graphitization of DLC film in hydrogen plasma exposure. G peak position shifts with exposure time and microwave power of hydrogen plasma. This trend is nearly similar to alteration in I_D/I_G ratio thereby establishing graphitization of t-aC structure. In general, hydrogen passivates the dangling bonds (DBs) at the surface and stabilizes sp^3 bonding.[15] Thus, the ratio of I_D/I_G is low while film is exposed for short time in low energy plasma. As the ion energy increases, the hydrogen becomes more energetic and percolates into the subsurface. Hydrogen ions also interact with sp^2 and C-H bonds. In the former case, it breaks the C=C bonds in graphite and stabilizes the sp^3 bonding. Whereas in the later case, it knocks out the H atom attached to carbon atom and causes formation of sp^2 phase, a process commonly known as hydrogen abstraction.[1] This is attributed to the increase in I_D/I_G ratio at high microwave energy. Conversely, oxygen plasma exposure always results in continuous reduction in I_D/I_G ratio and shift in G peak position. This is indicative of an increase in sp^3 bonding with increasing exposure time and microwave power. This is further attributed to preferential etching of sp^2 bonding, leading to enhance the sp^3 content. Nitrogen plasma exposure results in increase in I_D/I_G ratio and shift in G peak position which follows similar trend as depicted by hydrogen plasma. However, at higher microwave power, I_D/I_G ratio and shift in G peak position are reduced. At low plasma energy, C-N bonds are formed by substituting C-H bonds in DLC film.

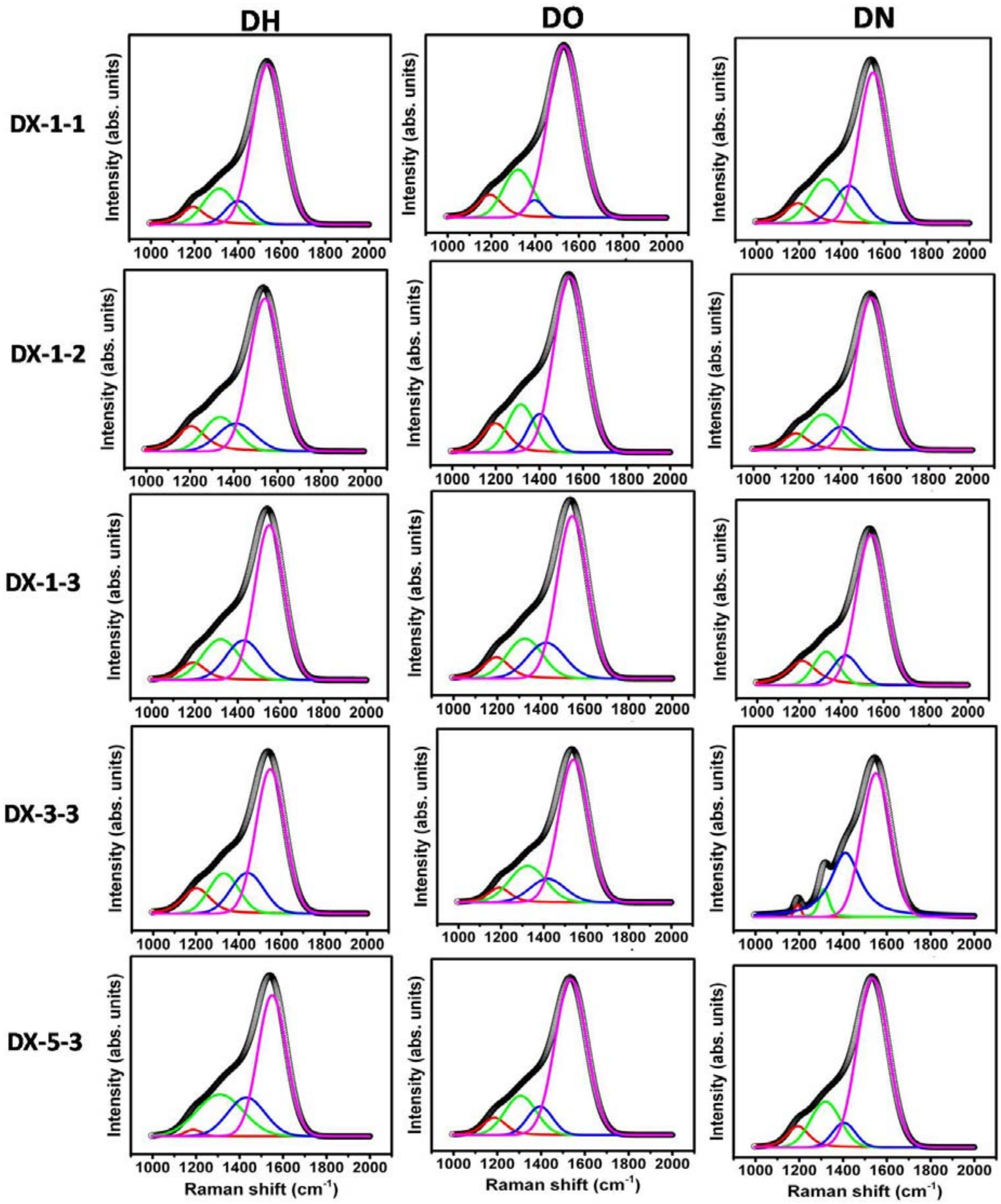

Figure 7.5 Rama spectra of plasma treated DLC films

(The films were designated as DX-1-1, DX-1-2, DX-1-3, DX-3-3, DX-5-3, where X indicates type of plasma i.e hydrogen (H), oxygen (O) and nitrogen (N). The first digit indicates microwave power (1-100 W, 3-300 W, 5-500 W) and the second digit indicates exposure time (1-10 minutes, 2-20 minutes, 3-30 minutes).

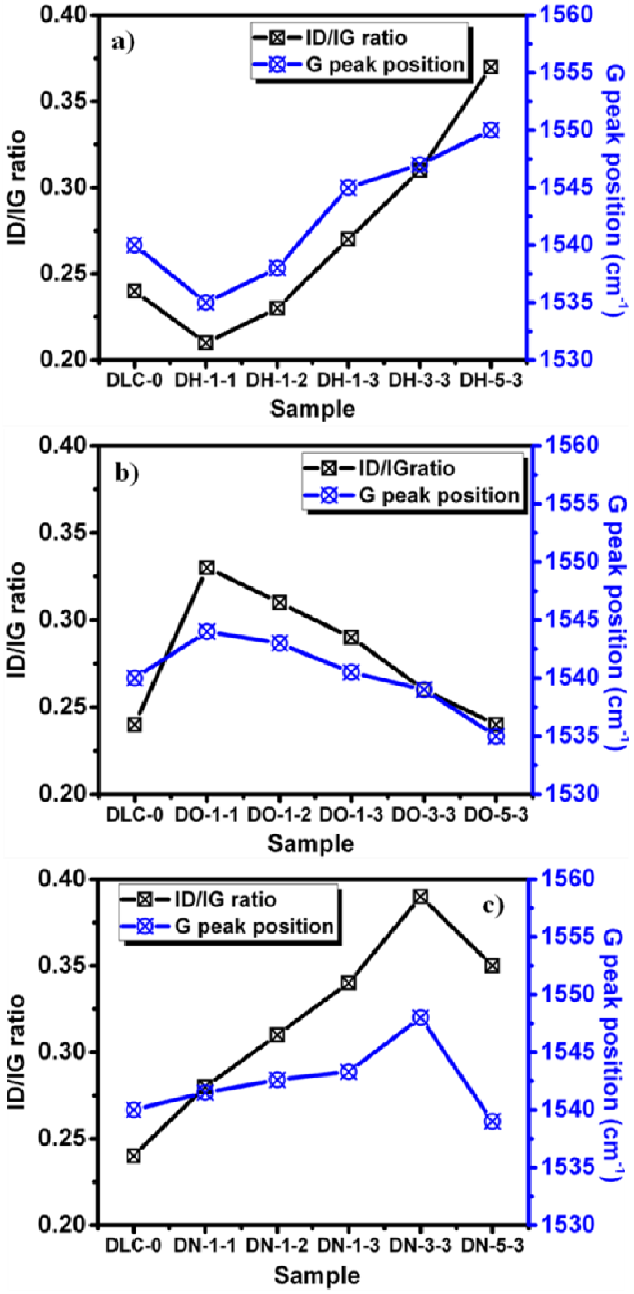

Figure 7.6 I_D/I_G ratio and G peak position of DLC films exposed to a) H_2, b) O_2 and c) N_2 plasmas

This leaves an excess electron in nitrogen atom which further bonds with electron available in π bonding configuration of carbon atom results in higher *sp*^{2} bonding.[1] This is affirmed by the blue shift in G peak position which is a signature of clustering of *sp*^{2} bonding in DLC film. However, nitrogen ions or radicals also cause chemical etching of DLC films. Etching increases with the ion energy and this is confirmed by the observations in FESEM images (Fig. **7.3**). This results in enhanced sp^3 bonding fraction when the film is exposed to higher energy of microwave plasma. Above analysis reveals insignificant changes in chemical structure of films upon plasma exposures. Plasma exposure not only incorporates the reactive species into the film but at the same time these species also interacts with film surface and chemically etches it out.**[20]** Raman spectra of the bias assisted plasma exposed films also possess typical signature of the DLC without significant changes. However, in case of the bias assisted plasma exposure the I_D/I_G ratio initially decreased and further raised at higher exposure times as shown in table-7.1. It is attributed to the selective chemical etching of sp^2C=C carbon by the H^+ ions during the plasma treatment and this process results in stabilization of sp^3C-C content. On the other hand, at higher exposure time, the I_D/I_G ratio increased for both with and without the substrate bias this is due to graphitization. In addition to this, the G peak position showed similar trend and it confirms the initial increase in sp^3 bonding. However, later it converted to sp^2 bonding. Raman spectroscopy cannot limit to the surface chemical structure changes. Hence the compositional changes in film surface induced by plasma exposure on surface were probed by XPS.

Figure **7.7** shows XPS survey spectra of three major peaks of plasma exposed DLC films i.e., C1*s* (~285 eV), N1*s* (~400 eV) and O1*s* (~530 eV).**[20]** Surface reconstruction and modification are obvious outcomes of microwave plasma exposure.**[19]** C/O ratio is high in as-deposited DLC film which shows that the oxygen concentration on the surface is negligible. However, at low microwave power, the oxygen content is high at DLC film surface upon hydrogen plasma exposure (Fig. **7.7a**)). This systematically decreases with increase in microwave power and exposure time. At low microwave power and short exposure time, the carbon dangling bonds density is high on surface. Under this condition, hydrogen plasma interacts with the surface carbon atoms of DLC. This brings about substantial desorption of carbon by hydrogen radicals present in plasma species. This energetic radical knocks off carbon atoms and creates active centre for trapping of atmospheric oxygen.[19] In this circumstances, re-passivating the dangling carbon bonds through hydrogen atom during plasma exposure is also a possible consequence. However, at high microwave power, hydrogen atoms do not interact with the DLC film surface because it diffuses into subsurface which in-turn restricts generation of fresh dangling bonds at surface. This prevents formation of oxygen trapping centers. Therefore, the chemical affinity of DLC surface for atmospheric oxygen species decreases. Oxygen concentration on the film surface increases when surface is exposed to oxygen and nitrogen plasmas (Fig. **7.7b-c**). In both these cases, oxygen concentration increases with increase in microwave power and exposure time. Reactive species generated from oxygen and nitrogen plasma interact with carbon and knocks them out of DLC film surface. This is well evident from the observed reduction in film thickness (Fig. **7.1**). Desorption of carbon atoms leaves behind fresh dangling bonds at the film surface. Such scenario increases the susceptibility of surface towards further adsorption of oxygen upon exposure to ambient atmosphere (Fig. **7.7b**)). In addition there are oxygen chemisorptions on DLC surface during exposure in oxygen plasma. On the other hand nitrogen concentration decreases in DLC film surface when microwave power and exposure time of nitrogen plasma is increased (Fig. **7.7c)**). At high microwave power, nitrogen desorbs from the surface while interacting with incoming energetic nitrogen. It is clear that oxygen absorption of DLC films exposed to oxygen and nitrogen plasma is considerably higher compared to the film exposed to hydrogen plasma.

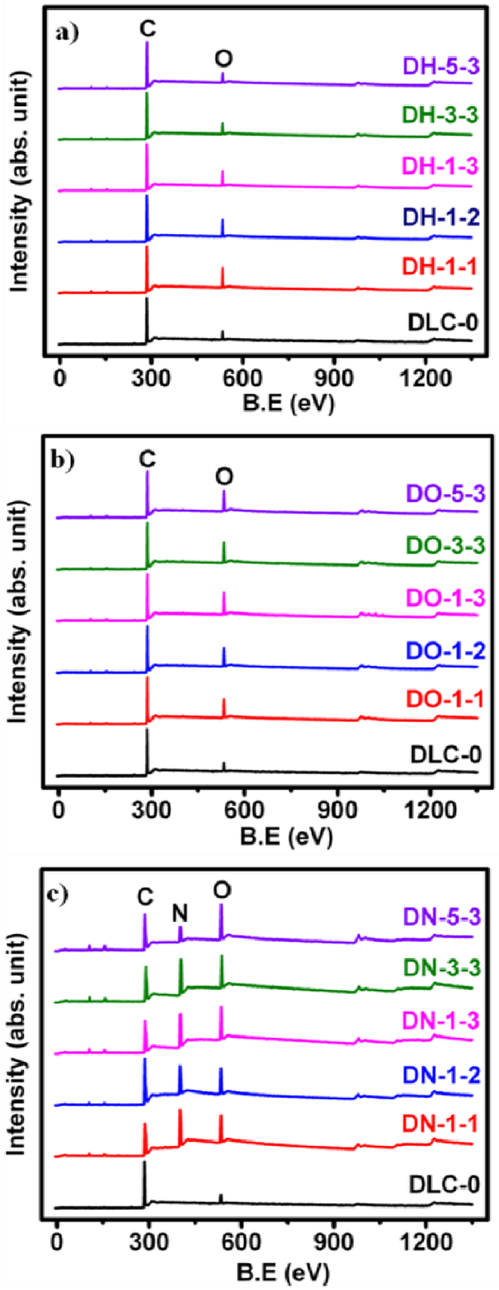

Figure 7.7 XPS survey spectra of DLC films exposed to (a) H_2 (b) O_2 and (c) N_2 plasmas

Systematic inverse trend between surface roughness and C/O ratio is observed in plasma exposed DLC films (Fig. **7.8**). Roughness and alteration in C/O ratio are related to reactivity of plasma species. In hydrogen plasma, surface roughness does not vary much because the hydrogen atoms do not cause significant surface reconstruction thereby resisting defect generation and carbon atom desorption. In contrast, hydrogen atoms passivate the reactive carbon dangling bonds.[19]

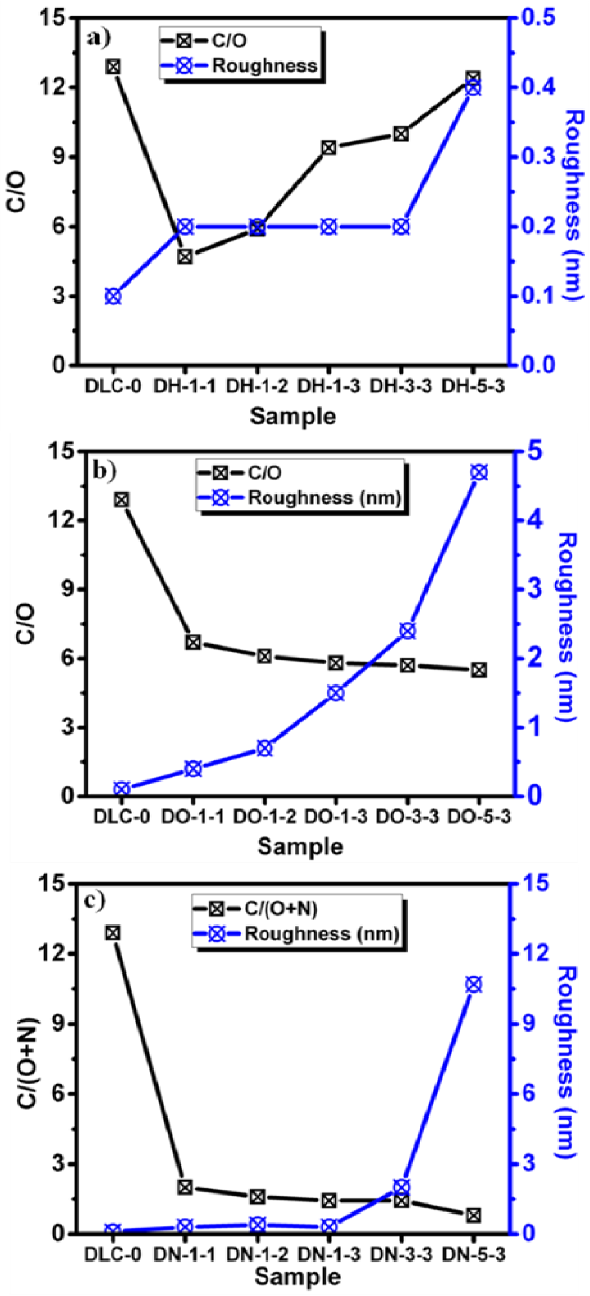

Figure 7.8 C/O ratio and roughness of DLC films exposed to (a) H_2 (b) O_2 and (c) N_2 plasmas

This is the reason that oxygen content on the surface is low and C/O ratio is highest in hydrogen plasma exposed DLC film surface. Therefore, the roughness slightly changes with C/O ratio (Fig. **7.8a**). However, concentration of oxygen species increases significantly in oxygen and nitrogen plasma exposed DLC films. This also caused an increase in surface roughness (Fig. **7.8b-c**). These effects are governed by reactivity of oxygen and nitrogen plasma that produces the surface defects via desorption of carbon atoms along with simultaneous adsorption of oxygen and nitrogen species.[20] High roughness leads to high surface energy and rougher asperities act as oxygen trapping centers.[12,20] The deconvoluted C1*s* peak of the bias assisted hydrogen plasma treated DLC films are shown in Fig. **7.9**.

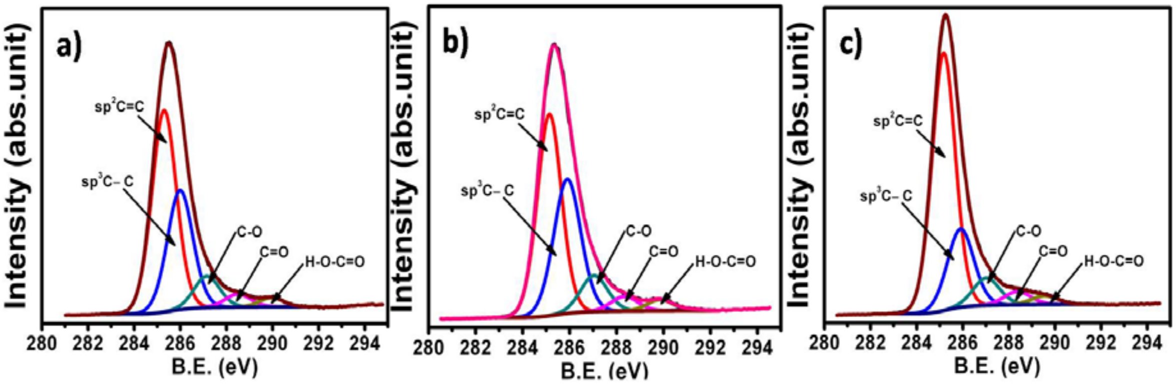

Figure 7.9 C1*s* spectra of bias assisted H_2 plasma exposed DLC films for a) 15, b) 30 and c) 60 mins

Table-7.1: Roughness, I_D/I_G ratio, *sp*^{2}/*sp*^{3} ratio, coefficient of friction (COF) and contact angle (CA) with plasma processing time

Sample name	Roughness (nm)	I_D/I_G ratio	*sp*^{3}/*sp*^{2} (XPS)	COF	CA (Degree)
S15	0.29	0.44	50/50	0.12	81
S30	0.32	0.39	60/40	0.15	75
S60	3.2	0.51	30/70	0.08	88

Significant amount of surface absorbed oxygen is observed in case of the bias assisted H_2 plasma exposed DLC films and it is increased with the exposure time which is due to increase in surface roughness.

7.3.3 Contact angle analysis

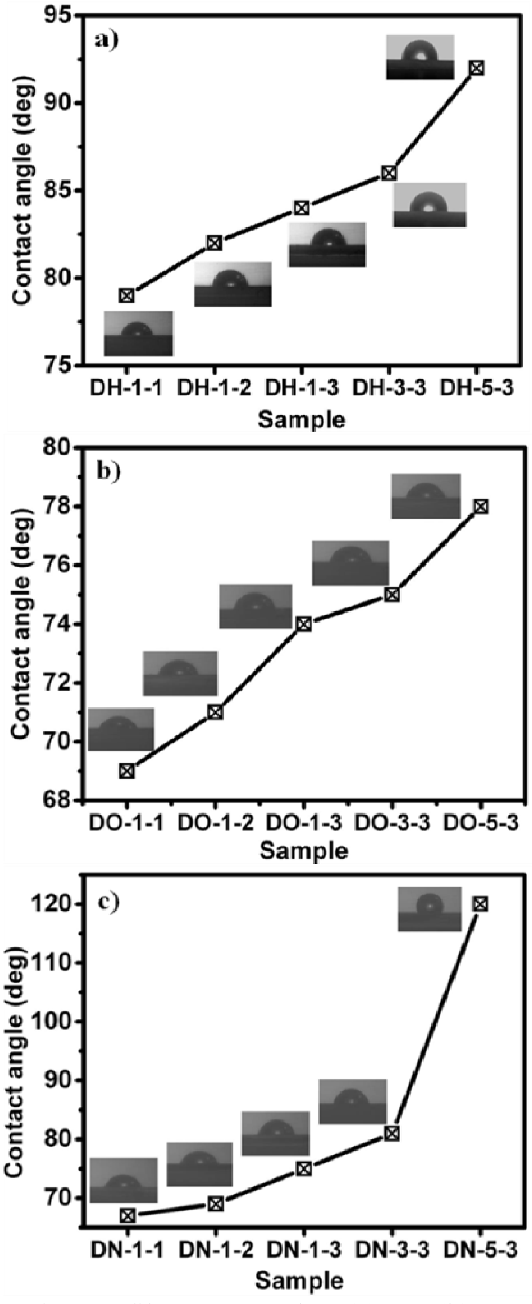

Figure 7.10 Contact angle of DLC films exposed to (a) H2 (b) O2 and (c) N2 plasmas

Contact angle measurements on plasma exposed DLC films are shown in Fig. **7.10**. It is shown that water contact angle of DLC film increases with increase in microwave power and exposure time. At lower exposure time, all the three plasma exposed films become hydrophilic as compared to the as-deposited DLC films (Fig. **7.10a-c**). Especially, nitrogen and oxygen plasma exposure render the film surface more hydrophilic (Fig. **7.10 b-c**). However, the increase in exposure time and microwave power increases the water contact angle and this value becomes close to the as-deposited DLC film. Upon hydrogen plasma exposure, dangling carbon bonds of DLC surface interacts with hydrogen atoms/ions/radicals present in the plasma and undergoes surface reconstruction.[19, 20] Alongside hydrogen chemisorptions, trace levels of oxygen ingress also occurs as seen in XPS analysis.

A plausible interaction mechanism of water droplet with film surface is schematically shown in Fig. **7.11 (a-c)**. The droplet interacts with DLC surface forming hydrogen-oxygen network through hydrogen bonding. This happens when carbon dangling bonds of DLC surface is passivated by hydrogen atoms forming covalent bond and the hydrogen atom interacts with oxygen of water molecules. Hydrogen atoms of water molecules may also interact with hydrogen atom which saturates the carbon dangling bonds in DLC surface. This interaction is weak electrostatic in nature and hinders wetting by water droplet. Further, covalent bond is formed between adsorbed oxygen and carbon dangling bonds of the DLC surface. The interaction induces asymmetric polarization thereby promoting hydrogen bonding with water molecules. The negative charge centers created by oxygen atoms can coordinate with several hydrogen bonds belonging to water. The strength of hydrogen bonding is stronger than the weak electrostatic force that brings in hydrophilicity to surface.[26, 27] The XPS analysis shows reduced oxygen content in the DLC surface. Hydrogen bonding causing enhanced hydrophilicity and restricts oxygen chemisorption. Such interaction is expected to be negligible because adsorbed oxygen is less on the hydrogen plasma exposed DLC film.

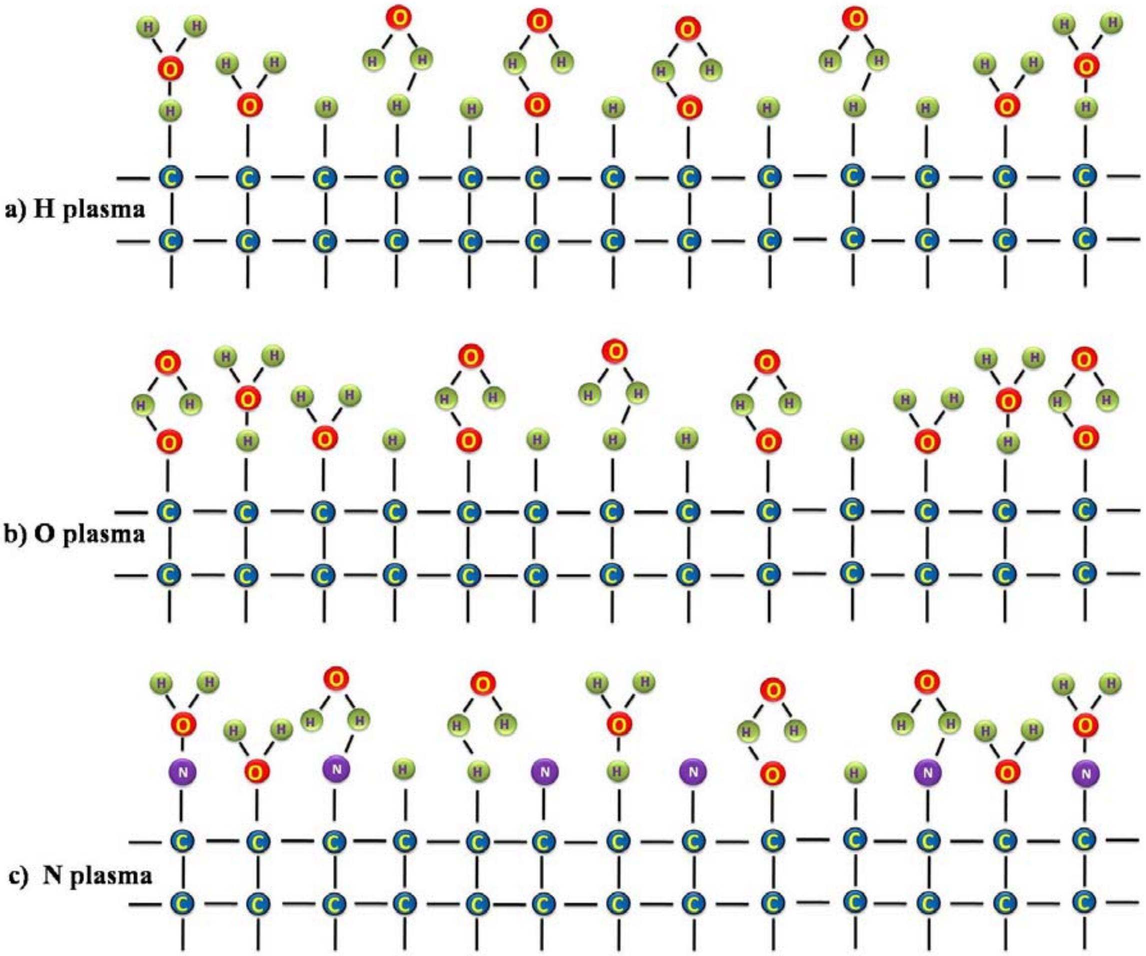

Figure 7.11 Schematic representation of DLC film surface exposed to (a) H_2, (b) O_2 and (c) N_2 plasmas

The surface roughness of hydrogen exposed DLC surface does not change much and the effect of roughness on contact angle can be ignored. Oxygen and nitrogen plasma exposed films are found to be much more hydrophilic as compared to hydrogen plasma exposed DLC films (Fig. **7.11 b-c**). However, resistance to water wetting characteristic increases with microwave power and exposure time. This is attributed to oxygen and nitrogen adsorption on the surface. In case of oxygen plasma exposure, oxygen content on the DLC surface increases with microwave power and exposure time as evident from XPS analysis. This indicates adsorption of more oxygen that establishes hydrogen bonding between adsorbed oxygen thereby forming C-O bond on DLC surface and water molecules (Fig. **7.11b)**). Therefore, it brings in the -C-O-H_2O bonding network. This adsorbed oxygen atoms might form the covalent bonding with dangling carbon bonds.[19] Implantation at high microwave power leads to more energetic oxygen bombardment on DLC surface which causes desorption of surface carbon atoms.[20] The dangling bonds formed under this processes causes carbon-oxygen covalent network to be established (Fig. **7.11b)**). Covalent chemical bond possibly forms between water molecules and unsaturated carbon atom of DLC surface when adsorbed oxygen content is less on the surface. This occurs when microwave power and plasma exposure time are low. A plasma exposed DLC surface containing unsaturated carbon dangling bonds have a tendency to physisorb or chemisorb either H_2O or O_2 molecules from ambience leading to saturation. The sorption phenomenon is more or less inactivates the surface leading to reduction in contact angle which was indeed observed in this case.

Nitrogen plasma exposure of DLC film surface showed increase in oxygen and decrease in nitrogen species with microwave power and exposure time. In this condition, the proposed operating interaction mechanisms are shown schematically in Fig. **7.11 c)**. Nitrogen adsorption on film surface dominates at low microwave power and exposure time. This leads to formation of covalent bonds between adsorbed nitrogen and dangling carbon bonds of DLC network. Here, the negative polarity on the nitrogen atom becomes high and interacts covalently with negatively charged oxygen atoms of water molecules that lead to hydrophilic behavior (Fig. **7.11 c)**). This explains that chemical affinity of surface becomes stronger when nitrogen content is more on the surface, leading to more water wetting characteristic. Hydrogen bonding network is possible when covalently adsorbed nitrogen in DLC network interact with hydrogen atoms of water molecules forming N-H coordination (Fig. **7.11 c)**).[27] However, oxygen content is high at higher microwave power and exposure times. The dominant mode of interaction involves formation of hydrogen bonding between water molecules and adsorbed oxygen atom on the DLC surface. This interaction is weaker than covalent interaction existing between adsorbed nitrogen and oxygen atom of water molecules. Thus wetting characteristics gets influenced by the adsorbed oxygen content on the DLC surface. At high microwave power irrespective of gaseous constituent used, surface defect density increases. The chemical etching and diffusion of implanted species are predominant in increasing in defect density.[20] Hydrogen being a lighter atom compared to carbon it does not cause high surface roughness. This normally diffuses and passivates the carbon dangling bonds on the surface and subsurface region.[19, 20] Whereas, the atomic masses of oxygen and nitrogen are comparable to the carbon. As energy increases these heavier species collide with the surface and transfer the energy and momentum, leading to resputtering of film surface.[1] Moreover, carbon atom becomes unstable and it is etched away from the surface when oxygen and nitrogen like reactive species form a covalent bonding with dangled carbon atoms. The surface thinning and etching is well evident from the cross section of the film acquired at different microwave power and exposure times (Fig. **7.3**). This is the main reason for significant increase in surface roughness in nitrogen and oxygen plasma exposed DLC film. Surface roughness can also be considered to influence the contact angle. High roughness acts as a cavity on the surface where air pressure is more effective. These pressurized pockets repel the water droplets which can be explained by Cassie and Baxter model.[28] However, this model is more reliable to explain the contact angle of water droplet in microscopic scale. Therefore, the relationship of contact angle with chemical modification and reconstruction of DLC surface is explained here more reliably on the basis of bonding configuration.

7.3.4 Tribology studies

Fig. **7.12** illustrates the friction coefficient and wear rate of plasma treated films. At first instance it is clear that plasma exposure resulted in higher friction coefficient than the untreated film irrespective of the plasma gas. The wear rate also increased with the microwave power in all the three cases. The increase in friction coefficient can be attributed to change in surface chemistry and surface roughness. The topography measurements showed increase in roughness and this value increased significantly while film was exposed to oxygen and nitrogen plasma. In addition to this, a notable increase in C/O, C/(O+N) ratio also observed in all the three cases. It has been reported that the oxygen absorption (C=O) of DLC film results in higher friction coefficient.[25] Apart from the higher friction coefficient, the run-in-period behavior is also observed. Run-in-period is the transient state before reaching the steady state friction coefficient. The run-in-period is prominent in the films exposed to hydrogen and nitrogen plasma. The films exposed to hydrogen plasma for 10 mins shown an extended run in period up to 60 meters of sliding and a significant reduction with increase in exposure time and power. However, this behavior disappeared at very high plasma power. Similar behavior is observed in the nitrogen plasma exposed films. Surprisingly, run-in-period also disappeared in the oxygen plasma exposed films. The run-in-period is attributed to the absorbed oxygen and the width of the run-in-period behavior is corroborated well with the C/O ratio.

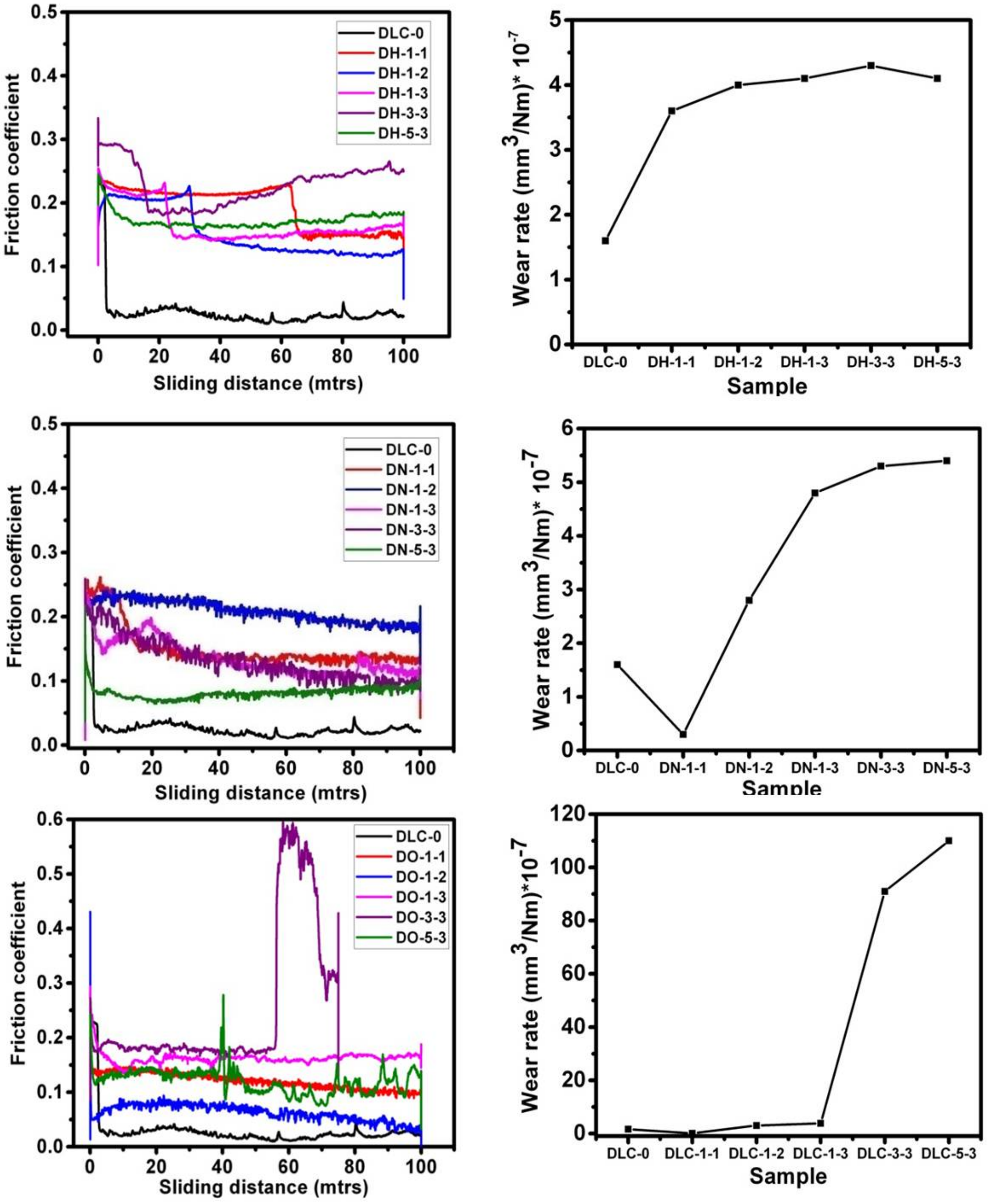

Figure 7.12 Friction plot and corresponding wear rate of plasma exposed DLC films (a,b) hydrogen, (c,d) nitrogen and (e,f) oxygen plasmas

Friction coefficient of hydrogen and oxygen plasma exposed DLC films increases with increase in contact angle. This can be explained by following mechanism. In real tribological contact, the interacting hydrophobic surfaces become dry that can lead to direct surface-surface solid interaction. The shear rigidity of solid surfaces is stronger which increases the adhesion and friction. Therefore, the stability of atmospheric water vapor on hydrophobic DLC surfaces at high tribo-contact pressure is weak. This establishes the direct contact of DLC surface with Al_2O_3 ball, leading to high wear and friction when contact angle is high. In contrast, water vapor traps in hydrophilic contacting surfaces make a thin liquid layer. This provide protective layer and it easily slides. Furthermore, water vapor helps to chemically heal the dangling bonds formed on deformed surface through passivation.

7.4 Conclusions

Hydrogen, oxygen and nitrogen ions were used at various, microwave powers and exposure times for post plasma modification of DLC surface. Ultra-smooth as-deposited DLC film surface becames significantly rougher in oxygen and nitrogen plasma. The origin of this roughness is explained by adsorption-desorption of implanted species and carbon atoms from the tetrahedral DLC network, leading to chemical reconstruction of the surface. Contact angle of water droplet increased when surface is highly reconstructed by oxygen and nitrogen plasma. This feature was described by forming the hydrogen bonding and weak electrostatic network between the water droplet and adsorbed species. However, wetting properties were enhanced when adsorbed atoms interacted with water molecules. Additionally the surface re construction and absorbed oxygen played significant role in altering the friction coefficient. However, irrespective of plasma type and exposure time, friction coefficient increased because of the altered surface roughness and chemistry.

7.5 References

1. J. Robertson, *Mat. Sci. Engg.* **2002**, 37, 129.
2. C. A. Charitidis, *Int. J. Refrac. Met. & Hard Mat.* **2010**, 28, 51.
3. A. Erdemir and C. Donnet, *J. Phys. D: Appl. Phys.* **2006**, 39, 311.
4. R. Blossey, *Nature Mat.* **2003**, 2(5), 301.
5. N. R. Chio, *et al., Nature Nano technol.* **2007**, 2, 354.
6. S. Meng, *et al.*, *Phys. Rev. Lett.* **2006**, 97, 036107.
7. R. K. Roy and K. R Lee, *J. Biomed. Mat. Res. B Appl. Biomater.* **2007**, 83(1), 72.
8. J. W. Yi, *et al.*, *Langmuir* **2010**, 26 (22), 17203.
9. M. K. Kuntumalla, *et al.*, *Phys. Chem. Chem. Phys.* **2015**, 17, 21331.
10. F. Liu, *et al.*, *ACS Nano* **2010**, 4 (5), 2643.
11. H. Zhuang, *et al.*, *J. Phys. Chem. C* **2010**, 114, 20207.
12. B. Cortese and H. Morgan, *Langmuir* **2012**, 28, 896.
13. S. Tian, *et al.*, *Langmuir* **2014**, 30, 12647.
14. B. Sun, *et al.*, *Langmuir* **2006**, 22, 9598.
15. T. Wang, *et al.*, *Langmuir* **2014**, 30, 1089.
16. L. Zhang, *et al.*, *RSC. ADV.* **2015**, 5, 9635.
17. Y. Rahmawan, *et al.*, *Langmuir* **2010**, 26 (1), 484.
18. M. Karlsson, *et al.*, *Langmuir* **2010**, 26 (2), 889.
19. S. R. Polaki, *et al.*, *Tribo. Int.* **2015**, 81, 283.
20. D. Caschera, *et al.*, *Langmuir* **2013**, 29, 2775 – 2783.
21. Y. N. Chen, *et al.*, *J. Phys. Chem. C* **2015**, 119, 16148-16155.
22. S. Bai, *et al.*, *RSC. ADV.* **2014**, 4, 33739.

23. K. Hayashi, *et al.*, *J. Phys. Chem. C* **2011**, 115, 22981.

24. S. Bai, *et al.*, *J. Phys. Chem. C* **2012**, 116, 12559.

25. H. I. Kim, *et al.*, *Tribo. Lett.* **2006**, 21(1), 53.

26. L. Mayrhofer, *et al.*, *J. Am. Chem. Soc.* **2016**, 138, 4018.

27. G. R. Desiraju, *et al. Acc. Chem. Res.* **2002**, 35, 565 – 573.

28. A. B. D. Cassie and S. Baxter, *Trans. Faraday Soc.* **1944**, 40, 546.

8.1 Conclusions

Argon dilution of the feedstock gas enhances the growth rate of DLC films. This improves the film density by stabilizing *sp*^{3} bonding. Hydrogen ingress into films also found to be marginal with dilution. On the other hand with increase in methane concentration in the feed stock gas soft and polymer-like hydrogenated DLC film forms. Substrate biasing not only improved film density but also reduced the hydrogen content. However, high bias voltage reduced film density due to increase in *sp*^{2} bonding because of ion bombardment with high energy. This resulted in evolution of graphitic second phase in the DLC matrix. This caused reduction of elastic modulus. The elastic modulus mapping using AFAM showed a microscopic evidence for the graphitic clustering described by the subimplantation growth model.

The DLC films grown at high substrate bias exhibited high friction coefficient and also films failed mechanically. Increase in sliding speed resulted in reduction of friction coefficient due to graphitization of the DLC films. However, the wear rate increased with the sliding speed. This was substantiated by contact resonance frequency mapping across the wear track. Conversion of *sp*^{3} to *sp*^{2} phase with sliding speeds was investigated by Raman spectroscopy mapping across the wear track. Significant increase in friction coefficient as well as wear rate was observed with increase in normal load.

The nitrogen doping of DLC films enhanced *sp*^{2} C=C bonding and also encouraged their clustering in amorphized *sp*^{3} matrix. The clustering phenomenon was achieved at low bias voltages compared to the un-doped films. The cluster size increased with nitrogen concentration. Consequently elastic modulus is reduced and friction coefficient increased. However, the wear resistance improved by 2 orders.

The adsorbed oxygen showed a considerable influence on the friction coefficient in nitrogen doped DLC film. Nearly vanishing friction coefficient (0.004) and ultra antiwear properties were observed in CH_4 atmosphere. This was explained by surface passivation by hydrogen ions liberated upon dissociation of CH_4 occurs during the sliding. Inert gases Ar and N_2 also played an effective role in reduction of friction coefficient. However, very high friction and high wear were observed in O_2 reach atmosphere. Except in ambient conditions, both undoped and nitrogen doped DLC films showed similar friction and wear behavior in CH_4, Ar, N_2 and O_2. Tribology studies in different gas media ascertained the role of surface chemistry and passivation on friction behavior of DLC films.

Exposure to hydrogen, oxygen and nitrogen plasmas at various energies and exposure time durations caused surface reconstruction of DLC films. This altered the microstructure and surface chemistry due to chemical etching of the DLC films. This was moderate in H_2, N_2 and severe in O_2 plasmas. Surface modification by plasma exposure demonstrated the possibility of tuning wetting characteristics of DLC films. Hydrophilic characteristics of DLC films were observed when it was exposed in O_2 plasma medium. On the other hand both H_2 and N_2 exposed films resulted in hydrophobicity. Apart from the surface chemistry, the surface roughness was also found to be a key parameter deciding the wetting characteristics. Surface roughness was mainly influenced by chemical etching.

Future prospects

- Adhesion of DLC films with varying microstructure grown on metallic substrates needs to be investigated.
- Metal embedded DLC films needs investigation for multifunctional behavior.
- Tribology studies on DLC films at high temperature need to be carried out to establish real system applications.
- Tribo chemical stability also needs to be established.
- Tribothermal stability of DLC film with a nanocrystalline diamond or graphene layer on top or composite to be explored.
- Bio compatibility of DLC films needs to be explored.